

The Pennsylvania State University
School of Engineering
Department of Mechanical & Nuclear Engineering

**DEVELOPMENT OF A REAXFF REACTIVE FORCE FIELD FOR
SILICON/OXYGEN/HYDROGEN/FLUORIDE INTERACTIONS AND APPLICATIONS
TO HYDROXYLATION AND FRICTION.**

A Dissertaion in
Mechanical and Nuclear Engineering

by
Jejoon Yeon

© 2016 Jejoon Yeon

Submitted in Partial Fulfillment
of the Requirements
for the Degree of

Doctor of Philosophy

May 2016

The dissertation of Jejoon Yeon was reviewed and approved* by the following:

Adri C. T. van Duin
Professor of Mechanical and Nuclear Engineering
Professor of Chemical Engineering
Dissertation Advisor
Chair of Committee

Aman Haque
Professor of Mechanical and Nuclear Engineering

Liming Chang
Professor of Mechanical and Nuclear Engineering

Seong H. Kim
Professor of Chemical Engineering

James D. Kubicki
Professor of Geological Sciences
University of Texas El Paso

Karen A. Thole
Professor of Mechanical and Nuclear Engineering
Head of the Department of Mechanical & Nuclear Engineering

*Signatures are on file in the Graduate School

ABSTRACT

Molecular dynamics (MD) simulations with the ReaxFF reactive force field were carried out to find the atomistic mechanisms for tribo-chemical reactions occurring at the sliding interface of fully-hydroxylated amorphous silica and oxidized silicon as a function of interfacial water amount. The ReaxFF-MD simulations showed a significant amount of mass transfer across the interface occurs during the sliding. In the absence of water molecules, the interfacial mixing was initiated by dehydroxylation followed by the Si-O-Si bond formation bridging two solid surfaces. In the presence of sub-monolayer thick water, the dissociation of water molecules can provide additional reaction pathways to form the Si-O-Si bridge bonds and mass transfers across the interface. However, when the amount of interfacial water molecules was large enough to form full monolayer, the degree of mass transfer was substantially reduced since the silicon atoms at the sliding interface were terminated with hydroxyl groups rather than forming interfacial Si-O-Si bridge bonds. The ReaxFF-MD simulations clearly showed the role of water molecules in atomic scale mechano-chemical processes during the sliding and provided physical insights into tribochemical wear processes of silicon oxide surfaces observed experimentally.

In addition to this, we performed reactive force field molecular dynamics simulation to observe the hydrolysis reactions between water molecules and locally strained SiO_2 geometries. We improved the Si/O/H force field from Fogarty et al.¹, to more accurately describe the hydroxylation reaction barrier for strained and non-strained Si-O structures, which are about 20 kcal/mol and 30 kcal/mol, respectively. After optimization, energy barrier for the hydroxylation shows a good agreement with DFT data. The observation of silanol formation at the high-strain region of a silica nano-rod also supports the concept that the adsorption of water molecule: hydroxyl formation favors the geometry with higher strain energy. In addition, we found three

distinct hydroxylation paths – H_3O^+ formation reaction from the adsorbed water, proton donation from H_3O^+ , and the direct dissociation of the adsorbed water molecule. Because water molecules and their hydrogen bond network behave differently with respect to temperature ranges, silanol formation is also affected by temperature. The formation of surface hydroxyl in an amorphous silica double slit displays a similar tendency: SiOH formation prefers high-strain sites. Silanol formation related with H_3O^+ formation and dissociation is observed in hydroxylation of amorphous SiO_2 , similar with the results from silica nano wire simulation. These results are particularly relevant to the tribological characteristics of surfaces, enabling the prediction of the attachment site of the lubrication film on silica surfaces with a locally strained geometry.

TABLE OF CONTENTS

List of Figures	vii
List of Tables	xii
Acknowledgement	xiii
Chapter 1 Introduction	1
1.1. Lubrication and tribo-chemistry	1
1.2. Hydroxylation of SiO ₂ surface and relationship with atomic strain energy of surface	4
1.3 Silicon-Fluorine reaction and etching	7
Chapter 2 The ReaxFF Reactive Force Field method	10
2.1. About the ReaxFF method	10
2.2. Brief introduction of ReaxFF	11
2.2.1. Bond order and bond energy	11
2.2.2. Valence angle energy	12
2.2.3. Torsion angle energy	12
2.2.4. Lone pair energy	13
2.2.5. Van der Waals energy	13
2.2.6. Coloumb energy	14
Chapter 3 Silica force field improvement and application to strain related hydrolysis reactions	15
3.1 Introduction	15
3.2. Relationship between hydroxylation of SiO ₂ surface and local atomic strain energy	16
3.2.1. Validation of the force field for strained Si-O bond hydrolysis	16
3.2.2. Application to Silica Nanowire	20
3.2.3 Reaction path for hydroxylation on the edge area of silica nano wire	22
3.2.4. Analysis of hydroxyl formation with respect to different temperatures	26
3.2.5. Hydroxyl formation on amorphous silica surface: ReaxFF MD simulation results	34
Chapter 4	44
Molecular dynamics simulations of friction in amorphous silica surfaces	44
4.1. Introduction	44
4.2. Friction simulation of amorphous SiO ₂ surface under various environments	44
4.2.1. System preparation and simulation conditions	44
4.2.2. Tribological reactions at the sliding interface	47
4.2.3. Interfacial mixing during the slide for 1ns	51

4.2.4. Separation of the interface after sliding for 1 ns	58
Chapter 5.....	65
Development of a ReaxFF description for fluorine etching.....	65
5.1. Introduction to force field development.....	65
5.2. Force field optimization of Si/F parameters.....	66
5.3. Force field optimization for F/F and H/F interaction.....	69
5.4. Etching of Si 001 surface using F ₂ and HF molecule	71
5.4.1. System Preparation.....	72
5.4.2. Etching of Fluorine gas to Si(100) surface: ReaxFF MD simulation results.....	73
Chapter 6 Conclusion.....	78
References.....	82

LIST OF FIGURES

Figure 2-1. Comparisons of ReaxFF method with other way of simulation method	10
Figure 3-1. Picture of strained Si dimer (left) and non-strained silica dimer (right)	16
Figure 3-2(a). Energy barrier for hydroxylation on non-strained Si dimer structure with the Fogarty force field.....	17
Figure 3-2(b). Energy barrier for hydroxylation on strained Si dimer structure with the Fogarty force field. ¹	17
Figure 3-3(a). Energy barrier for hydroxylation of the non-strained silica dimer structure for the SiO-2015 force field.	18
Figure 3-3(b). Energy barrier for hydroxylation of the strained silica dimer structure for the SiO-2015 force field.....	19
Figure 3-4(c). Relative strain energy (kcal/mol) view of silica nanowire. Red atoms represent higher strained atoms, blue atoms mean lower strain energy ones.....	20
Figure 3-4(b). Silica nano wire. Grey atoms are Si atoms, and Red atoms are Oxygens.	20
Figure 3-4(a). Silica nano rod in the 200 water molecules in the 30x30x30 Å ³ periodic box. Water density was 0.222 kg/dm ³	20
Figure 3-5(b). Silica nanowire, 500ps exposure at 700K temperature. All strained Si atoms at the edge sites are occupied by silanols.	21
Figure 3-5(a). Silica nanowire after 650ps exposure at 400K temperature. 5 silanols are formed at the edge area. Green and blue atoms represents the O and H of the silanol.	21
Figure 3-6. Snapshots of hydroxylation reaction, involving the formation of hydronium ion at 400K. Grey atoms are Si, red atoms are O, white atoms are H, and blue atoms are O of hydroxyl.	23
Figure 3-6(b). 76.26ps after MD simulation. One of the H atom of adsorbed water molecule is attracted to nearby secondary water molecule	23
Figure 3-6(a). 76.21ps after MD simulation. Adsorbed water molecule at the edge Si of silica nano wire.	23
Figure 3-6(d). 76.32ps after MD simulation. Formation of hydroxyl. H ₃ O ⁺ ion moved across the periodic boundary.....	23
Figure 3-6(c). 76.265ps after MD simulation. Proton donation occurred.....	23
Figure 3-7(c). 195.375ps after MD simulation. Proton donation.....	24

Figure 3-7(d). 195.45ps after MD simulation. Si-O bond breaks, and SiOH formed.....	24
Figure 3-7. Snapshots of hydroxylation reaction, involving the dissociation of hydronium ion at 900K. All color settings of atoms are the same as figure 3-6	24
Figure 3-7(a). 195.3ps after MD simulation. H ₃ O ⁺ approaches to bridge O.....	24
Figure 3-7(b). 195.37ps after MD simulation. One of the H of H ₃ O ⁺ is attracted to the bridge O of strained structure.....	24
Figure 3-8(a). 121.76ps after MD simulation. Adsorption of water to Si.....	25
Figure 3-8(b). 121.815ps after MD simulation. One of the H of adsorbed H ₂ O is attracted to the bridge O of strained structure.	25
Figure 3-8(c). 121.82ps after MD simulation. Proton donation.....	25
Figure 3-8(d). 121.87ps after MD simulation. Si-O bond breaks, and two silanols formed.	25
Figure 3-8. Snapshots of hydroxylation reaction, involving the dissociation of adsorbed water molecule at 1500K. All color settings of atoms are the same as figure 6. Water molecules, unrelated with reaction, are removed for clarity.	25
Figure 3-9. Maximum number of silanols during simulation for each temperature after 800ps MD simulation.....	27
Figure 3-10(b). Si – O _{water} RDF from 700K to 1000K.....	28
Figure 3-10(a). Si – O _{water} RDF at 300K, 400K, 500K, and 600K.....	28
Figure 3-10(c). Si – O _{water} RDF from 1200K to 1500K.....	29
Figure 3-10(d). RDF among water molecules	29
Figure 3-11. Average number of isolated water molecules and water clusters.....	32
Figure 3-12(c). Graph of potential energy and temperature with respect to time during annealing of quartz. A 0.002 K / iteration temperature ramp was used in these simulations.	35
Figure 3-12(b). Amorphous silica, after annealing	35
Figure 3-12(a). Quartz, before annealing.....	35
Figure 3-13(b). Si-O-Si bond angle distribution of amorphous SiO ₂ slab.....	36
Figure 3-13(a). Density distribution of slab in depth direction per 1 Å.....	36

Figure 3-13(c). Si-O radial distribution of amorphous SiO ₂ slab.....	37
Figure 3-14. Surface atoms from of the amorphous silica slab, surface Si atoms, colored by strain energy, and surface O atoms, colored by strain energy, from left to right. Red color represents higher strain energy, blue color represents lower strain energy.	38
Figure 3-15. Number of silanols on the slab surface during hydroxylation simulation at different temperatures.	39
Figure 3-16. Vertical view of amorphous SiO ₂ surface after 300K simulation. Red atoms are Si atoms of hydroxyls (Left). Strain energy view of surface Si atoms after 300K hydroxylation simulation. (Right) Red circles represents the position of silanols. Si atoms with relatively high strain energy are generally become the Si of surface hydroxyl.	40
Figure 3-17. Vertical view of amorphous SiO ₂ surface after 500K simulation. Red atoms are Si atoms of hydroxyls (Left). Strain energy view of surface Si atoms after 500K hydroxylation simulation. (Right) Red circles represents the position of silanols. Number of hydroxyls are increased when compared to 300K case, and all of them follows the position of relatively high strained surface Si atoms.....	41
Figure 3-18(c). 26.665ps after simulation. Hydronium formation. (Red circle).....	42
Figure 3-18(d). 26.95ps after simulation. Proton hopping to other water molecule. (Red circle).	42
Figure 3-18(a). 26.57ps after simulation. Adsorbed water on a strained silicon structure. (Red circle) Bright grey shows Si, red atoms are O, white atoms are H, blue atoms are O of water, and green atoms are H of water.....	42
Figure 3-18(b). 26.66ps after simulation. Donation of proton to the nearby water molecule. (Red circle).....	42
Figure 3-19(d). 9.925ps after simulation. One of Si-O bond breaks, forming single silanol on the surface	43
Figure 3-19(c). 9.88ps after simulation. Unstable Si-OH-Si structure.	43
Figure 3-19(a). 9.83ps after simulation. Hydronium inside the water phase. Repeated color scheme with figure 4-18.....	43
Figure 3-19(b). 9.875ps after simulation. Proton donation from hydronium to a high-strained surface bridge oxygen.....	43
Figure 4-1. Configuration of systems for the ReaxFF MD simulations of mechano-chemical wear of silicon oxide surfaces. The number of interfacial water molecules is varied, from left to right, 0, 20, 50 and 100.....	45

Figure 4-2(b). Tracking of number of hydroxylation on the surface of Si (100) and a-SiO ₂ ...	46
Figure 4-2(a). Tracking of oxidation state of Si(100) crystal slab	46
Figure 4-3. Snapshot views of reactions involving a hydroxylated Si atom (A) of the a-SiO ₂ surface and hydroxyl groups of the hydroxylated Si (100) surface in the absence of water at 700K. The sliding time is shown in each frame. Large solid circles marked with letters and numbers are the atoms involved in reactions being monitored in the series of snapshots. Small transparent circles are the atoms that are discussed in the figure. Black solid lines are periodic boundaries.....	48
Figure 4-4. Snapshot views of reactions of an oxygen atom (1) of a water which eventually forms a covalent bond bridging the a-SiO ₂ surface and the oxidized Si (100) surface. The system temperature is 500K and the initial amount of water is 20 molecules in the system. The sliding time is shown in each frame. The color codes in the figures are the same as Figure 4-2.....	49
Figure 4-5. Snapshot views of reactions involving a hydroxylated Si atom (A) of the a-SiO ₂ surface and hydroxyl groups of the hydroxylated Si (100) surface in the presence of 100 water molecules at 300K. The sliding time is shown in each frame. The color codes in the figures are the same as Figure 4-2.	50
Figure 4-6. Mixing of atoms across the interface during the slide in the presence of 20 water molecules at 500K. The sliding time is shown in each frame. The color codes in the figures are the same as Figure 2. The Si and O atoms dissociated from their original solid surfaces and transferred to the opposite solid surfaces as well as the O and H atoms dissociated from H ₂ O are presented as solid enlarged circles.....	52
Figure 4-7(a). Number of water molecules during sliding.....	53
Figure 4-7(b). Number of silanols during sliding.	53
Figure 4-8. Mixing of atoms across the interface during the slide in the presence of 100 water molecules at 300K. The sliding time is shown in each frame. The color codes in the figures are the same as Figure 4-6.....	54
Figure 4-9. Total amount of interfacial mixing, as a function of number of water molecules and system temperature, occurred after sliding at a speed of 10 m/s for 1 ns. The applied normal load is 1 GPa.	55
Figure 4-10. Potential energy change during the sliding of the a-SiO ₂ /oxidized-Si(100) interface system containing 0, 20, 50, and 100 water molecules at 300K, 500K, and 700K. Higher temperature shows smooth and declining potential energy curves, while lower temperature shows numerous peaks and increasing tendency of potential energy.....	57

Figure 4-11. Snapshot views of the vertical separation at a 20 m/s speed for 100 ps after sliding for 1 ns in the absence of water molecule at 500K. The separation time is shown in each frame. The color codes in the figures are the same as Figure 2.	59
Figure 4-12. Snapshot views of the vertical separation at a 20 m/s speed for 100 ps after sliding for 1 ns in the presence of 100 water molecules at 500K. The separation time is shown in each frame. The color codes in the figures are the same as Figure 2.....	60
Figure 4-13. Changes in potential energy of the system during the separation, for the systems of 0, 20, 50, and 100 water molecules at 300K, 500K, and 700K.....	61
Figure 4-14. Total amount of atoms displaced from their original surfaces after sliding at a speed of 10 m/s for 1 ns followed by vertical separation at 20 m/s for 100 ps. The applied load normal to the surface was 1 GPa.	62
Figure 5-1. Energy curve for (a) Si-F bond dissociation, (b)F-Si-F angle, and (c)F-Si-Si angle, and (d) Si-F overcoordinated dissociation energy in SiF ₅ . (e) SiF ₂ formation on the surface 1, F ₂ approach from edge, (f) SiF ₂ formation on the surface 2, F ₂ approach from center. Si-F bond energy and F-Si-F valence angle energies are calculated from SiF ₄ , while F-Si-Si angle used Si ₂ F ₆ molecule.....	67
Figure 5-2. Pictures of geometries for Si-F trainset.....	69
Figure 5-3. (a) Clustering anomalies of HF molecules (left), and (b) F ₂ molecules (right).....	70
Figure 5-4. Energy curve for ReaxFF and QM comparison	71
Figure 5-5. Si(100) slab with reconstructed surface Si atoms	72
Figure 5-6. Result features of the etching of Si(100) slab with 100 F ₂ molecules.....	73
Figure 5-7. Result features of the etching of Si(100) slab with 200 F ₂ molecules.....	74
Figure 5-8. Result features of the etching of Si(100) slab with 300 F ₂ molecules.....	74
Figure 5-9. Result features of the etching of Si(100) slab with 400 F ₂ molecules.....	75
Figure 5-10. Number of species during etching simulations for different F ₂ density. Decreasing speed of F atoms, which means adsorption of F anions to the surface, is faster in 400 F ₂ simulation results than others.	76
Figure 5-11. Surface features from etching simulation after 200ps. Yellow = Si, Pink = F, Cyan = Si of SiF ₄ , and Red = F of SiF ₄	76

LIST OF TABLES

Table 3-1. Different types of silanol formation reaction for different temperature.	30
Table 3-2. Average number of independent water and weakly bonded water clusters. Larger cluster ranges from 4 water to 20 water molecules. The mass of larger cluster is an averaged value.	31
Table 3-3. Comparison of properties of the amorphous silica from ReaxFF and from literature.	38
Table 5-1. Various energy relation comparison between ReaxFF and QM after Si-F interaction training. (all kcal/mol).....	68
Table 5-2. Various relative energy comparison before / after training of ReaxFF force field. Those energies were compared with same number of isolated HF or F ₂ molecules.	71

Acknowledgement

This research is supported as part of the NSF/SI2 program, a National Science Foundation / Software Infrastructure for Sustained Innovation program, under Grant #1047857. I greatly appreciate to my academic advisor, Dr. Adri van Duin, and all current and previous group members of our research group, as well as the co-workers of my research, for helpful discussions, suggestions, and insights. I also appreciate to my family and my wife, Sunyoung Lim, for great support for me. Lastly, I greatly thanks to my friends in US and Korea for all those supports and advices for me.

Chapter 1

Introduction

1.1. Lubrication and tribo-chemistry

Friction and wear of sliding interfaces are not just two-body contact problems involving two ‘static’ solid surfaces. They are consequences of dynamic processes. The mechanical shear of the solid interface can alter the surface structures through dynamic reconstruction and deformation.²⁻⁸ These processes are also very sensitive to the chemical environments to which sliding interfaces are exposed. The molecules impinged and adsorbed on the surface could be involved in chemical reactions affecting adhesion, deformation, and reconstruction processes of the sliding contact.^{9,10}

Nanoscale friction and lubrication of silicon are of great interests especially since the advent of microelectromechanical systems (MEMS).¹¹⁻¹³ Silicon is the first choice of materials for fabrications of MEMS devices because it can be processed through various microfabrication techniques developed for semiconductor industries.^{14,15} However, silicon and silicon oxide materials have poor tribological properties, which poses significant challenges and limitations in the reliability of MEMS devices with physically moving, colliding, and rubbing components. Thus, it is important to understand the fundamental mechanisms of tribological behaviors of silicon materials in nanoscale.¹⁶⁻²²

The chemistry involved in wear of the sliding contact of silicon materials in humid environments is very complicated. In a reciprocating ball-of-flat tribo-testing, the wear of silicon wafer drastically increased upon increasing of water vapor partial pressure in the environment from zero to 50% relative humidity (RH), while the wear was suppressed upon introduction of n-pentanol vapors.²³ At a nanoscale friction test carried out using atomic force microscopy (AFM), the silicon surface showed a protrusion upon scratch with a silica ball in dry environments,²⁴ which was quite different from the material loss observed in the macroscale pin-on-disc test in the same environment.²³ As RH increased from 0% to 50%, this nanoscale protrusion disappeared and the wear of the substrate was observed. Since all mechanical loading and sliding conditions were kept constant, these RH dependences were attributed to tribochemical reactions of water which was speculated to involve the formation of Si–O–Si covalent bonds bridging two solid surfaces.²⁴ A more recent AFM wear tests over the full RH range from 0% to 100% revealed that the silicon wear was maximum at RH around 50% and then decreased upon further increase of RH.²⁵ It was speculated that as multilayers of water grow on the surface at high RH conditions, the probability for the asperities to come close enough to form Si_{tip}–O–Si_{substrate} bridges would decrease.²⁵ It was also reported that the RH dependence of silicon wear is different at low and high sliding speeds in AFM tests.²⁶

The surface chemical reactions induced by shear actions of a tribological interface are further complicated as additional variables are involved. For example, the water-induced wear could be suppressed when alcohol molecules are co-adsorbed.^{27,28} But, the alcohol effect is negated when the water vapor pressure is sufficiently high.^{27,28} In the

case of soda lime silica glass, the surface sodium ions are easily leached and exchanged with protons and water molecules.²⁹ The chemical reactivity of water molecules occupying the leached sodium ion sites appears to be quite different from that of water molecules adsorbed on the silica surface.²⁹ All these data suggest that very complex tribochemical reactions take place at the sliding interface of silicon in the presence of water.

Molecular details of such complicated reactions could be attained from computational studies. For example, density functional theory (DFT) calculations showed large differences in activation energy for solvolysis reactions of silicon oxide surface with water and alcohol molecules.²³ However, it should be noted that DFT calculations were done in the absence of any mechanical shear of the interface. The mechanical properties could be studied better with molecular dynamics (MD) simulations.^{30–35} However, conventional MD simulations use non-reactive force fields so that they cannot describe chemical reactions and transition states. Recently, many reactive force fields have been developed and available; most representative ones are REBO,³⁶ COMB,³⁵ are ReaxFF.³⁷ Among these, ReaxFF is most versatile and widely used for various systems including surface corrosions and failure.^{38–43}

In this study, we carried out MD simulations with ReaxFF to understand tribochemical reactions taking place at the sliding interface between the hydroxylated surfaces of amorphous SiO₂ and oxidized Si(100) solids. ReaxFF-MD simulations revealed molecular details of interfacial reactions involving the surface atoms and functional groups of the two solid surfaces as well as water molecules present in the

sliding interface.^{23,44} The reaction dynamics are much more complicated than the simple schematic representations proposed in the previous experimental studies.^{24,25} Most of interfacial reactions were initiated by the dissociation of Si-O bonds and subsequent reactions varied depending on the system temperature and the initial amount of water present in the interface.

1.2. Hydroxylation of SiO₂ surface and relationship with atomic strain energy of surface

Amorphous silica is the one of the most important material on the Earth, thanks to its excellent mechanical properties, such as dielectric constant, and mechanical resistance.⁴⁵ Silica has been an important material for various applications, such as glass, wafer, electronic devices and nano-tech devices.^{11,12,46}

In addition, among all the studies related with silicon, silica-water interaction has been a central research topic, due to its importance and influence on theoretical science and practical applications. More importantly, the silica/water combination is very inexpensive and ubiquitous, which is why silica-water has often been preferred by researchers compared to other chemical combinations present in the natural environment.^{47,48} Many studies have been performed to understand the interfacial surface chemistry regarding water-silica system, such as how surface silicon-hydroxyls modulate interfacial properties, or how this chemistry is affected by surface characteristics,^{49,50} or by the effect of tensile or compressive stress on reaction between silica surface and water.⁵¹

The hydrolysis reaction between water and the silica surface is initiated by physisorption of the water molecule onto the surface, followed by its dissociation and chemisorption as a hydroxyl group.⁵² Hydroxyls on the surface are known to greatly modify surface properties, due to their unique ability to form hydrogen bond networks. It has been observed that undercoordinated surface atoms and strained sites are responsible for structural deformation, such as crack formation, corrosion, or other surface chemistry. Similarly, hydrolysis reaction also favors defects and holes on the surface.⁵³

A significant research effort has been executed to understand and utilize silanols and Si-OH-related surface activity. Recent experimental techniques, such as XANES, are capable of in-situ measuring of electronic structure at the silica-liquid interface.⁵⁴ NMR and IR spectroscopy on silica surface expanded the understanding of various types of silanols.⁵⁵ However, experimental approaches are often not appropriate to represent surface topography and surface structure information in the atomic size scale, and on the picosecond time-scale connected with chemical reactions.

Computational chemistry methods enable us to simulate and visualize the processes of chemical reactions as well as track the behavior of atoms and molecules during reaction. First principle ab-initio simulations have been applied to compute the water-silica interactions by researchers, providing the clues for understanding of interfacial nature in atomic scale. For example, Y. He et al.⁵¹ showed the relationship between external stress and long range surface-water interaction, and role of other water molecules during reaction. Also, they predicted the pre-dissociation adsorption of water on silica surface using a Born Oppenheimer model. C. Mischler et al.⁵⁶ studied silica-

liquid interaction using a mixed classical MD and ab-initio code, with BKS and Car-Parrinello potential, to simulate reaction on the surface. M. H. Du et al.⁵⁷ also applied a DFT-assisted classic potential MD code, revealed various trends of hydrogen bond network between crystal phase and amorphous phase of silica. They also pointed out the effect of system size on hydration energy. Y. Ma et al.⁵⁸ investigated how undercoordinated Si atoms and third-party water molecules around OH group lead the dissociation of adsorbed H₂O molecule. F. Musso et al.⁵⁹ indicated that silica-water interaction strengthens hydrogen bonding between surface hydroxyls and water molecules. However, high computational cost and limit of system size are a significant drawback for DFT and other first principle based approaches.

Empirical force field methods enable us to study silica-water interfacial science and reaction mechanisms in a larger scale, because it can save significant amount of computational cost, when compared to quantum mechanics simulations.⁶⁰⁻⁶³ T. S. Mahadevan et al.⁶⁴ developed a dissociative water potential, and represented the silanol formation on water-silica interface. G. K. Lockwood and S. H. Garofalini⁶⁵ group's recent study using dissociative potential for water molecules on the silicon oxide showed active proton transfer among water molecules and silica surface with H₃O⁺ formation. J. Fogarty et al.¹ proposed silica/water interaction properties using the ReaxFF reactive potential molecular dynamics.

Following Garofalini and Fogarty's observations, in this research, MD simulation using the ReaxFF potential for water-amorphous silica system was performed, which represented the effect of strain energy on hydroxylation. Specially, strained silicon and

oxygen atoms on the surface were closely analyzed, as well as undercoordinated atoms and non-bonding-oxygen. We studied a SiO₂ based nanotube structure to check the force field in small, highly strained geometry, and how water molecule interacts with and reacts to the strained site of this geometry. Thereafter, we investigated the surface chemistry of large amorphous silica structures.

In this work, first, the relationship between water and silica surface has been studied, especially for defects and strained sites on the surface. Second, reaction kinetics and Si-OH formation on the interface is observed. Lastly, effect of neighboring water molecule and hydrogen bond network on hydroxylation is explained. This research enables a better understanding on the interfacial science related to hydrolysis reactions and provides a bridgehead for further tribological and chemical research.

1.3 Silicon-Fluorine reaction and etching

The history of plasma etching technique for Si based wafer and circuits is nearly 40 years old. Etching is an essential technology in the modern society. Without etching, there would be no smartphones, laptops, or any other small electronic devices. Since the etching technique allows us to fabricate highly integrated circuits with complex, narrow patterns, all small smart devices around us are owed to the development of etching technology.^{66,67}

Silicon and Si based materials has been amongst the most widely used semiconductors, because of excellent physical and chemical properties. Specially, SiC shows outstanding electronic properties, such as large bandgap, high thermal conductivity, high saturation velocity,

⁶⁸ as well as good mechanical properties, like hardness comparable with diamond or Al_2O_3 , high Young's modulus and wear resistance. ⁶⁹

Fluorine containing plasma, such as fluorocarbon plasma, has been employed as the main working gas in Si related material etching technology, thanks to its chemical inertness in acid in wide temperature range. ^{70,71,72,73}

However, most of previous studies were mainly targeted for macroscopic etching properties, such as the effect of pressure and temperature, and plasma reactor technology, while only few studies have been focused on chemistry on the surface, and exact mechanisms of interactions on the surfaces. ^{74,75,76} To fully understand the precise detail of fast and radical interfacial chemistry of etching, research of molecular / atomic scale is essential.

Computational approaches can be an excellent way to investigate atomic / molecular scale investigation of surface chemistry of etching. Many quantum level researches revealed important energy relations and energy barriers regarding Si and F interactions. Garrison and Goddard calculated dissociation energies of SiF_n ($n=1-5$) using generalized valence bond dissociation consistent configuration interaction wave function. ^{77,78} King et al. used BHLYP functional predicted electron affinities of $\text{SiF}_1 \sim \text{SiF}_5$ ⁷⁹, with good agreement with experimental dissociation energies. ⁸⁰ Hiraoka et al. progressed structure / stability study of SiF_n s and CO, OH, and H relations in B3LYP level quantum simulation, and experimental approach. ⁸¹

Molecular dynamics simulations provides an attractive method for researching reactive surface chemistry for Si-F interaction, since it simulate larger systems with more atoms, with relatively cheaper computational cost. Darcy et al. used Stillinger-Weber potential to study reaction energy and heat of formation of SiF_n ($n=1-4$), Si_2F_6 and Si_3F_8 . ⁸² Abrams and Graves developed Tersoff type empirical potential for Si-C-F system. ⁸³ Gou et al. used Tersoff-Brenner REBO potential to calculate various Si - F interactions, such as Si - CF gas reaction energy

research and F_2 - SiC etching simulation.^{84,76,85,86} E. Carter and her coworkers studied Si-F reaction energy and relations for etching chemistry using first-principle ab initio method simulations.^{87,88,89}

Here, we developed ReaxFF force field to research the interactions between Silicon and Fluorine. ReaxFF can conduct massive scale simulation with large amount of atoms, with relatively lower computational cost, but still, have decent accuracy comparable with DFT level simulations, as well as good at transition state prediction.^{90,91} Thanks to these strong points, ReaxFF already showed its full ability to simulate large scale etching of TiO_2 with Chloride gas, and provided excellent force field for TiO_2 system.^{91,92}

Based on pre-developed water-Si / Na force field,¹ our purpose is, first, to establish a ReaxFF force field parameters to for the reaction of solid Si / SiO_2 with F_2 / HF gas system, second, to simulate large scale etching simulation of Si-F system. In addition, proper Si/F parameters will be greatly helpful to future researches, such as molecular dynamics study on tribochemistry. Since the most of the anti-wear coating materials for Al or Si surface contain Fluorine, ability to accurately simulate the interaction between Si and F would be essential to calculate mechano-chemical reactions during lubrication.

Chapter 2

The ReaxFF Reactive Force Field method

2.1. About the ReaxFF method

The ReaxFF Reactive force field has been developed by van Duin and co-workers, to simulate large system ($> 10^6$ atoms) with relatively cheaper computational cost, but with the comparable accuracy of quantum based simulation results.³⁷ As shown in figure 1, in this way, ReaxFF can perform MD simulation using empirical method's strong point, and quantum based calculation's advantage.

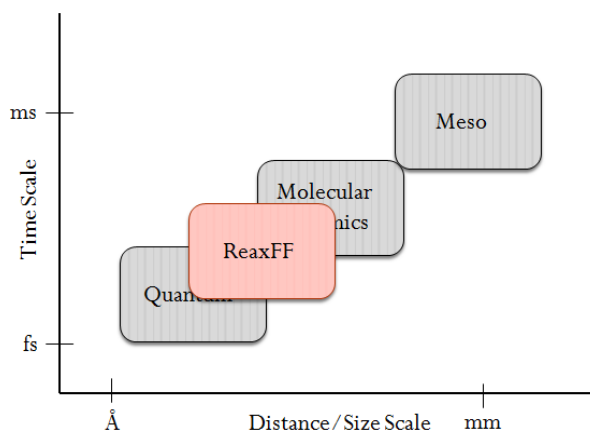


Figure 2-1. Comparisons of ReaxFF method with other way of simulation method

The way of calculation in the ReaxFF is based on bond-order dependent concept, so that it allows to predict highly accurate transition state modeling, when bonds are forming or breaking away.³⁷ Second, in order to calculate the contributions of these energies, all bond orders are calculated and modified at every iteration, thus allowing ReaxFF to form a precise relationship

between the bond distance and the bond order.^{93,94,95} Third, as a multi-body potential, ReaxFF calculates the long-range interactions among all atom pairs. Lastly, ReaxFF uses an electronegativity equalization model to calculate charges and polarization effects.^{96,97} Initially, a ReaxFF potential was developed to simulate hydrocarbon based system,³⁷ later, the method was developed further for organics, metals, and water related systems.^{90,98,1}

2.2. Brief introduction of ReaxFF

ReaxFF calculates the energy of system for several particular section, and sum up as shown in equation 2.1

$$E_{\text{system}} = E_{\text{bond}} + E_{\text{under}} + E_{\text{over}} + E_{\text{val}} + E_{\text{tor}} + E_{\text{lp}} + E_{\text{vdw}} + E_{\text{coul}} \quad (2.1)$$

More explanations are available in van Duin et al.⁷⁸ and Chenoweth et al.⁸⁴

2.2.1. Bond order and bond energy

ReaxFF calculates the bond energy from bond order relationship, and bond orders are calculated from equations using bond length. In addition, ReaxFF consider sigma / pi / double pi bond when calculates bond order / bond energy. Bond orders are gathered from following equation 2.2

$$BO'_{ij} = BO_{ij}^{\sigma} + BO_{ij}^{\pi} + BO_{ij}^{\pi\pi}, \text{ where}$$

$$BO_{ij}^{\sigma} = \exp[p_{\text{bo}1} \left(\frac{r_{ij}}{r_0^{\sigma}}\right)^{p_{\text{be}2}}], \quad BO_{ij}^{\pi} = \exp[p_{\text{bo}3} \left(\frac{r_{ij}}{r_0^{\pi}}\right)^{p_{\text{be}4}}], \quad BO_{ij}^{\pi\pi} = \exp[p_{\text{bo}5} \left(\frac{r_{ij}}{r_0^{\pi\pi}}\right)^{p_{\text{be}6}}] \quad (2.2)$$

The exponential terms for each sigma, pi, and double pi bond orders are the empirical function of uncorrected bond order for each bond types, respectively. $P_{\text{bo}i}$, $i=1$ to 6 are the

parameters for the bond orders, which are optimized using experimental and QM data during force field training process. Using this uncorrected bond order BO_{ij} , with the over/under-coordination penalty calculated from each atom,³⁷ corrected bond order BO_{ij} is calculated. and then the bond energy us calculated as shown in equation 2.3

$$E_{\text{bond}} = -D_e^\sigma BO_{ij}^\sigma \exp[\text{pbe1}(1-(BO_{ij}^\sigma)^{\text{pbe2}}) - D_e^\pi BO_{ij}^\pi - D_e^{\pi\pi} BO_{ij}^{\pi\pi}] \quad (2.3)$$

Again, pbe1, pbe2, D_e^σ , D_e^π , and $D_e^{\pi\pi}$ are bond dissociation section parameter in the force field file, which are optimized during training process using DFT and experimental data.

2.2.2. Valence angle energy

Equation 2.4 is used to calculate valence angle energy for the atomic system of atom i,j, and k, where k is the atom of the center.

$$E_{\text{val}} = f_7(BO_{ij})f_7(BO_{jk})f_8(\Delta_j)p_{\text{val1}}[1 - \exp \{-p_{\text{val2}}(\Theta_0 - \Theta_{ijk})^2\}] \quad (2.4)$$

As one can check from this equation, the valence angle also contains bond order terms in the equation, as well as angle of three atoms are considered. Function 7 (f_7) and function 8 (f_8) are the bond order/valency correlation functions,³⁷ while Δ_j is included for the over / under-coordination effect of central atom j to angle energy, and p_{val1} and p_{val2} are the parameters to be trained with QM or experimental data.

2.2.3. Torsion angle energy

Similar with valence angle energy equation, the torsion angle energy equation for 4 atoms of i,j,k, and l, is also a function of bond order, as shown in equation 2.5.

$$E_{\text{tor}} = f_{10}(\text{BO}_{ij}, \text{BO}_{jk}, \text{BO}_{kl}) \sin \Theta_{ijk} \sin \Theta_{jkl} \left[\frac{1}{2} V_1 (1 + \cos \omega_{ijkl}) + \frac{1}{2} V_2 \exp\{p_{\text{tol1}} (\text{BO}_{jk}^{\pi} - 1 + f_{11}(\Delta_j, \Delta_k))^2\} (1 - \cos 2 \omega_{ijkl}) + \frac{1}{2} V_3 (1 + \cos 3 \omega_{ijkl}) \right] \quad (2.5)$$

Function 10 (f_{10}) and function 11 (f_{11}) can be found at the previous reference,³⁷ and the p_{tol1} is the parameter to be optimized during training process for dihedral energy.

2.2.4. Lone pair energy

Equation 2.6 refers to the lone pair penalty energy. Lone pair means the valence electron pair which is not shared with other atoms, In ReaxFF, number of lone pair is the difference between the sum of bond orders of specific atom, and the number of outer shell electrons for that atom.

$$E_{\text{lp}} = \frac{p_{\text{lp2}} \Delta_i^{\text{lp}}}{1 + \exp(-75 \Delta_i^{\text{lp}})} \quad (2.6)$$

Where the p_{lp2} is the parameters to be trained, and the Δ_i^{lp} equals to the sum of lone pairs.

2.2.5. Van der Waals energy

In ReaxFF, a distance-corrected Morse is applied to take into account the van der Waals force effect, as shown in equation 2.7

$$E_{\text{vdw}} = \text{Tap} D_{ij} \left[\exp \left\{ \alpha_{ij} \left(1 - \frac{f_{13}(r_{ij})}{r_{\text{vdw}}} \right) \right\} - 2 \exp \left\{ \frac{1}{2} \alpha_{ij} \left(1 - \frac{f_{13}(r_{ij})}{r_{\text{vdw}}} \right) \right\} \right] \quad (2.7)$$

Tap in this equations is called a taper term, preventing discontinuous energy result when the charged species passes through the non-bonding cutoff radius. Function 13 (f_{13}) can be found from van Duin et al.'s ref³⁷, and r_{vdw} and D_{ij} can be optimized during training.

2.2.6. Coloumb energy

A shielded Coulomb potential is applied to consider orbital overlap among atoms, as shown in equation 2.8

$$E_{\text{coul}} = T_{\text{ap}} C \frac{q_i q_j}{(r_{ij}^3 + r_{ij}^{-3})^{-3}} \quad (2.8)$$

In ReaxFF, Geometry dependent Electron Equilibrium Method (EEM) is applied to calculate the charge for each atoms, which considers the polarization effects.^{96,97}

Chapter 3

Silica force field improvement and application to strain related hydrolysis reactions

3.1 Introduction

Previous computational approaches with reactive potential predicted the energy relation for hydroxylation, and role of hydronium.^{64,65} In this study using ReaxFF potential, first, we reparametrized the Si-O-water interaction parameters, in order to accurately simulate the energy barrier of hydroxylation to silicon. Second, with the advanced force field, ReaxFF MD simulation was calculated to reveal the relationship between atomic strain energy and hydroxylation, with smaller silica nano wire, and with amorphous SiO₂ slab. In addition, after series of hydroxylation MD simulation under various temperature condition, and importance of 2~3 paired water dimer / polymers connection was observed.

To discuss details, section 1 explains the validation and optimization of force field (Figure 2 and 3) using two Si dimer geometries (Figure 1). Section 2 introduce the silica nano wire (Figure 4), and observation of hydroxylation on silica nano wire which prefers the strained edge sites (Figure 5). In section 3, representative examples for three distinctive reaction pathways around strained sites are shown: (i) hydroxylation involving formation of H₃O⁺ (Figure 6), (ii) hydroxylation involving dissociation of H₃O⁺ (Figure 7), and (iii) hydroxylation involving dissociation of adsorbed water molecule (Figure 8). Section 4 discusses the analysis of number of hydroxylation (Figure 9), RDF of water – Si (Figure 10), and analysis of water clusters (Table1, Table2, and Figure 11), revealed the effect of water cluster on hydrolysis reaction and hydronium

formation. Lastly, section 5 describes the effect of locally strained structures on amorphous SiO_2 slab on hydroxylation, showing silanol formation favored the surface atoms with high strain energy. (Figure 12, 13, and 14) Reaction pathways for the hydroxylation on slab surface are also shown. (Figure 15 and 16). All visualizations were performed by Molden, Atomeye, and Ovito.⁹⁹

3.2. Relationship between hydroxylation of SiO_2 surface and local atomic strain energy

3.2.1. Validation of the force field for strained Si-O bond hydrolysis

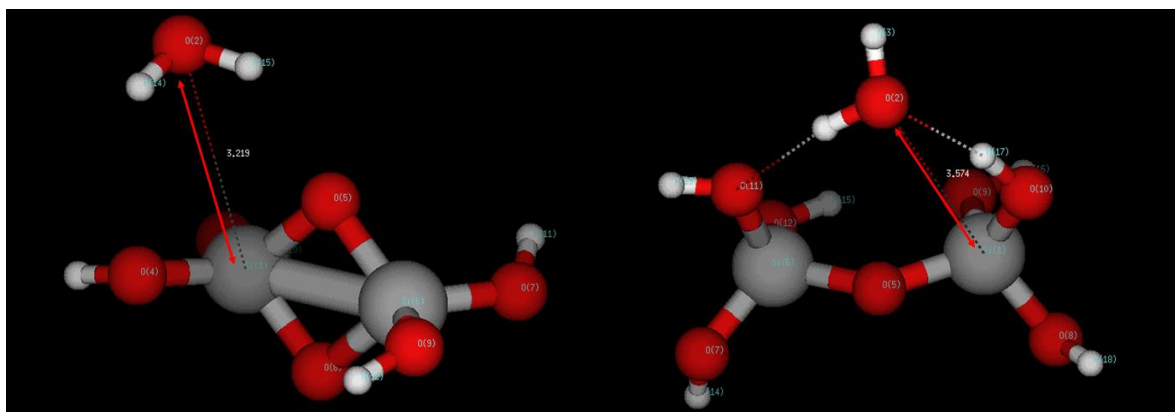


Figure 3-1. Picture of strained Si dimer (left) and non-strained silica dimer (right)

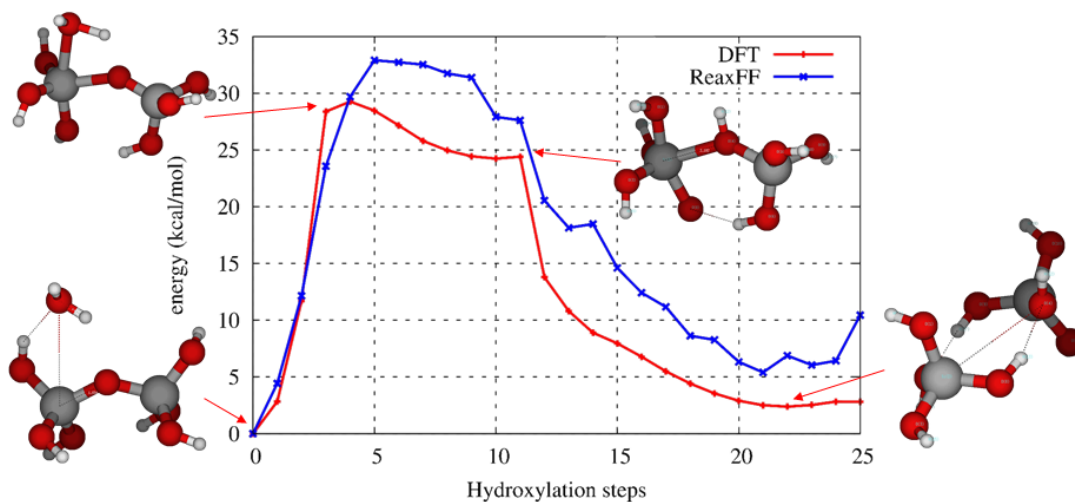


Figure 3-2(a). Energy barrier for hydroxylation on non-strained Si dimer structure with the Fogarty force field.

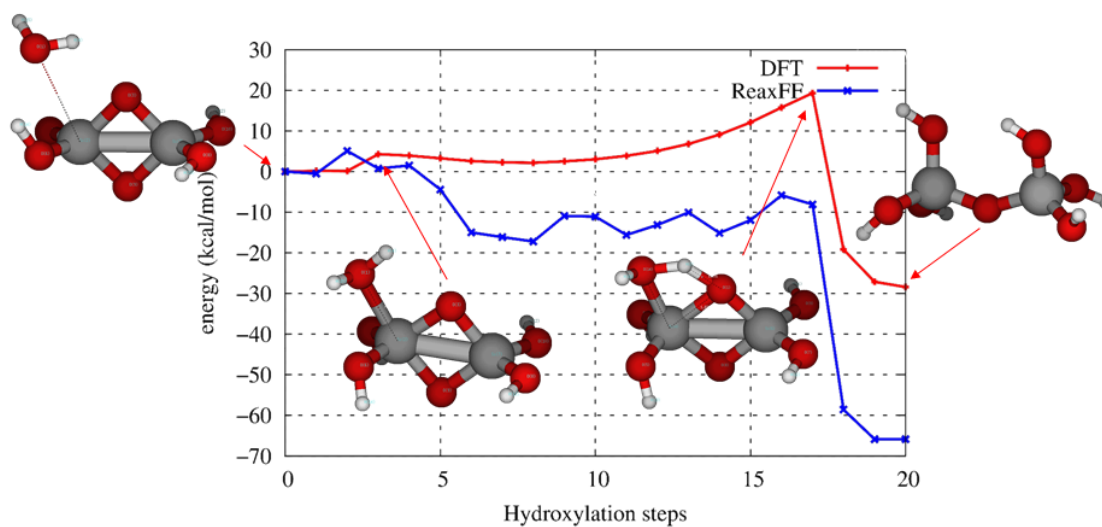


Figure 3-2(b). Energy barrier for hydroxylation on strained Si dimer structure with the Fogarty force field. ¹

Using DFT and ReaxFF, energy scan for the transition state was performed in order to

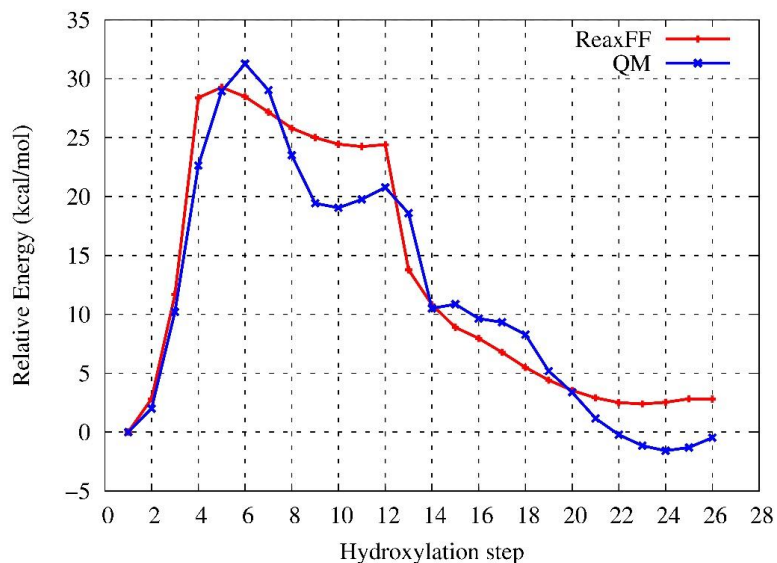


Figure 3-3(a). Energy barrier for hydroxylation of the non-strained silica dimer structure for the SiO-2015 force field.

examine and compare how the reaction energy barrier for silanol formation varies with strained geometric conditions. As shown in figure 3-1, we prepared two geometries of a silica dimer: One has the 4-membered Si-O-Si-O ring structure with a high strained energy, and the other has only one bridge oxygen with relatively low strain energy. All DFT calculations were carried out using B3LYP functional with the 6-311G++G(d,p) basis set, and ReaxFF potential developed by J. Fogarty et al. 1 was applied to check the ReaxFF hydroxylation energy barrier.

As a result, energy barriers calculated by previous Si-O-water interaction parameters 1 were shown to be slightly insufficient when compared to DFT result. Figure 3-2(a) and 3-2(b) present the energy curves as a water molecule approaches one of Si atoms of the strained and non-strained silica dimer structure, respectively. Both hydroxylation reactions are initiated by adsorption of water molecule to a Si atom of dimer, and proton donation occurs to the bridge oxygen. Then, one of the Si-O bonds breaks, forming a system with 2 silanol groups. As we can see in figure 3-2(a), the energy curve for a non-strained silica dimer correctly followed the energy

curve from DFT. On the other hand, for strained Si-O ring structure, the energy barrier in figure 3-2(b) for hydroxylation was underestimated when compared to that of DFT, indicating easier hydroxylation for strained structure, for the force field for Si-O-water interaction from J. Fogarty et al. ¹

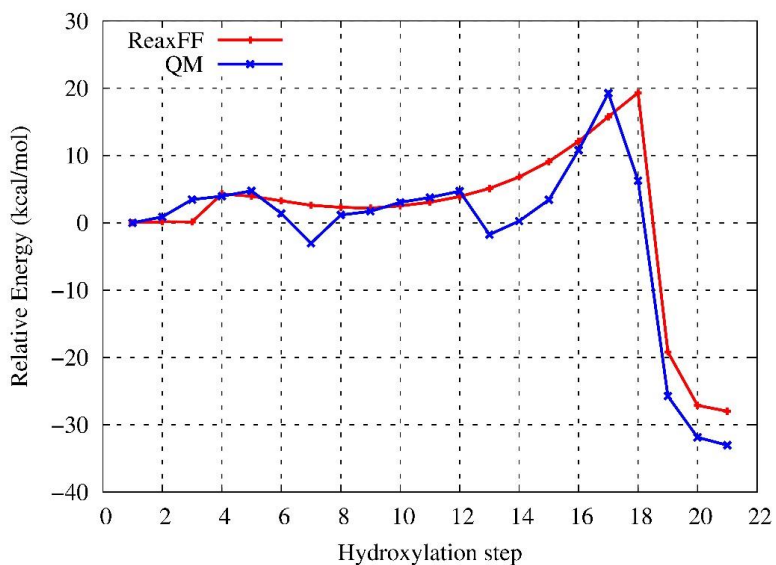


Figure 3-3(b). Energy barrier for hydroxylation of the strained silica dimer structure for the SiO-2015 force field.

In order to improve the ReaxFF performance for the strained silica dimer, we added the two DFT energy curves for hydroxylation on the strained silica dimer, and non-strained silica dimer to the Fogarty et al. training set ¹, and re-parameterized the force field, generating the SiO-2015 parameter set. The energy curve result for two hydroxylation reaction after force field optimization is shown in figure 3-3(a) and figure 3-3(b). After parametrization, hydroxylation energy barrier of new force field is about 31 kcal/mol for non-strained Si dimers, and 20 kcal/mol for strained Si dimer. Optimized parameters are Si-O bond and off diagonal, Si-O-Si / O-Si-O / O-Si-Si angle, and H-O-H hydrogen bond parameters. In addition, as a future plan, force field

training for hydroxylation energy barrier with 2 or more water molecules, and Na-SiO₂ system is planned.

3.2.2. Application to Silica Nanowire

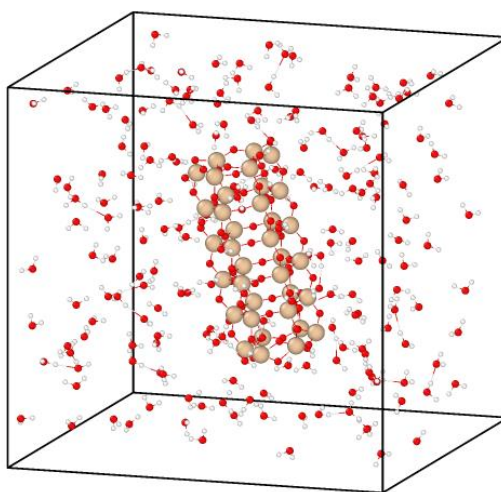


Figure 3-4(a). Silica nano rod in the 200 water molecules in the 30x30x30 Å³ periodic box. Water density was 0.222 kg/dm³.

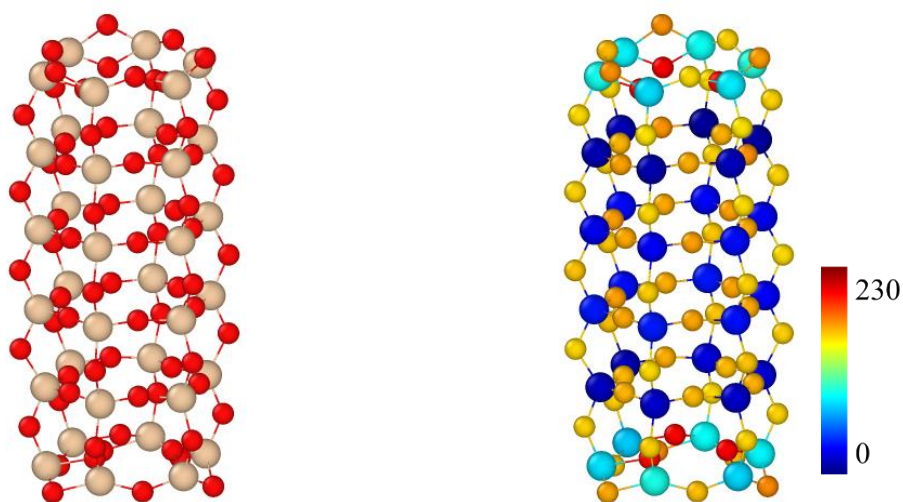


Figure 3-4(b). Silica nano wire. Grey atoms are Si atoms, and Red atoms are Oxygens.

Figure 3-4(c). Relative strain energy (kcal/mol) view of silica nanowire. Red atoms represent higher strained atoms, blue atoms mean lower strain energy ones.

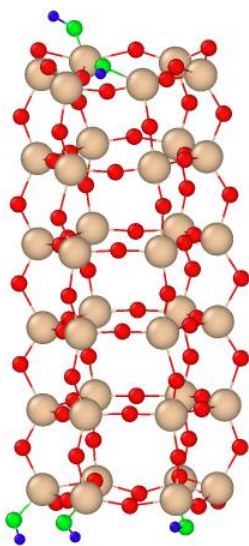


Figure 3-5(a). Silica nanowire after 650ps exposure at 400K temperature. 5 silanols are formed at the edge area. Green and blue atoms represents the O and H of the silanol.

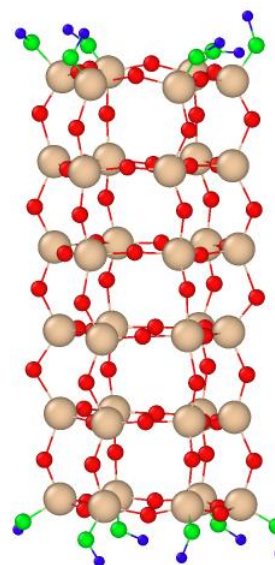


Figure 3-5(b). Silica nanowire, 500ps exposure at 700K temperature. All strained Si atoms at the edge sites are occupied by silanols.

As a test of the SiO-2015 force field, calculation of SiO₂ nanowire and 200 water molecules were simulated to check the relationship between strain energy and formation of silanol in a smaller and simpler system. The silica nanowire structure of this research has also been used in previous studies.^{100,101} System configuration is shown in figure 3-4(a). Figure 3-4(b) is the picture of silica nano wire, and figure 3-4(c) presents the strain energy of each atom in silica nano wire.

The silica nano wire in our study, which was used in previous research to find the dependence of silica – water reaction¹⁰¹, has distinctively strained region at the edge of structure. As seen in figure 3-4(b) and 3-4(c), the silica nanowire, which is non-periodic and hollow, consists of 36 silicon and 72 oxygen atoms. This nanowire's top and bottom surfaces are opened to vacuum, thus creating a highly strained, Si-O-Si-O 4 membered ring structure at the edge. This type of four-membered ring structure is rare in real silica slab, but we used this model as a

representation highly strained geometry. of Figure 3-4(c) clearly shows the strained Si and O atoms at the edge area, represented by different colors with a relatively higher strain energy, while the atoms in the body are less strained. There are total 12 of Si atoms at the edge of the silica nano wire, which contains higher relative strain energy than other Si atoms do. Average relative strain energy of Si atoms in non-strained structure was 15.97 kcal/mol, while that of Si atoms in strained structure was 78.09 kcal/mol. The orthogonal periodic box has a volume of 3 were performed by applying the Berendsen thermostat to all atoms in the system, with 100fs of temperature damping constant, and 0.1fs of timestep. System temperature was set from 300K to 1500K, and simulations were performed at every 100K. The reason behind the choice of wide temperature range was, first, to check the behavior of water clusters as environment approaches the supercritical state of water vapor, and second, to reveal how the hydroxylation is influenced by high temperature. 1500K is high temperature, but reaction research on hydroxylation with water under supercritical condition is also crucial to various industries, such as power plant and reactor design, and processing of hazardous material.¹⁰²⁻¹⁰⁴ The simulations were performed at 100K temperature intervals, to distinguish the effect of different temperatures.

Initial observation of MD simulation showed that the hydroxyl formation was initiated from the edge area. Figure 3-5(a) and 3-5(b) show the pictures of silica nano wire and Silanols formed at the edge of the Silica nano wire, in the 400K at 650ps and 700K at 500ps respectively. Clearly, hydroxyl formation occur preferably at the strained Si-O sites of silica nano wire, which implies that the approaching and adsorption of the water molecule also prefer the strained edge site of the silica nano wire.

3.2.3 Reaction path for hydroxylation on the edge area of silica nano wire

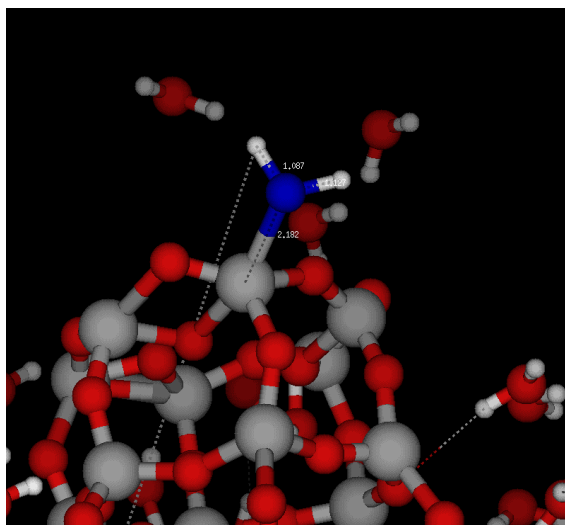


Figure 3-6(a). 76.21ps after MD simulation. Adsorbed water molecule at the edge Si of silica nano wire.

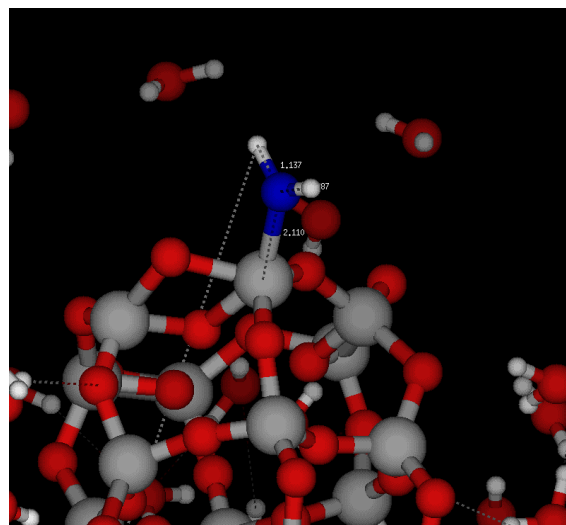


Figure 3-6(b). 76.26ps after MD simulation. One of the H atom of adsorbed water molecule is attracted to nearby secondary water molecule

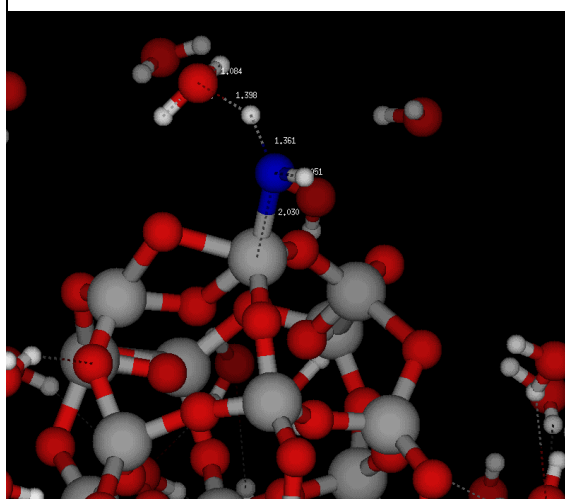


Figure 3-6(c). 76.265ps after MD simulation. Proton donation occurred.

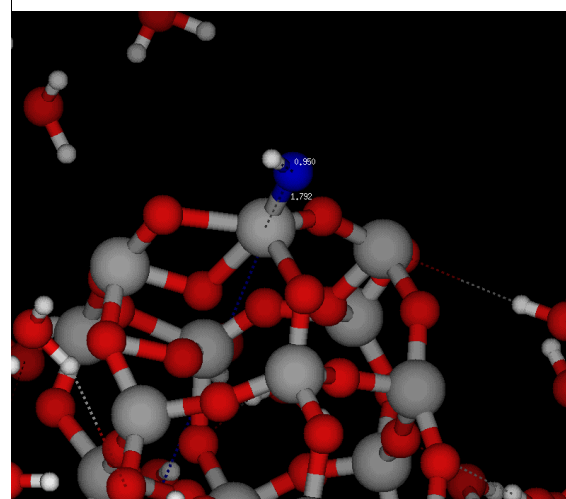


Figure 3-6(d). 76.32ps after MD simulation. Formation of hydroxyl. H_3O^+ ion moved across the periodic boundary.

Figure 3-6. Snapshots of hydroxylation reaction, involving the formation of hydronium ion at 400K. Grey atoms are Si, red atoms are O, white atoms are H, and blue atoms are O of hydroxyl.

As G. K. Lockwood et al.⁶⁵ observed in a previous study using a dissociative potential, the hydronium ion plays an important role in the silanol formation reactions. Figure 3-6 describes

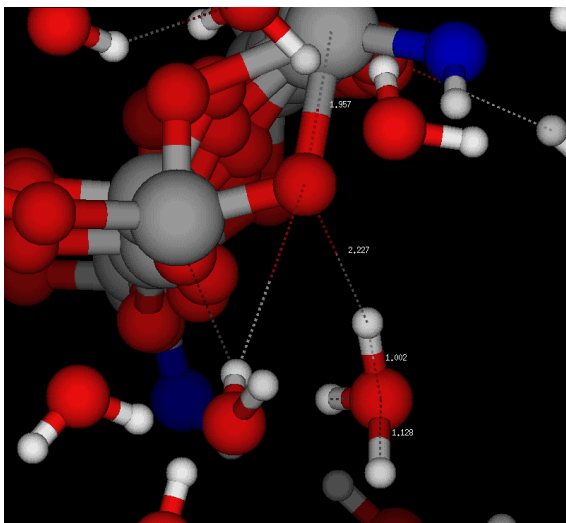


Figure 3-7(a). 195.3ps after MD simulation. H_3O^+ approaches to bridge O.

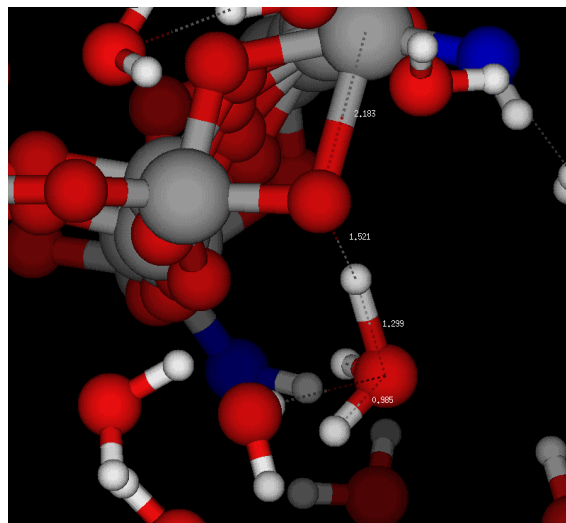


Figure 3-7(b). 195.37ps after MD simulation. One of the H of H_3O^+ is attracted to the bridge O of strained structure.

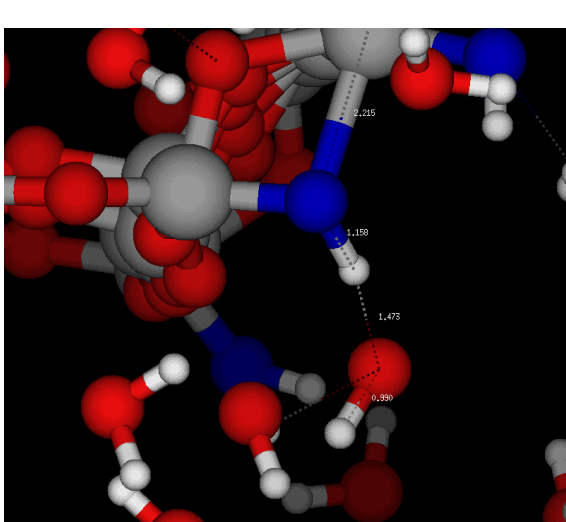


Figure 3-7(c). 195.375ps after MD simulation. Proton donation.

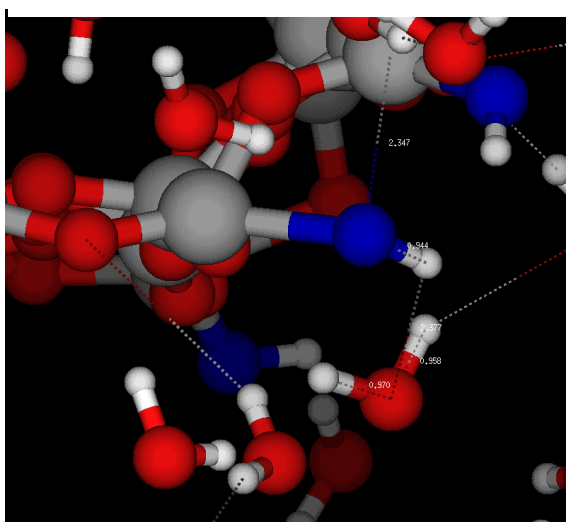


Figure 3-7(d). 195.45ps after MD simulation. Si-O bond breaks, and SiOH formed.

Figure 3-7. Snapshots of hydroxylation reaction, involving the dissociation of hydronium ion at 900K. All color settings of atoms are the same as figure 3-6

the process of hydroxylation at 400K, which includes the formation of a H_3O^+ ion. At 76.21ps (Figure 3-6a), a water molecule adsorbed to the Si atom of the edge of silica nano wire. At

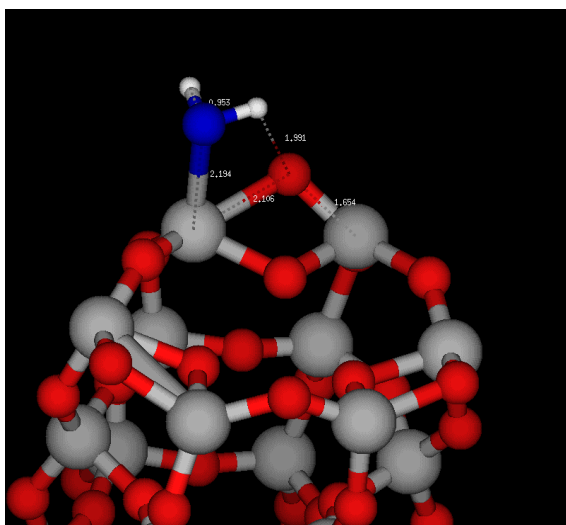


Figure 3-8(a). 121.76ps after MD simulation. Adsorption of water to Si.

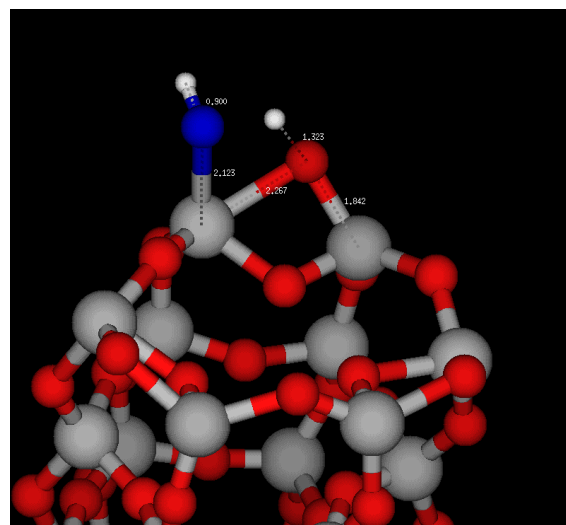


Figure 3-8(b). 121.815ps after MD simulation. One of the H of adsorbed H₂O is attracted to the bridge O of strained structure.

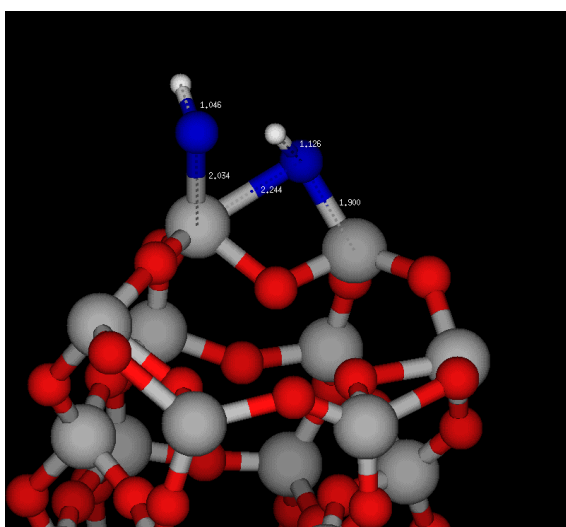


Figure 3-8(c). 121.82ps after MD simulation. Proton donation.

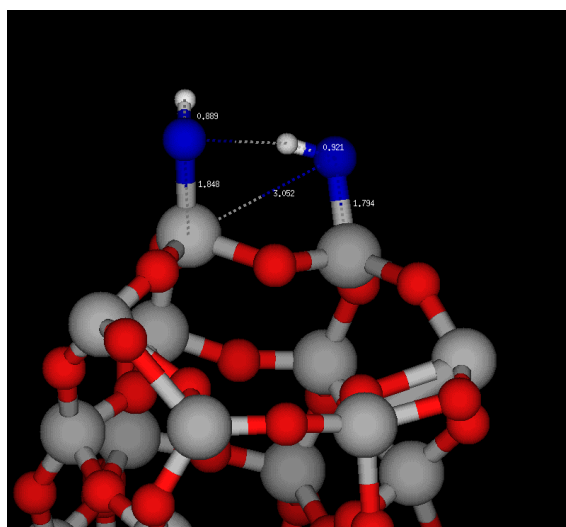


Figure 3-8(d). 121.87ps after MD simulation. Si-O bond breaks, and two silanols formed.

Figure 3-8. Snapshots of hydroxylation reaction, involving the dissociation of adsorbed water molecule at 1500K. All color settings of atoms are the same as figure 6. Water molecules, unrelated with reaction, are removed for clarity.

76.26ps (Figure 3-6b), a secondary water molecule closely approached the adsorbed water molecule. At 76.265ps (Figure 3-6c), proton donation was occurred. Finally, at 76.32ps (Figure 3-

6d), a H_3O^+ and a silanol were formed. The hydronium ion, generated in figure 3-6d, moved away from the hydroxyl group, forming a hydrogen bond network with other nearby water molecules and hydroxyls. This process creates unstable 5-coordinated Si, which easily forms new hydroxyl with nearby water molecules or hydronium ions, showing similar results with previous study by J. Kubicki et al.¹⁰⁵

In addition, dissociation of hydronium ion was also a major route for silanol formation. Figure 3-7(a)-(d) show an example of H_3O^+ deprotonation path at 900K condition. At 195.3ps (Figure 3-7a), a H_3O^+ approaches Si-O-Si-O ring structure at the edge of the silica nano wire. At $t=195.37\text{ps}$ (Figure 3-7b), one of the H^+ ions of hydronium interacts with bridge oxygen of silica nano wire, which has a relatively high strain energy. At 195.375ps (Figure 3-7c), H_3O^+ deprotonates one of H^+ to the O and become H_2O . Lastly, at 195.45ps (Figure 3-7d), one of the Si-O bonds is elongated, forming a hydroxyl and H_2O molecule as a product.

Not only hydronium ions, but also water molecules can induced the hydroxylation reaction, especially at higher temperature, (typically $T > 1000\text{K}$). Figure 3-8(a)-(d) present an example of the formation of silanol due to the direct dissociation of an adsorbed water molecule, which tends to be observed at higher temperatures in our simulations. At 121.76ps (Figure 3-8a), a water molecule was adsorbed on the Si atom at the edge area of silica nano wire. At 121.815ps (Figure 3-8b), one of the H atoms at the adsorbed water approaches the bridge oxygen, stretching O-H distance to $1.1 \text{ \AA} \sim 1.2 \text{ \AA}$. At 121.82ps (Figure 3-8c), after H moves to the bridge oxygen, Si-O distance increases to more than 2 \AA . At 121.87ps after simulation (Figure 3-8d), 2 hydroxyls were formed as one of the Si-O bonds dissociated.

3.2.4. Analysis of hydroxyl formation with respect to different temperatures.

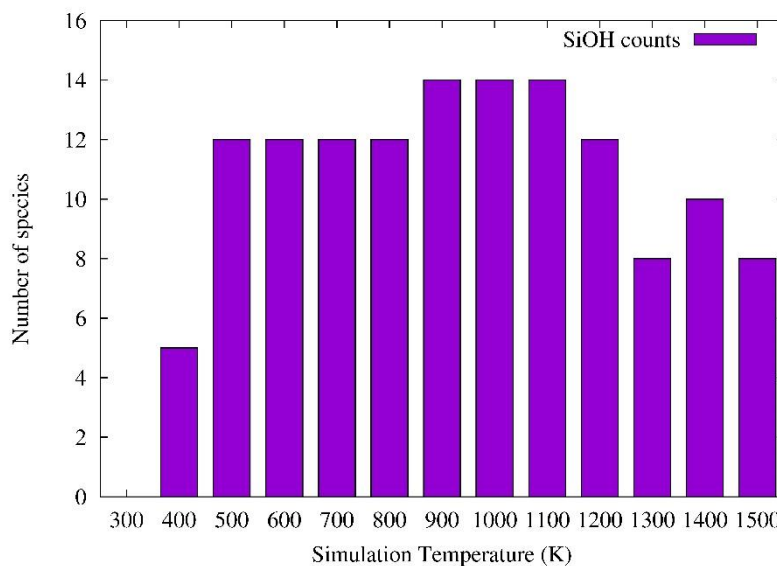


Figure 3-9. Maximum number of silanols during simulation for each temperature after 800ps MD simulation.

Our observations from the reaction pathways of hydroxylation imply that there is a relationship among temperature, water clusters, and the kinetics of hydroxyl formation. Accordingly, an analysis of the reaction path for hydroxylation was performed to reveal the connection among them. Figure 3-9 shows the maximum number of silanols during each simulation. According to the figure 3-9, the maximum number of silanols during the simulations is not proportional to the temperature. Instead, the number of silanols shows the maximum number of 14 at 900K, 1000K, and 1100K, and minimum number of 5 at 400K. In 300K simulation, no silanol formation is observed. Based on our observation of reaction kinetics from 900K to 1100K, 2 hydroxyls – 13th and 14th - are generated at the Si atom of body area of silica nano wire by proton donation from H_3O^+ , only after all 12 strained Si atoms at the edge of the silica nano wire are fully hydroxylated.

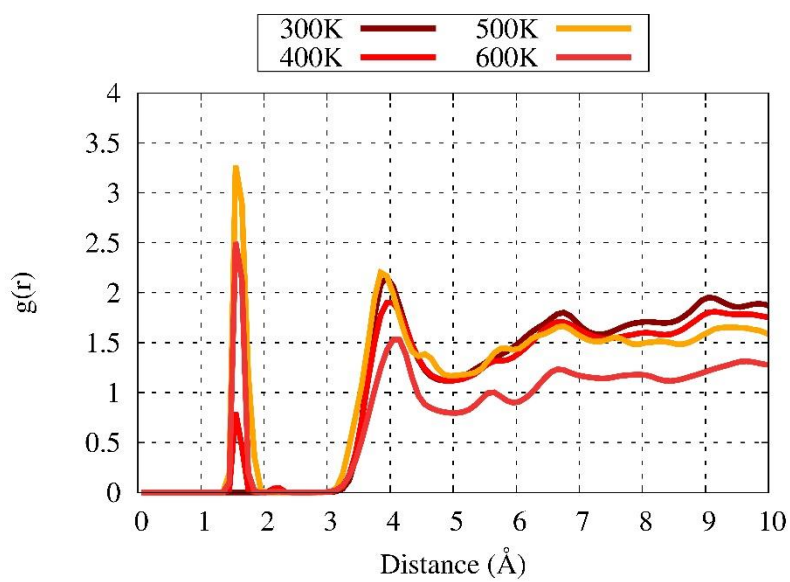


Figure 3-10(a). Si - O_{water} RDF at 300K, 400K, 500K, and 600K

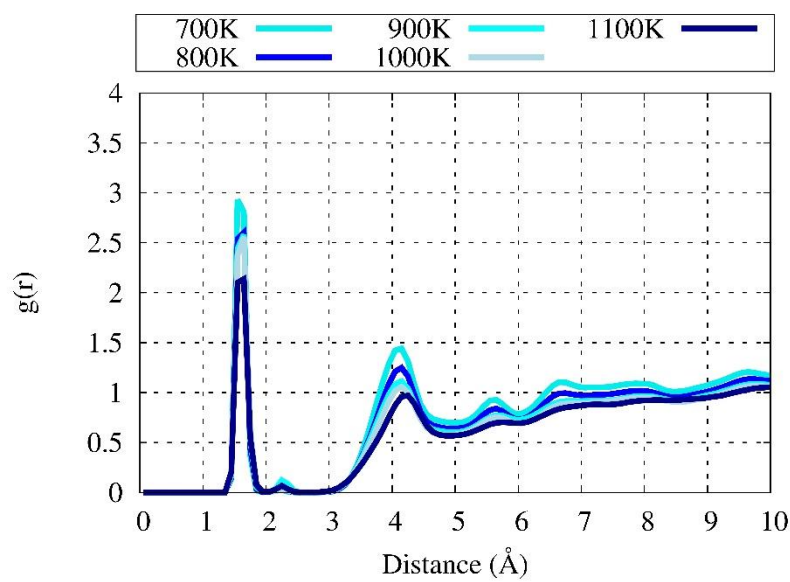


Figure 3-10(b). Si - O_{water} RDF from 700K to 1000K

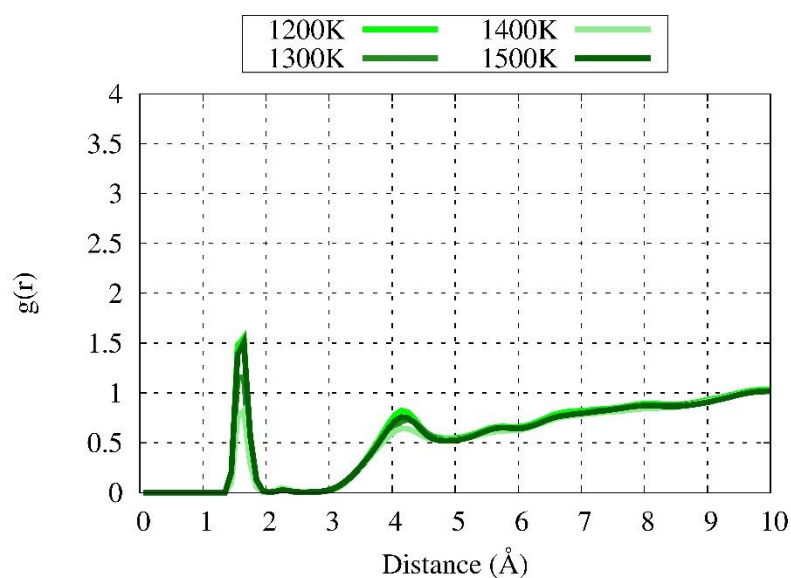


Figure 3-10(c). Si – O_{water} RDF from 1200K to 1500K

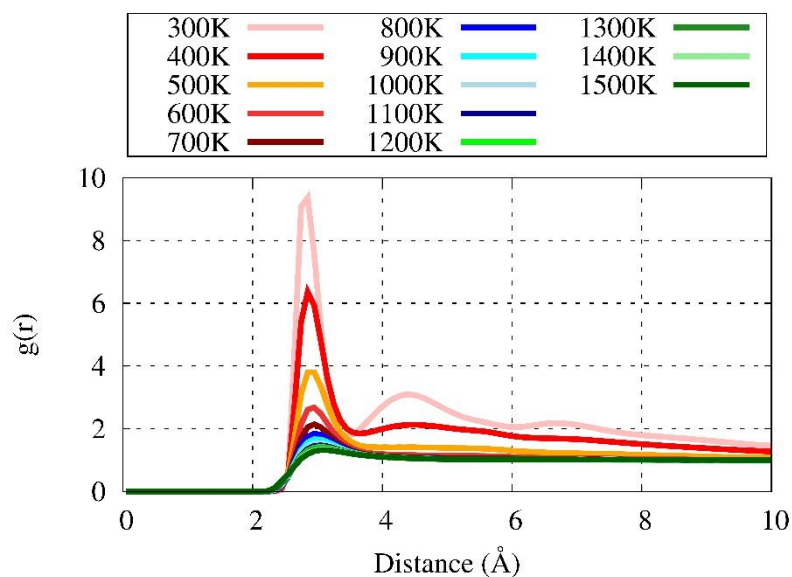


Figure 3-10(d). RDF among water molecules

To check how water molecules behave and interact with silica nano wire under various temperature conditions, the RDF between water and Si, and RDF among waters were calculated. Water-Si RDF was calculated from the RDF of O_{water}-Si_{nanowire}, which is shown in Figure 3-10(a), 3-10(b), and 3-10(c). Figure 3-10(d) shows the RDF among the water molecules.

Temperature	total	H3O+ formation reaction	Deprotonation from H3O+	H2O dissociation
300K	0	0	0	0
400K	5	3 (60%)	2 (40%)	0
500K	12	6 (50%)	6 (50%)	0
600K	12	6 (50%)	6 (50%)	0
700K	12	6 (50%)	6 (50%)	0
800K	12	6 (50%)	6 (50%)	0
900K*	14	7 (50%)	7 (50%)	0
1000K*	14	7 (50%)	7 (50%)	0
1100K*	14	7 (50%)	5 (36%)	2 (14%)
1200K	12	6 (50%)	4 (33%)	2 (17%)
1300K	8	3 (38%)	3 (38%)	2 (24%)
1400K	10	4 (40%)	4 (40%)	2 (20%)
1500K**	8	3 (38%)	2 (25%)	4 (37%)

Table 3-1. Different types of silanol formation reaction for different temperature.

* From 900K to 1100K, silanol formation in the body area of silica nano wire was observed, by proton donation from H3O+ ion.

** At 1500K, one of the silanol was restored to the H2O, by H3O+ + SiOH -> 2H2O reaction.

According to the first peak of $O_{\text{water}}\text{-Si}_{\text{nanowire}}$ RDF data, (positioned at $R_{\text{Si-O}}$ around 1.55\AA) at 300K and 400K (Figure 10a), water molecules hardly approach the Si atoms, resulting in no or a few water adsorption. Accordingly, the chance for the formation of silanols is lower than that in higher temperature condition. On the other hand, from 500K to 1100K (Figure 3-10a and 3-10b) a significant increase of the first peak of RDF is observed, which indicates a higher number of approaching of water molecules to the Si atoms. In addition, as temperature increases higher than 1200K (Figure 3-10c), the first peak of $O_{\text{water}}\text{-Si}_{\text{nanowire}}$ RDF decreases and overall curve is flattened. RDF among water molecules (RDF of $O_{\text{water}}\text{-O}_{\text{water}}$, Figure 3-10d) imply similar

trends with the RDF of $O_{\text{water}}-Si_{\text{nanowire}}$. 300K water RDF presents the highest first peak, and existence of second and third peak, which suggests the strong hydrogen bond network among the water molecules. From 500K to 1100K of temperature, hydrogen bond network is weakened, as well as all peaks of RDF curves. After 1200K, because of the high velocity of the water molecules, all hydrogen bond networks are broken, and the curves are greatly flattened. These RDF data also supports the existence of optimal temperature ranges for the silanol formation, which was suggested in figure 3-9.

Temperature	isolated water	2 water	3 water	>3 water cluster	Mass of >3 water cluster (AMU)
300K	17.8	3.4	-	9.7	3397.2
400K	54.8	12.5	5.2	17.8	2101.5
500K	95.7	17.4	5.8	17.0	1084.6
600K	124.9	18.4	4.6	13.6	593.6
700K	137.7	16.9	-	10.4	527.1
800K	146.2	15.7	2.8	6.0	270.0
900K	151.8	14.6	2.3	6.2	255.4
1000K	154.6	14.1	-	7.6	334.9
1100K	157.8	13.7	-	7.7	326.3
1200K	159.4	13.3	-	8.2	334.2
1300K	162.1	13.4	-	11.9	383.8
1400K	163.1	13.3	-	12.3	392.6
1500K	163.4	12.8	-	13.3	405.9

Table 3-2. Average number of independent water and weakly bonded water clusters. Larger cluster ranges from 4 water to 20 water molecules. The mass of larger cluster is an averaged value.

However, still, it is unclear how the reaction pathways of hydroxylation are related with temperature. To find this, we investigated how hydroxyls were formed with each temperature condition. Table 3-1 presents how silanols were formed during all simulations. Our observation indicated that all of reaction pathways generally followed the examples shown in figure 3-6, 3-7,

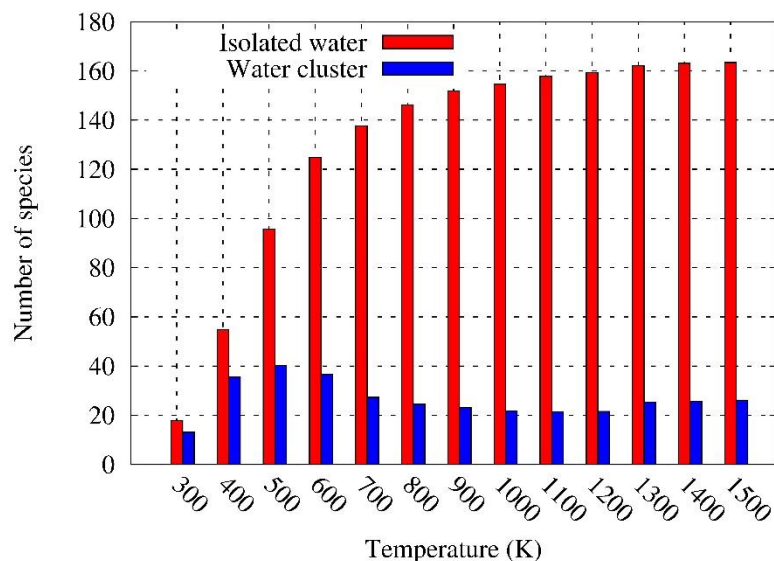


Figure 3-11. Average number of isolated water molecules and water clusters

and 3-8. According to this data, the dominant pathways for silanol formation are strongly affected by temperature. Among three methods of hydroxylation, the majority of them are originated from the reaction regarding the hydronium ion. Especially, from 300K to 1000K of temperature ranges, all of the silanols are closely related with the formation and dissociation of the H_3O^+ ion. On the other hand, silanol formation due to the direct dissociation of a water molecule is observed only from 1100K and higher temperature range. In addition, its ratio becomes the maximum at the 1500K, the highest temperature in our study. This unimolecular silanol formation path is due to strong vibration of O-H bond of adsorbed water molecules, facilitated by high temperature environment. Because of its rapid vibrational motion, once being adsorbed by silica nano wire, water molecules can donate their H atom to the bridge oxygen of silica nano wire more easily, compared to a lower temperature environment.

To answer why the hydrolysis reaction pathways differ with respect to temperature, we analyzed the cluster of water molecules: how many water molecules established hydrogen bond interactions.

Table 3-2 contains the average number of isolated water, water clusters that consisted of two or three water molecules, and the larger clusters with many water molecules interacting in hydrogen bond networks. Using the xyz trajectories of water molecules and silica nano wire from each 800ps simulations, we run the single point MD simulations with a low bond order cutoff value of 0.1. This enables us to distinguish the hydrogen bond networks among water molecules from other chemical connections. Figure 3-11 shows the number of isolated water molecules, and number of water clusters. A water clusters consist of at least two water molecules.

Observation from water cluster analysis (Table 3-2 and Figure 3-11) implies the existence of relationship between the hydroxylation mechanism, temperature, and water cluster. First, water loses its autocatalytic reaction at high temperature ($>1200\text{K}$), since the hydrogen bonding connections of water cluster are disrupted. Accordingly, the number of water dimers declined as temperature increases after 600K (Table 3-2), and the number of hydroxyls also declined (Figure 3-9). This influences the pathway for hydrolysis reaction, as the ratio of dissociation of adsorbed water increased from 1100K (Table 3-1). Based on our observations of reaction path, (Figure 3-6 and 3-7) hydrolysis reaction involving formation or dissociation of hydroxyl requires water dimers and neighboring waters to donate or to receive proton ions. In this case, the absence of water dimer structure induced the lack of hydroniums, which leads the increased number of hydroxylation by dissociation of water. This result is also presented in RDF data, showing the absence of second and third peak in water RDF curves at temperature greater than 1100K (Figure 10d), and lower first peak intensity at $\text{O}_{\text{water}}\text{-Si}_{\text{nanowire}}$ RDF (Figure 10c). This RDF results also indicate the decreased number of water dimer structure at corresponding temperature range.

Water dimer and large water cluster structures can survive and sustain their H-bond connections in the lower temperature range. According to the data from Table 3-2, at the temperature range from 500K to 1000K, the average number of water dimer structures was larger

than that at either lower or higher temperatures. This implies that water molecules in such temperature range established more sustainable hydrogen bond network, which offered stable supply of neighboring water molecules to donate or receive the proton. This results increased chance of hydrolysis reaction involving hydronium ions, as well as greater number of hydroxyls than that at extreme low- or high-temperature range ($T < 500\text{K}$ or $T > 1300\text{K}$ range) RDF curves for $\text{O}_{\text{water}}\text{-Si}_{\text{nanowire}}$ for temperature from 500K to 1000K (Figure 3-10a, and 3-10b) show a strong second peak around 4\AA , ($g(r) > 1$ at $R_{\text{Si-O}} \approx 4.1\text{\AA}$), which suggests strong hydrogen bond network and neighboring water molecules. Meanwhile, the second peak of $\text{O}_{\text{water}}\text{-Si}_{\text{nanowire}}$ for high temperature ($T > 1200\text{K}$) shows weaker intensity ($g(r) < 1$ at $R_{\text{Si-O}} \approx 4.2\text{\AA}$), which means the dissociation of hydrogen bond networks, and water cluster connections.

In addition, this observation may imply the possible existence of the optimum temperature range for the hydrolysis reaction, where the reactivity of water with silica structures is maximized at such temperature.

3.2.5. Hydroxyl formation on amorphous silica surface: ReaxFF MD simulation results.

To check how the silanol formation is influenced by atomic strain energy of local sites on the surface, we prepared an amorphous SiO_2 slab with MD simulation.

An amorphous SiO_2 slab was fabricated from the orthogonal, high-density quartz super-cell structure. The initial quartz crystal consists of 1722 atoms in a $29.478 \times 34.038 \times 50\text{\AA}^3$ periodic box, with an initial density of 2.174 kg/dm^3 . To develop an amorphous silica structure, we annealed the quartz slab from 1500K to 3500K, with 0.02 K/fs of temperature variation rate under NVT ensemble. After annealing, amorphous slab was in a $31.9 \times 31.9 \times 50\text{\AA}^3$ periodic box.

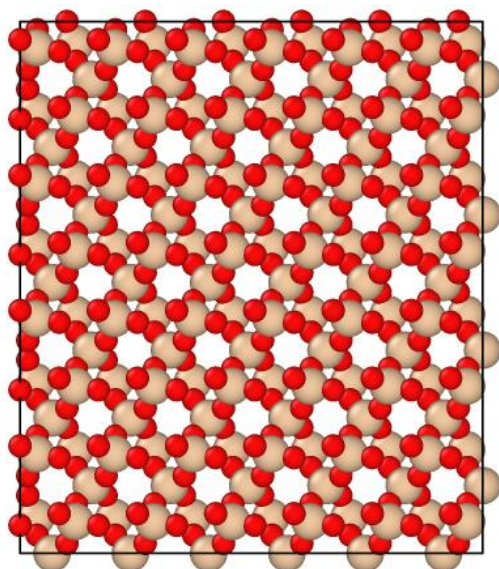


Figure 3-12(a). Quartz, before annealing

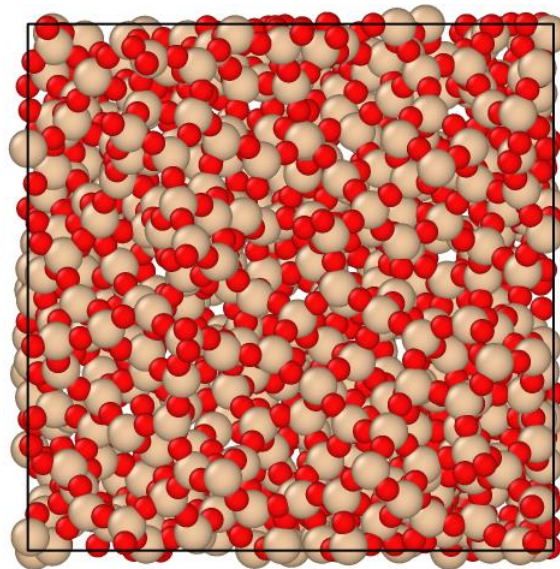


Figure 3-12(b). Amorphous silica, after annealing

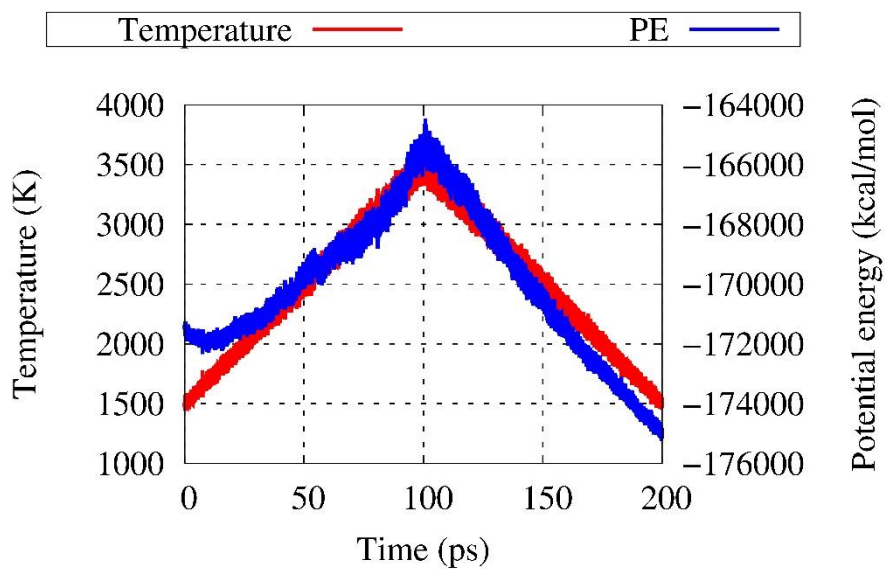


Figure 3-12(c). Graph of potential energy and temperature with respect to time during annealing of quartz. A 0.002 K / iteration temperature ramp was used in these simulations.

The system for annealing was vacuum slab, so that the z-dir surface of slabs were exposed to vacuum during annealing MD simulation. Figure 3-12(a) and 3-12(b) show the before

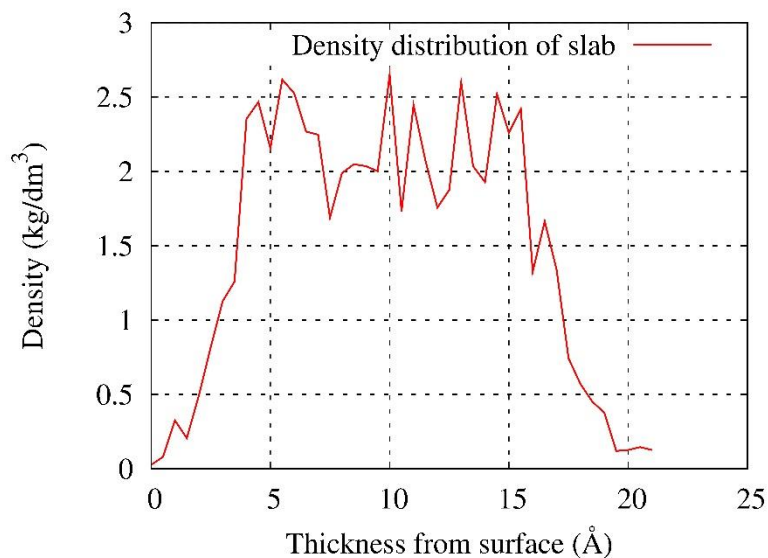


Figure 3-13(a). Density distribution of slab in depth direction per 1 Å

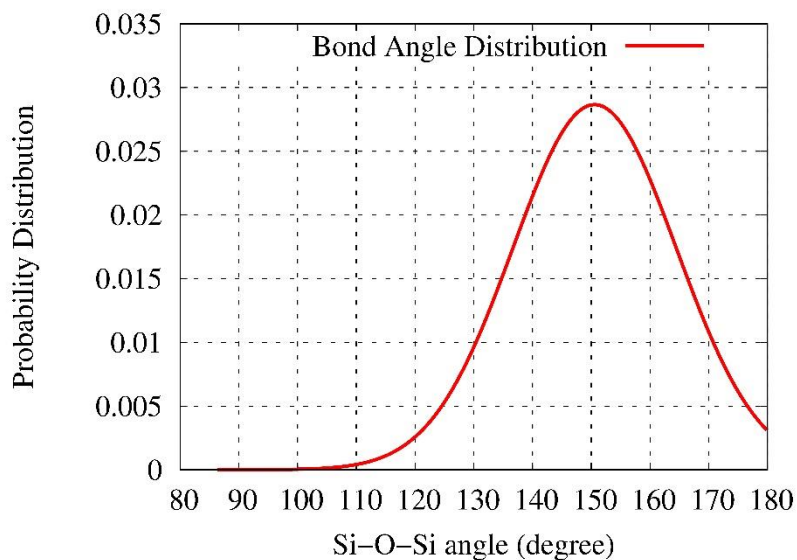


Figure 3-13(b). Si-O-Si bond angle distribution of amorphous SiO₂ slab.

and after of annealing of SiO₂ structure, and temperature and figure 3-12(c) is the graph of potential energy during the annealing progress.

The overall density of the annealed slab was 1.88 kg/dm³, but the density of bulk region

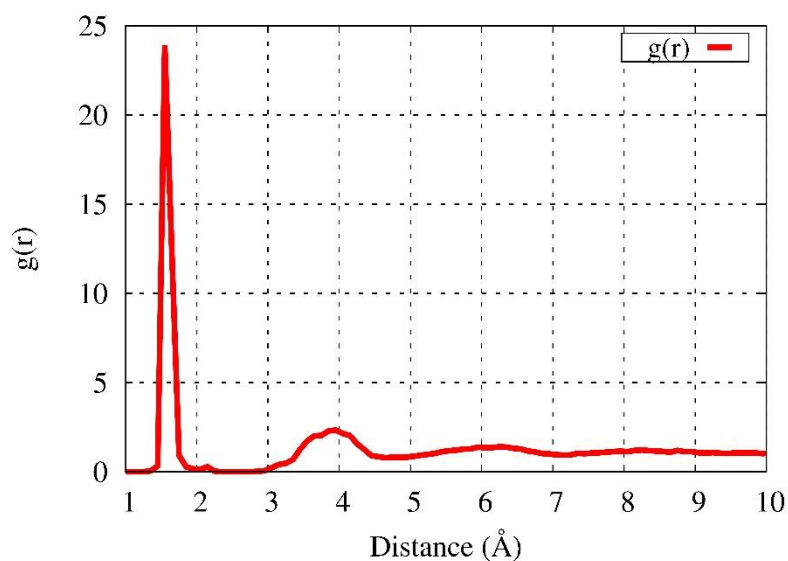


Figure 3-13(c). Si-O radial distribution of amorphous SiO₂ slab.

was around 2.1 kg/dm³, which is close to density of silica glass, 2.203 kg/dm³. The density profile (Figure 3-13(a)) shows the density distribution in subsurface direction. In addition, Si-O radial distribution function (figure 3-13(c)) and angle distribution of the slab (figure 3-13(b)) were analyzed, to check the credibility of annealed amorphous silica. All properties match well with the previous research data, as shown in Table 3-3 and Figure 3-13. Figure 3-14 shows various topological analytical results of the surface of the annealed structure. Surface atoms were collected from slab, by selecting the atoms with the highest z-coordinate, for every 1x1 Å² grid on the surface of the slab. Then, atomic strain energy was calculated for selected surface atoms. According to these results, the under-coordinated atoms have higher atomic strain energy than other atoms on the surface do. Atomic strain energy of ReaxFF is the chemical strain energy, which is closely related with the atomic potential energy. ReaxFF calculates all partial energies for all atoms for every iteration.

Properties	ReaxFF	QM & Expr
Bulk area density (g/cm ³)	2.1	2.2 ^{106,107}
Si-O RDF first peak (Å)	1.56	1.62 ^{106,107}
Si-O-Si angle (degree)	151	144 ^{106,107}
O-Si-O angle (degree)	110	109.5 ^{106,107}

Table 3-3. Comparison of properties of the amorphous silica from ReaxFF and from literature.

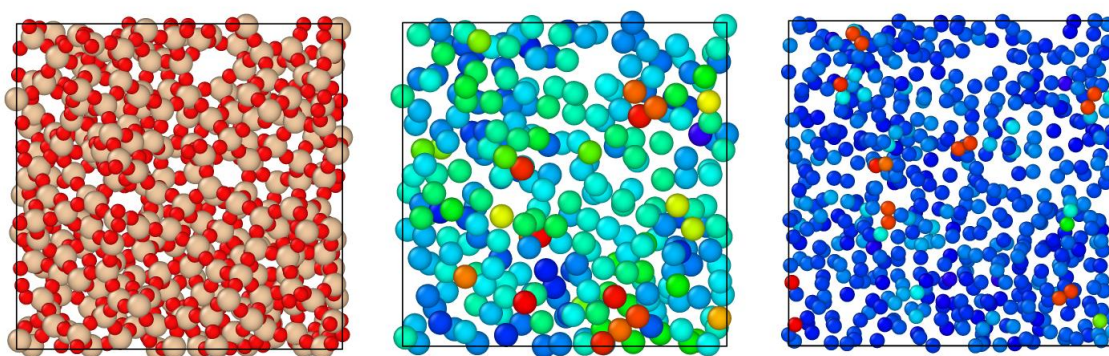


Figure 3-14. Surface atoms from of the amorphous silica slab, surface Si atoms, colored by strain energy, and surface O atoms, colored by strain energy, from left to right. Red color represents higher strain energy, blue color represents lower strain energy.

Based on our observations on surface atoms, undercoordinated atoms generally were placed in strained geometric position, usually off from their equilibrium bond distance and bond angle. In addition, fully coordinated atoms with high strain energy, with stretched Si-O bond distance and distorted angle/torsions, were also good candidates for adsorption and hydrolysis reaction by water molecules.

To evaluate the reactivity of this amorphous silica surface to water, 200 water molecules with a density of 0.204 kg/dm³ were deployed between two surfaces of the amorphous silica in random positions, thus forming a water vapor layer of 15Å thickness. The initial minimum distance among the molecules was maintained at 2.5Å to prevent any overlapping. Then, the

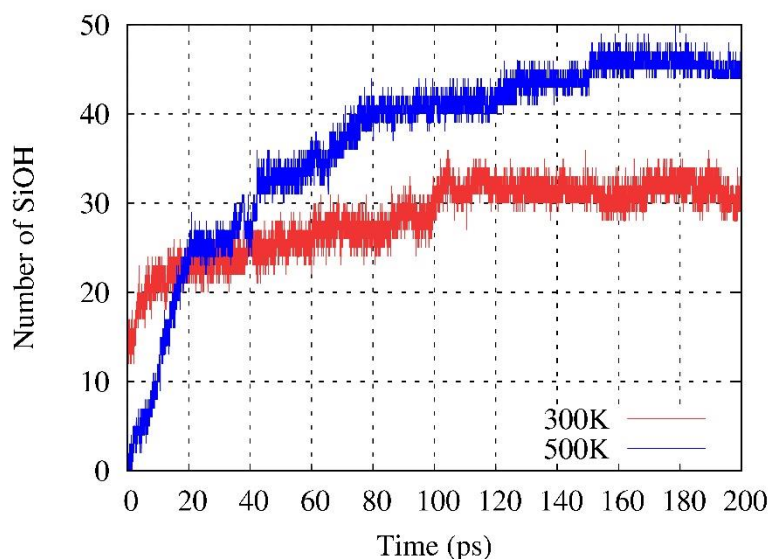


Figure 3-15. Number of silanols on the slab surface during hydroxylation simulation at different temperatures.

system was exposed to constant temperatures of 300K and 500 K with an NVT ensemble having 100 fs of damping constant. After 200ps exposure to water molecules, we observed the formation of surface hydroxyl. The time variation of the hydroxyl number density for the simulation at 300K and 500 K is shown in figures 3-15. Both simulations reached a steady state after 100ps (300K) and 160ps (500K).

Similar to the simulation of silica nano wire with water, hydroxylation of α -SiO₂ slab also favored atomically strained sites on the surface. Figure 3-16 and figure 3-17 show the relationship between silanol formation site and highly strained region of the surface. According to the results from both figures, the hydrolysis reaction clearly prefers the undercoordinated silicon atoms on the surface. The location of red-circled Si atoms of figure 3-16 and figure 3-17 indicates the relatively strained atoms than other atoms, and it matches well with hydroxyl formation sites. We observed that not only the undercoordinated atoms but also the fully coordinated atoms with high local strain energy are responsible for hydroxyl formation.

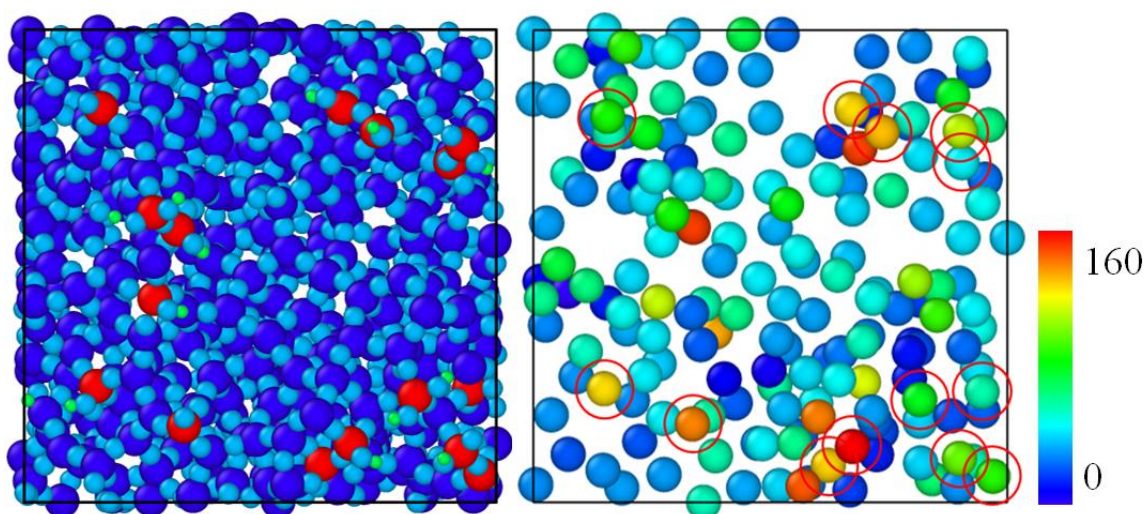


Figure 3-16. Vertical view of amorphous SiO_2 surface after 300K simulation. Red atoms are Si atoms of hydroxyls (Left). Strain energy view of surface Si atoms after 300K hydroxylation simulation. (Right) Red circles represents the position of silanols. Si atoms with relatively high strain energy are generally become the Si of surface hydroxyl.

Under 300K and 500K conditions, hydroxylation pathway on the a- SiO_2 slab was also similar with silica nano wire case: H_3O^+ ions participated the hydrolysis reaction. Figure 3-18 shows the formation of silanol and hydronium molecules on the surface of the amorphous SiO_2 slab, and proton donation from the hydronium molecules by the hopping process. The proton ions in our simulation approximately survives less than 100fs of time, according to averaged lifetime of all protons during our simulations. The most probable destination of hydrogen ion was a neighboring water molecule forming another hydronium, thus experiencing a proton hopping process. At 26.57ps (Figure 3-18a), hydroxylation starts from the adsorbed water molecule. At 26.66ps (Figure 3-18b), adsorbed water molecule donates its proton ion to the nearby water molecule. At 26.665ps (Figure 3-18c), hydronium ion formed. At 26.95ps (Figure 3-18d), hydronium is dissociated and one H atom migrates to the next water molecule, closely placed by hydrogen bond network. After successive hopping, proton forms another silanol, forming hydroxyl on the surface.

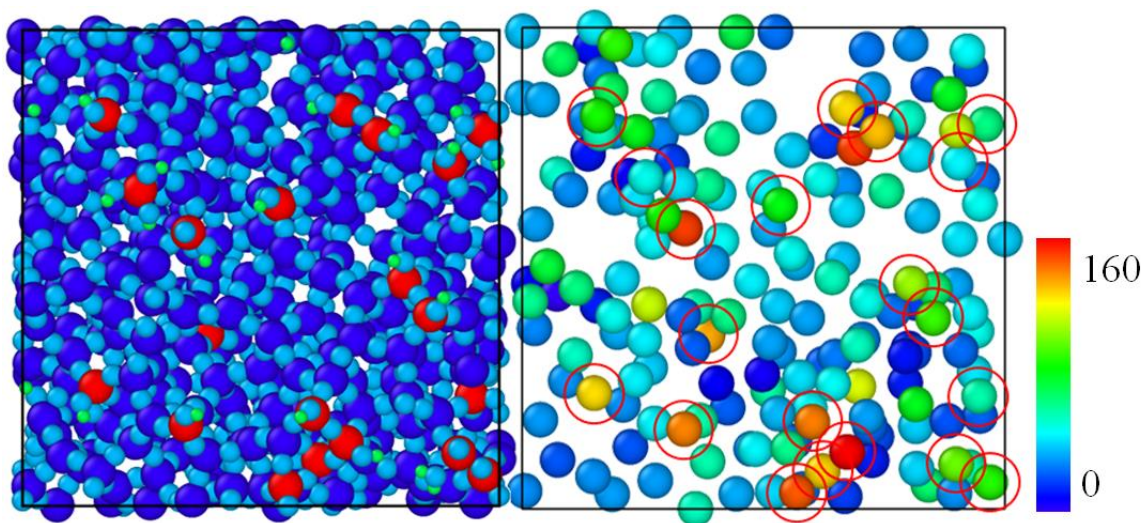


Figure 3-17. Vertical view of amorphous SiO_2 surface after 500K simulation. Red atoms are Si atoms of hydroxyls (Left). Strain energy view of surface Si atoms after 500K hydroxylation simulation. (Right) Red circles represents the position of silanols. Number of hydroxyls are increased when compared to 300K case, and all of them follows the position of relatively high strained surface Si atoms.

In addition, we observed that the donation of a proton to the bridge oxygen atom at surface is also related to the strain energy of the oxygen atom. Due to prolonged Si-O bonds on the amorphous surface, related Si and O atoms on such sites have higher strain energy, which creates a favorable environment for water and hydronium to donate their protons. Figure 3-19 shows the relationships between the hydroxyl formation site and the strained oxygen atom contour of the surface. At 9.83ps (Figure 3-19a), hydronium approached close to the surface. At 9.875ps (Figure 3-19b), proton migrated to the strained Si-O-Si structure on the surface from H_3O^+ ion. At 9.88ps (Figure 3-19c), Si-OH-Si structure was formed. Based on our observation, Si-OH-Si structure was very unstable, so that its survival time was within ~50 fs maximum. Subsequently, at 9.925ps after simulation (Figure 3-19d), this structure was dissociated into a single silanol and an undercoordinated Si atom, which becomes a new favorable site for additional hydroxyl formation on the surface.

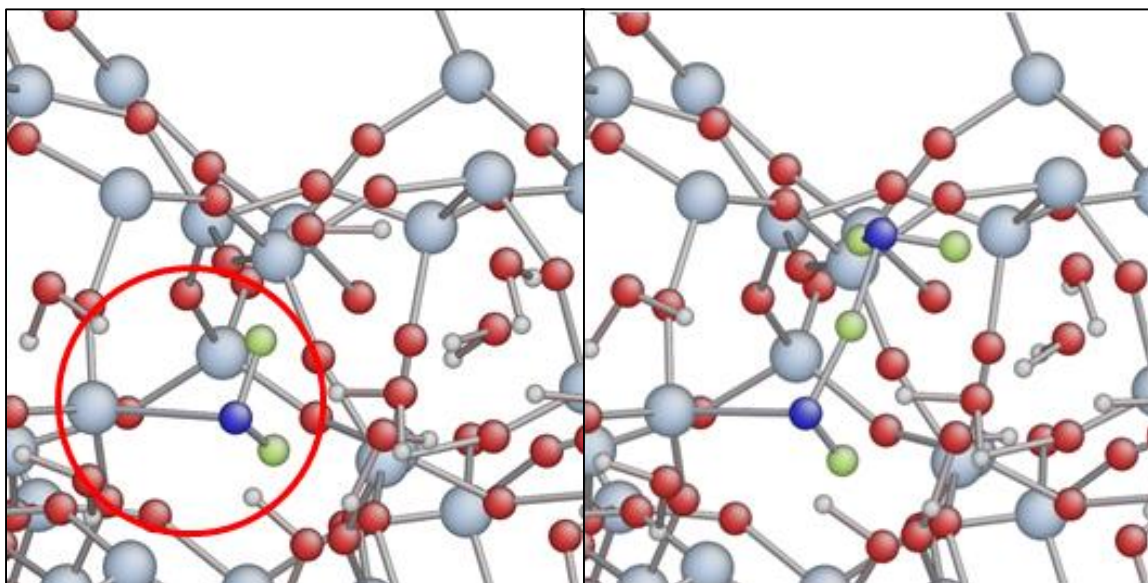


Figure 3-18(a). 26.57ps after simulation. Adsorbed water on a strained silicon structure. (Red circle) Bright grey shows Si, red atoms are O, white atoms are H, blue atoms are O of water, and green atoms are H of water

Figure 3-18(b). 26.66ps after simulation. Donation of proton to the nearby water molecule. (Red circle)

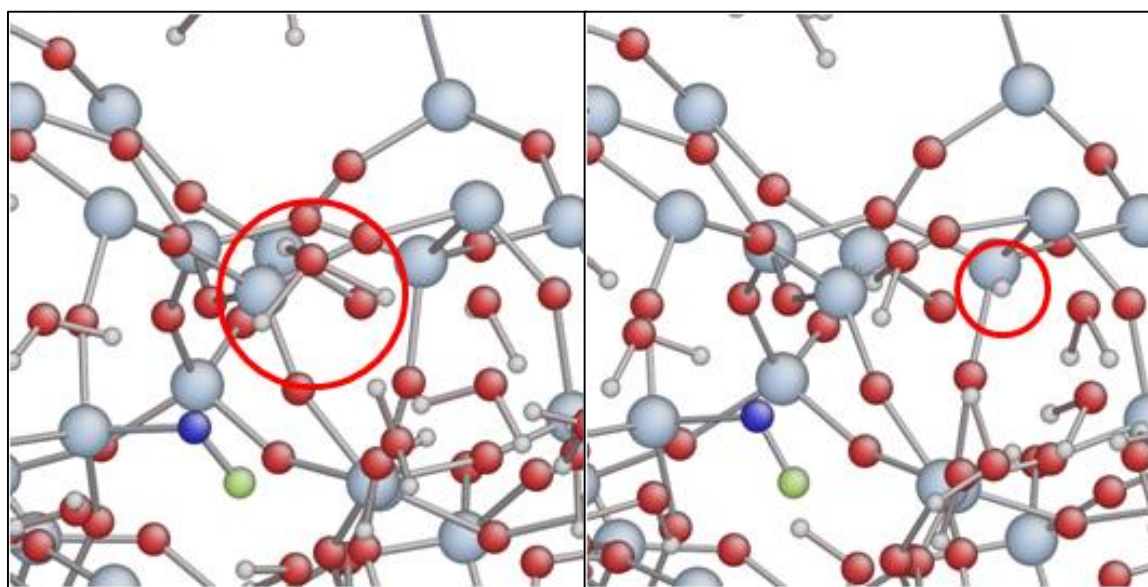


Figure 3-18(c). 26.665ps after simulation. Hydronium formation. (Red circle)

Figure 3-18(d). 26.95ps after simulation. Proton hopping to other water molecule. (Red circle).

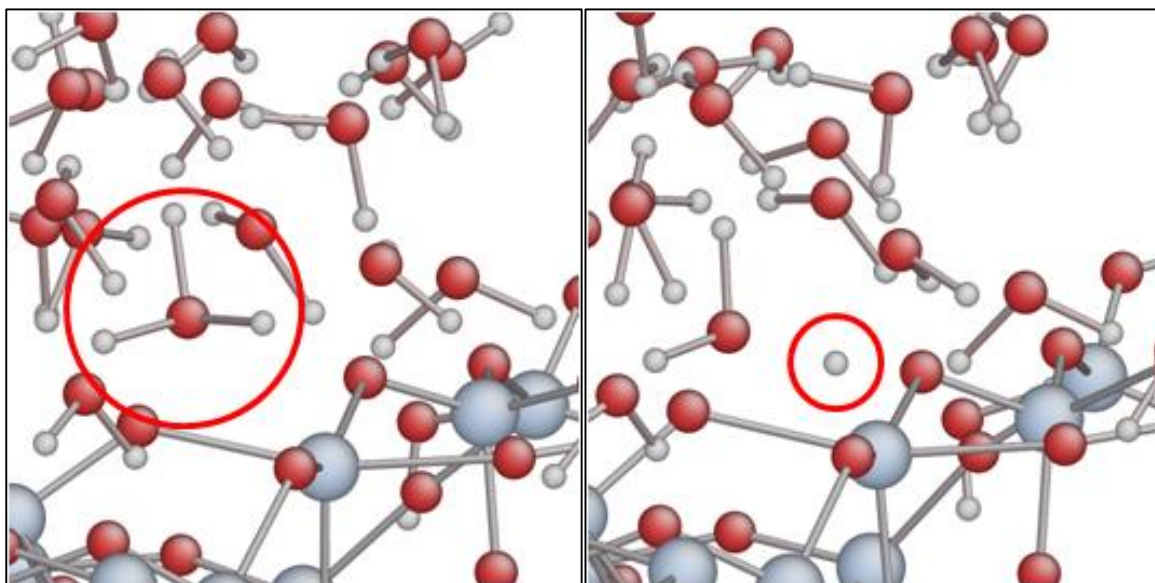


Figure 3-19(a). 9.83ps after simulation. Hydronium inside the water phase. Repeated color scheme with figure 4-18

Figure 3-19(b). 9.875ps after simulation. Proton donation from hydronium to a high-strained surface bridge oxygen.

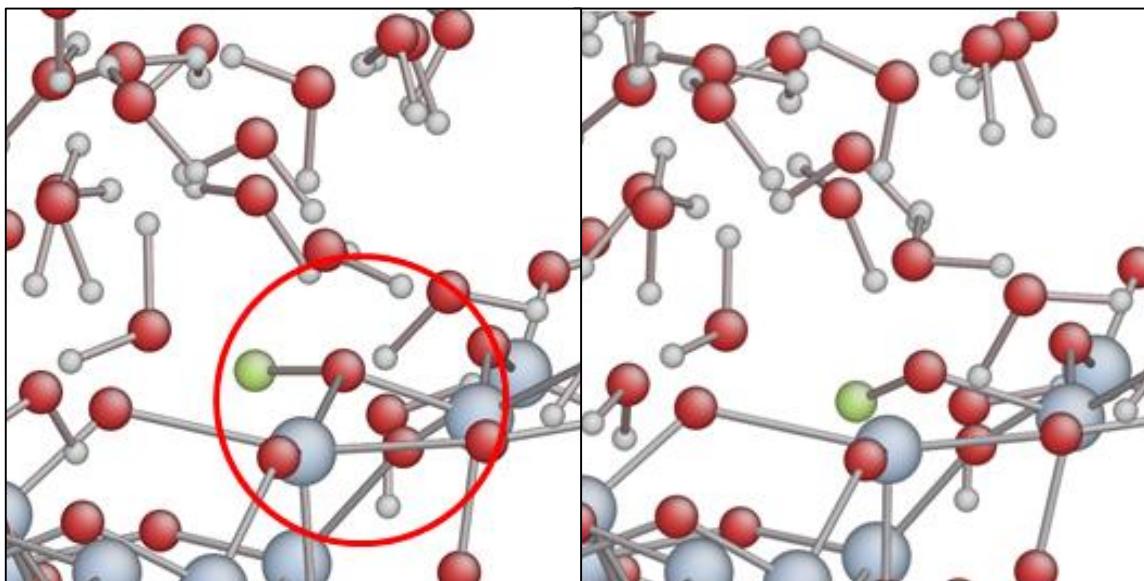


Figure 3-19(c). 9.88ps after simulation. Unstable Si-OH-Si structure.

Figure 3-19(d). 9.925ps after simulation. One of Si-O bond breaks, forming single silanol on the surface

Chapter 4

Molecular dynamics simulations of friction in amorphous silica surfaces

4.1. Introduction

The simulation results will be discussed in three sections. As representative examples, Section 1 discusses specific tribochemical reactions taking place at the sliding interface for three cases: (i) sliding at 700 K without water (Figure 4-2), (ii) sliding at 500K in the presence of 20 water molecules initially (Figure 4-3), and (iii) sliding at 300K in the presence of 100 water molecules initially (Figure 4-4). Section 2 discusses the overall mass transfer across the interface and energetics of the system during the slide for 1 ns (Figures 4-5 – 4-8), which vary depending on the interplay of tribochemical reactions induced by mechanical shearing. Section 3 elucidates the dynamic processes (Figures 4-9 and 4-10) and potential energy changes (Figure 4-11) as well as wear of the surfaces (Figure 4-12) upon separation of the interface after sliding for 1 ns.

4.2. Friction simulation of amorphous SiO₂ surface under various environments

4.2.1. System preparation and simulation conditions

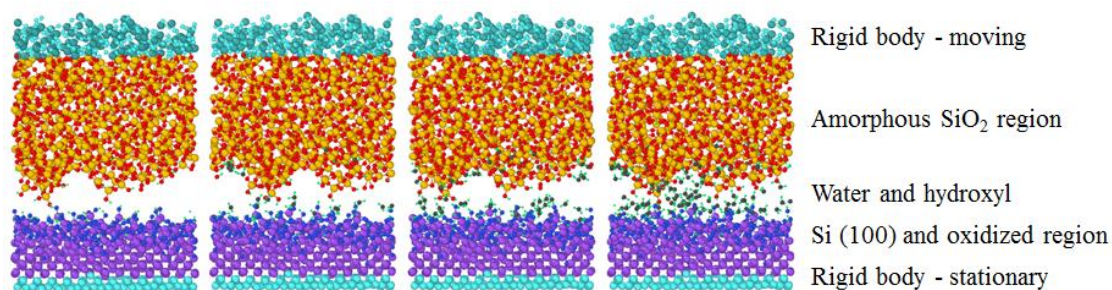


Figure 4-1. Configuration of systems for the ReaxFF MD simulations of mechano-chemical wear of silicon oxide surfaces. The number of interfacial water molecules is varied, from left to right, 0, 20, 50 and 100.

In previous experimental studies, counter-surfaces rubbing against a silicon wafer were either amorphous SiO₂ spheres with a 1~2 μm diameter attached to AFM cantilevers or macroscopic silica balls (a few mm in diameter).^{25,26,108} In the AFM study with silica spheres, the Hertzian contact diameter is on the order of 10 nm; the contact diameter in the macroscale ball-on-flat tribo-test is even larger (typically, >10~100 μm). Thus, we decided to mimic the experimental contact geometry using a slab-on-slab geometry (slab size = 3.2 nm wide). This also made it easy to control the number of water molecules confined within the sliding contact under periodic boundary conditions. When we attempted simulations with a ball-on-slab geometry (ball diameter = 1 nm and slab size = 3 nm) in the presence of 1 water molecules in the surrounding, the contact size was too small so that most water molecules remained outside the sliding contact.

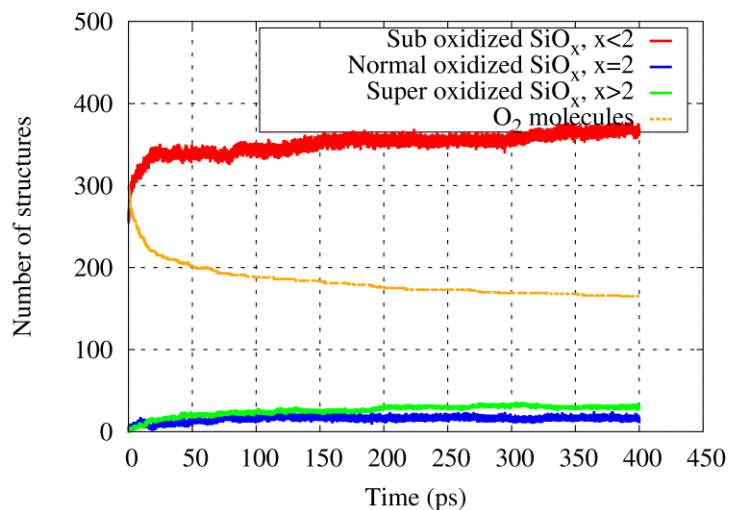


Figure 4-2(a). Tracking of oxidation state of Si(100) crystal slab

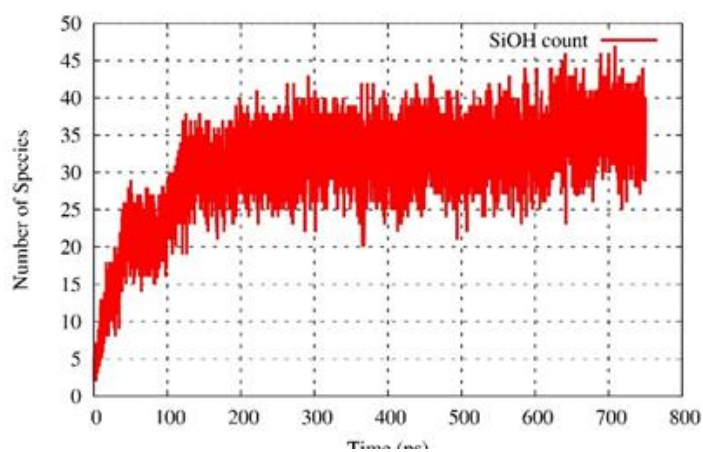


Figure 4-2(b). Tracking of number of hydroxylation on the surface of Si(100) and a-SiO₂

The ReaxFF force field used in our simulation was the one developed by Fogarty et al.,¹ which is currently the best ReaxFF potential for the Si/O/water interaction. An NVT ensemble with a Nose-Hoover thermostat was used for all MD simulations. To build an amorphous SiO₂ (a-SiO₂) slab, a quartz crystal was melted and annealed at 3000K and then cooled to 300 K. A native oxide layer on a Si(100) surface was created by oxidizing the Si(100) surface by reacting with 300 oxygen molecules at 300K for 400 ps through ReaxFF-MD simulations with 100fs temperature damping constant. After the oxidation reaction, a 0.5~0.6 nm thick oxide layer was

formed on the Si(100) surface, which was comparable with the previous simulation results.¹⁰⁹ Both a-SiO₂ and oxidized-Si(100) surfaces were hydroxylated by reacting with 300 water molecules at 300K in NVT MD simulations. At the end of the simulation, the number density of the surface silanol groups reached a steady state. Figure 4-2(a) and 4-2(b) represents the state of oxidation of Si(100) surface, and degree of hydroxylation for both slab.

Figure 4-1 represents the simulation setup for the tribochemical reactions occurring at the sliding interface of the a-SiO₂ slab and the oxidized-Si(100) slab. The size of periodic box for simulation was $3.19 \times 3.19 \times 7.0 \text{ nm}^3$. ReaxFF-MD simulations of tribochemical reactions were carried out in the following four steps: (i) vertical compression, (ii) equilibration, (iii) lateral slide at a speed of 10 m/s for 1 ns, and (iv) vertical separation at a speed of 20 m/s for 100 ps. Mimicking the previous AFM studies,^{25,26,108} a normal load applied to the top rigid body along the z-axis direction was maintained at 1 GPa during the simulation. The top rigid body region moved at a 0.01 nm/ps velocity along the x-axis direction. The bottom rigid body of the oxidized-Si(100) slab was fixed stationary.

The effects of water on tribochemical reactions were studied by adding 20, 50, and 100 water molecules into the space between two slabs (Figure 4-1). In our simulation dimension, 100 water molecules corresponded to about a full coverage of the surface. To test the effects of thermal activation on the wear process, simulations were carried out at three temperatures: 300K, 500K, and 700K. All MD simulations used a time step of 0.25 fs, and temperature damping constant was 100 fs, under the NVT ensemble and Nose-Hoover thermostat. Snapshot pictures of ReaxFF-MD simulation steps were produced using OVITO.⁹⁹

4.2.2. Tribological reactions at the sliding interface

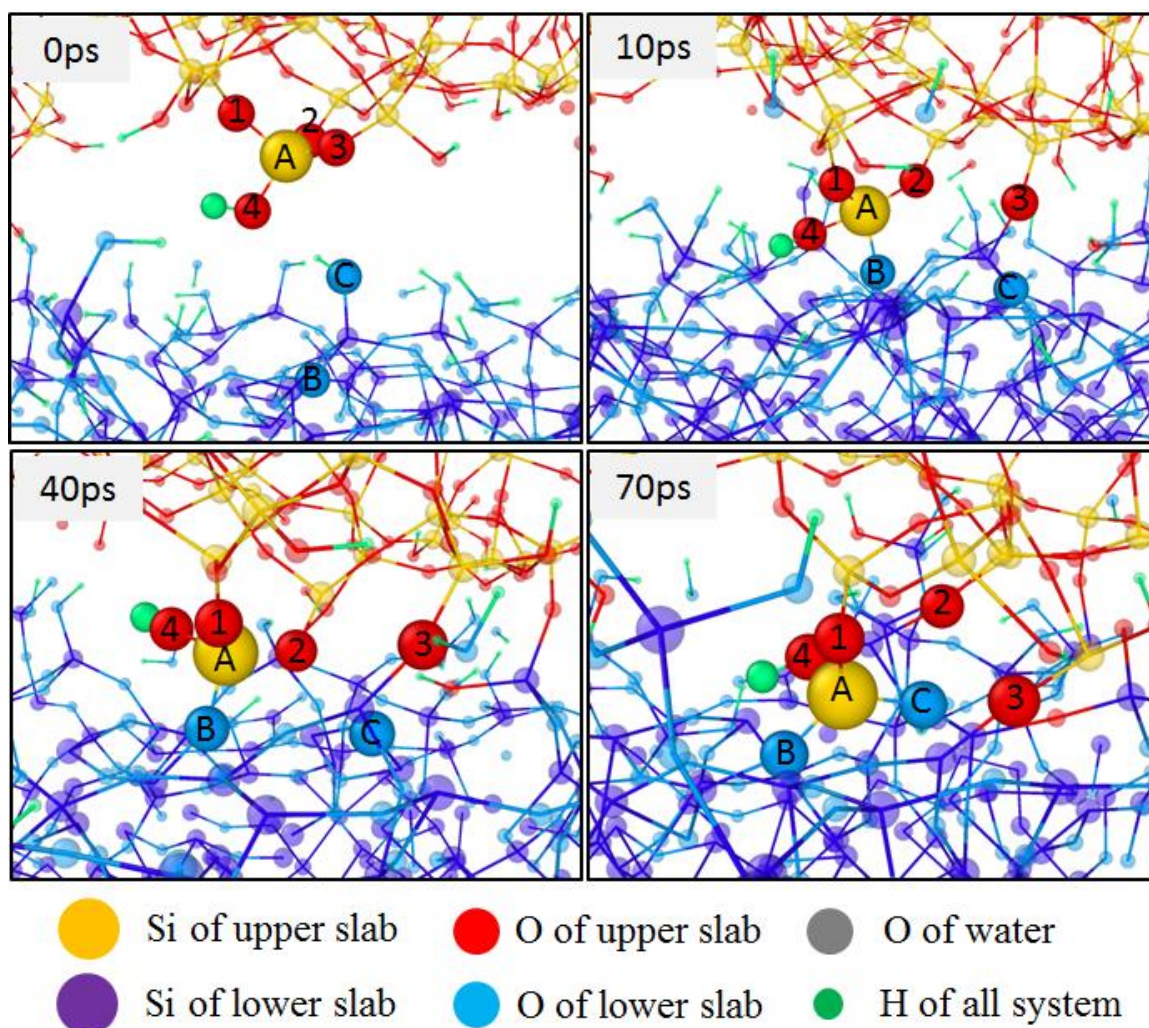


Figure 4-3. Snapshot views of reactions involving a hydroxylated Si atom (A) of the a-SiO₂ surface and hydroxyl groups of the hydroxylated Si (100) surface in the absence of water at 700K. The sliding time is shown in each frame. Large solid circles marked with letters and numbers are the atoms involved in reactions being monitored in the series of snapshots. Small transparent circles are the atoms that are discussed in the figure. Black solid lines are periodic boundaries.

In order to reveal the detailed reaction paths of tribochemical reactions occurring at the sliding interface, we monitored bond dissociations and formations of specific atomic species as a function of sliding time. Figure 4-3 shows chemical changes of a Si atom of the a-SiO₂ surface (marked with A in Figure 2) under dry condition at 700 K. Initially, it is terminated with one silanol group (Si^A-O⁴H). After 10 ps sliding, the Si^A-O³ bond is dissociated and the Si^A atom

forms a covalent bond with an oxygen atom (O^B) of the oxidized Si(100) surface. The O^3 atom, dissociated from Si^A of the a-SiO₂ slab, is bonded to a silicon atom in the oxidized Si(100) slab.

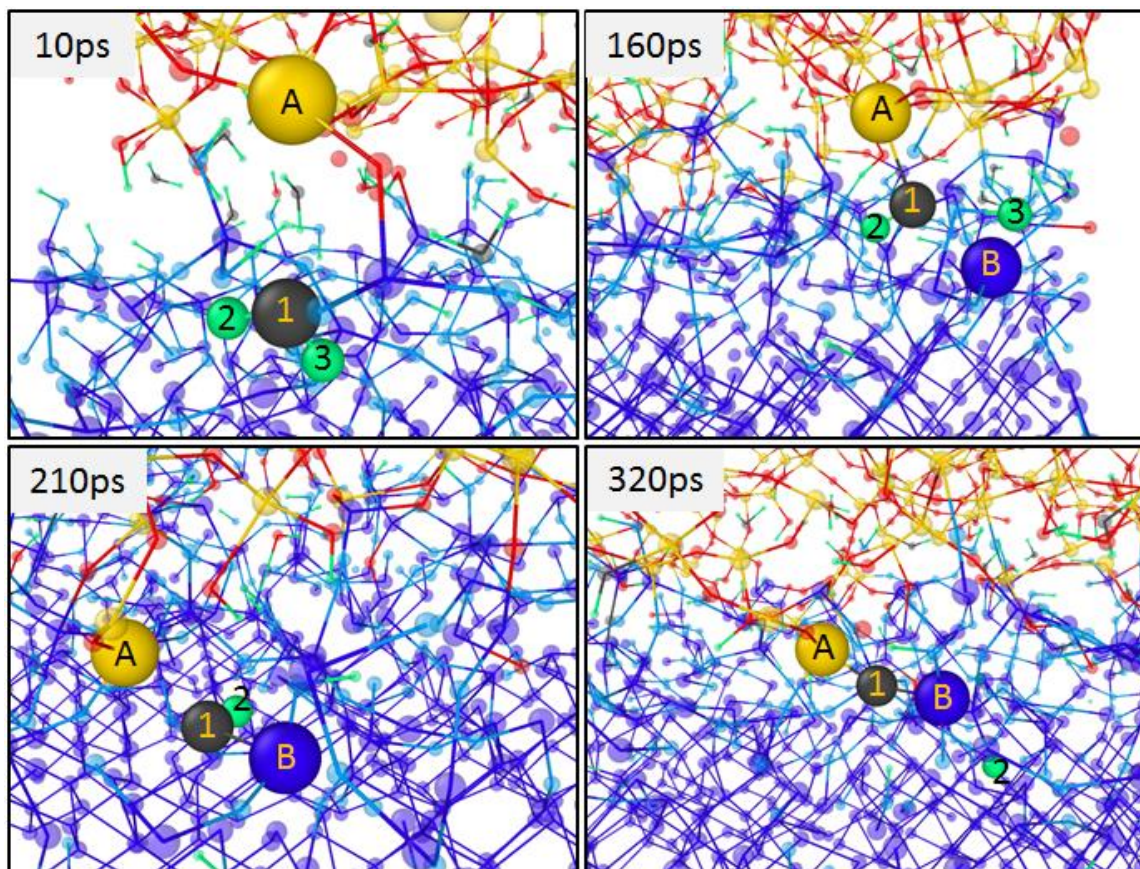


Figure 4-4. Snapshot views of reactions of an oxygen atom (1) of a water which eventually forms a covalent bond bridging the a-SiO₂ surface and the oxidized Si (100) surface. The system temperature is 500K and the initial amount of water is 20 molecules in the system. The sliding time is shown in each frame. The color codes in the figures are the same as Figure 4-2.

At 40 ps, it can be seen that the O^2 atom is dissociated from Si^A and bonded to another Si atom in the oxidized-Si(100) surface. The Si^A species is temporarily left in an under-coordinated state. At 70ps, the under-coordinated Si^A species of the a-SiO₂ surface reacts with another oxygen (O^C) of the oxidized-Si(100) surface. Through these sequential steps, the upper a-SiO₂ surface and the lower oxidized-Si(100) surface are now connected or bridged via Si^A-O^B , Si^A-O^C , O^2-Si^{lower} , and

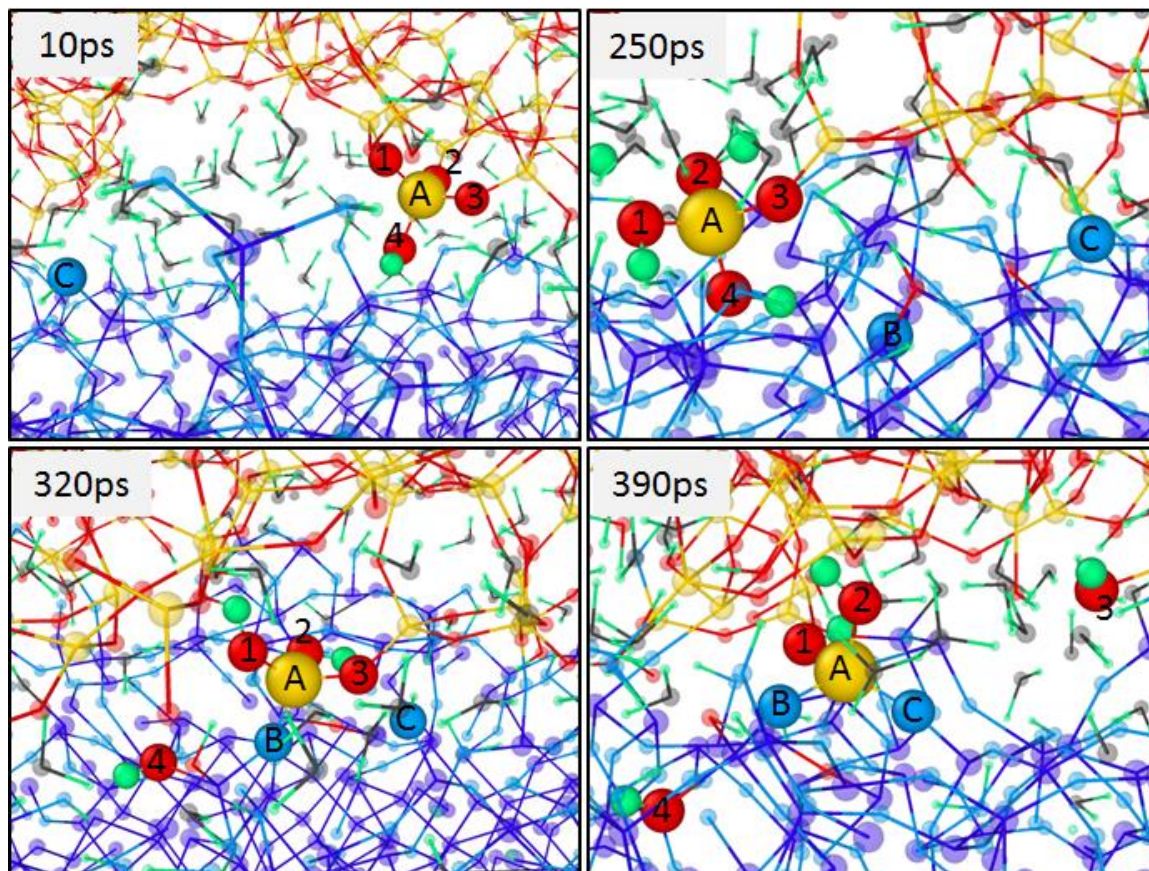


Figure 4-5. Snapshot views of reactions involving a hydroxylated Si atom (A) of the α -SiO₂ surface and hydroxyl groups of the hydroxylated Si (100) surface in the presence of 100 water molecules at 300K. The sliding time is shown in each frame. The color codes in the figures are the same as Figure 4-2.

O³-Si^{lower}. Note that the Si^A-O⁴H silanol group still remains intact at 70 ps; but later it also dissociates and forms another covalent bond with an oxygen atom of the lower slab. These “bridge” bonds are continuously formed across the sliding solid surfaces over the entire sliding duration.

When water molecules are present at the sliding interface, additional chemical reactions can take place. A series of chemical reactions involving an oxygen atom of a water molecule (marked as H²-O¹-H³) at the α -SiO₂/oxidized-Si(100) interface are illustrated in Figure 4-4. At 160 ps after sliding, this water molecule donates a hydrogen (H³) to the nearby oxygen atom and

forms a covalent bond with the Si^{A} atom, becoming a hydroxyl group ($\text{Si}^{\text{A}}\text{-O}^{\text{1H}}$) of the a-SiO₂ surface. At 210 ps, this hydroxyl group migrates to the Si^{B} atom of the oxidized-Si(100) surface, leaving the Si^{A} atom under-coordinated. At 320 ps, the O^{1} atom donates H^{2} to the other O atom in the oxidized-Si(100) surface, and forms a covalent bond again with the Si^{A} atom, forming a $\text{Si}^{\text{A}}\text{-O}^{\text{1}}\text{-Si}^{\text{B}}$ bridge bond across the interface. Thus, interfacial water molecules between the a-SiO₂ and oxidized-Si(100) surfaces can provide additional reaction channels to form the bridge bonds across the interface.

On the other hand, the presence of a large amount of water molecules can interrupt the interfacial bridge bond formation. Figure 4-5 depicts snapshots of simulations carried out with 100 interfacial water molecules at 300K, where a Si atom is transferred from the upper slab to the lower slab but the bridge bond is not formed. At 10 ps of sliding, the Si^{A} atom of the a-SiO₂ surface has one hydroxyl group ($\text{Si}^{\text{A}}\text{-O}^{\text{4H}}$) and its three oxygen atoms (O^{1} , O^{2} , O^{3}) are bonded to other silicon atoms of the a-SiO₂ surface. At 250 ps, two of these siloxane bonds (O^{1} , O^{2}) are broken and replaced with hydroxyl groups (O^{1H} , O^{2H}) through reactions with neighboring water molecules. At 320 ps, the Si^{A} atom transfers one of the hydroxyl groups (O^{4H}) to another silicon atom of the oxidized-Si(100) surface, and establishes a new interfacial $\text{O}^{\text{3}}\text{-Si}^{\text{A}}\text{-O}^{\text{B}}$ bridge bond. At 390 ps, the O^{3} atom is dissociated from the Si^{A} atom and transferred to another silicon atom of the a-SiO₂ surface as a hydroxyl group; at the same time, an oxygen from the oxidized-Si(100) surface reacts with the Si^{A} , forming a $\text{Si}^{\text{A}}\text{-O}^{\text{C}}$ bond. At this point, the Si^{A} atom is completely transferred from the a-SiO₂ surface to the oxidized-Si(100) surface, forming two siloxane bonds ($\text{Si}^{\text{A}}\text{-O}^{\text{B}}$, and $\text{Si}^{\text{A}}\text{-O}^{\text{C}}$) and germinal hydroxyl groups ($\text{Si}^{\text{A}}\text{-O}^{\text{1H}}$ and $\text{Si}^{\text{A}}\text{-O}^{\text{2H}}$).

4.2.3. Interfacial mixing during the slide for 1ns

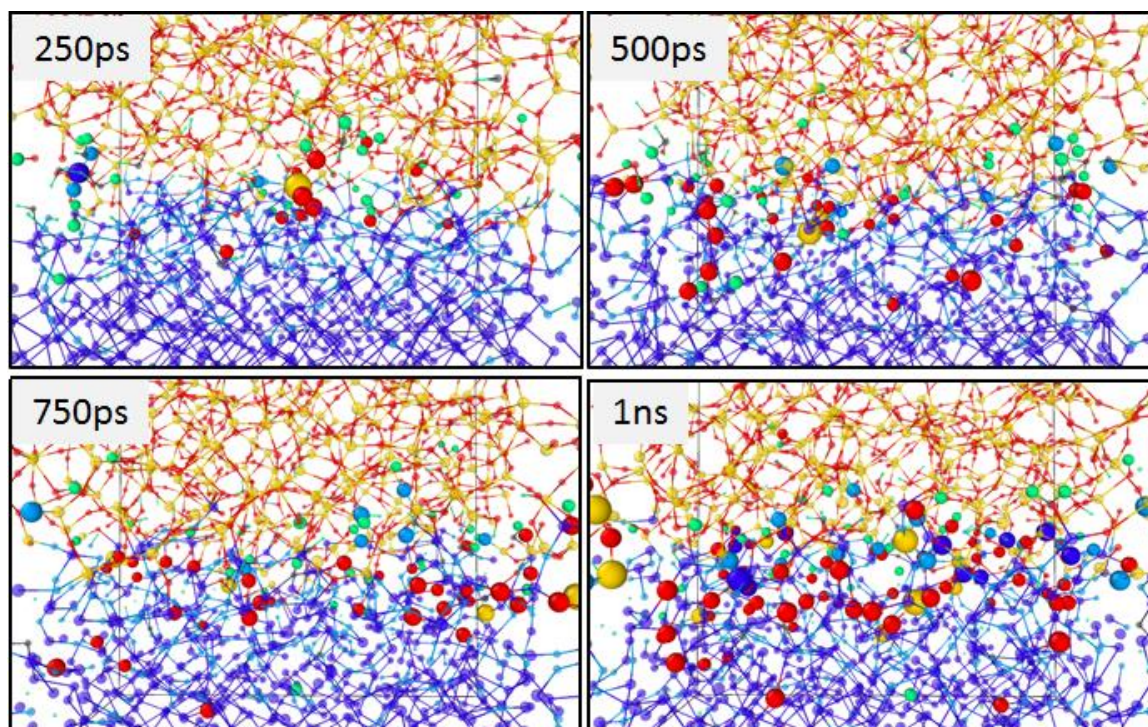


Figure 4-6. Mixing of atoms across the interface during the slide in the presence of 20 water molecules at 500K. The sliding time is shown in each frame. The color codes in the figures are the same as Figure 2. The Si and O atoms dissociated from their original solid surfaces and transferred to the opposite solid surfaces as well as the O and H atoms dissociated from H₂O are presented as solid enlarged circles.

The tribochemical reactions described in Section 1 occur simultaneously at multiple places during the entire sliding period. This leads to interfacial mixing of Si, O, and H atoms at the sliding interface. To distinguish the transferred atoms from the unaffected atoms and calculate the total amount of cross-interface mixing, we followed the trajectories of all atoms using the connectivity analysis. If any atoms were detached from the original slab, then they were counted as the transferred atoms, and their positions were tracked. The total amount of transferred atoms varied with the system temperature and the amount of interfacial water molecules.

Figure 4-6 shows the large area view of the sliding interface containing 20 water molecules at 250 ps, 500 ps, 750 ps, and 1 ns after sliding. In this sequence of pictures, it can be clearly seen that many atoms of each side are moved and transferred to the opposite side. The largest motions can be seen for oxygen atoms transferred from the a-SiO₂ surface to the oxidized-

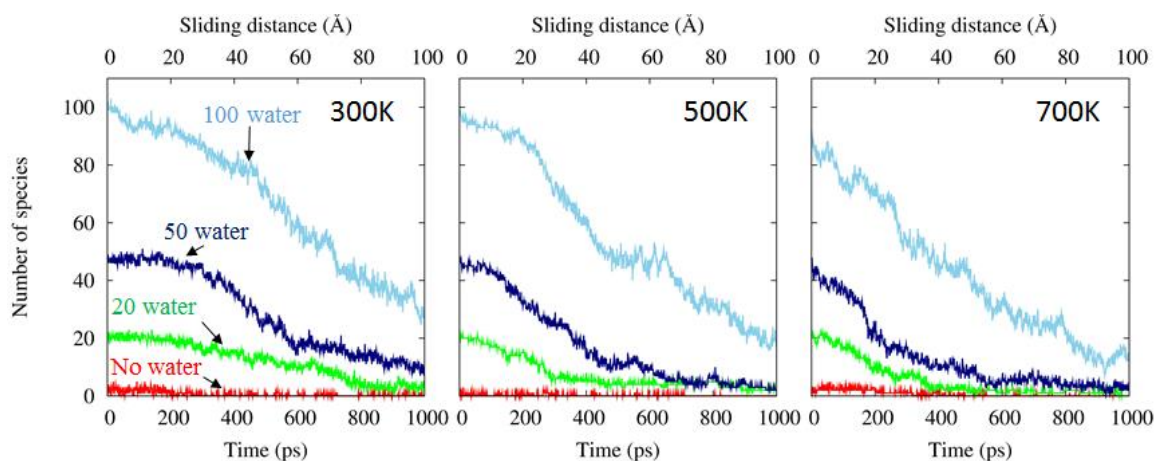


Figure 4-7(a). Number of water molecules during sliding.

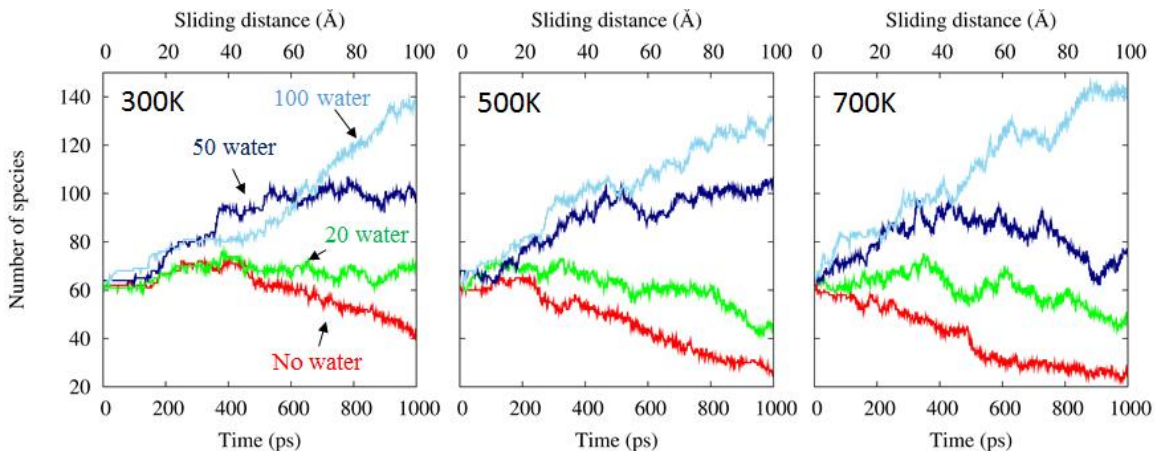


Figure 4-7(b). Number of silanols during sliding.

Si(100) surface (large red circles in Figure 4-6). This results in slight increase in the overall oxidation of the Si(100) surface. The dissociation of interfacial water molecules compensates the oxygen loss in the a-SiO₂ side, resulting in formation of hydroxyl groups (large green circles in Figure 4-6).

The dissociation rate of interfacial water is sensitive to the system temperature. The number of water molecules remaining intact during the course of sliding simulation is plotted in Figure 4-7(a). As presented in figure 4-7(a), the number of water molecules were declined during the sliding. Water molecules were hydroxylated, or dissociated to O and H atoms, and adsorbed

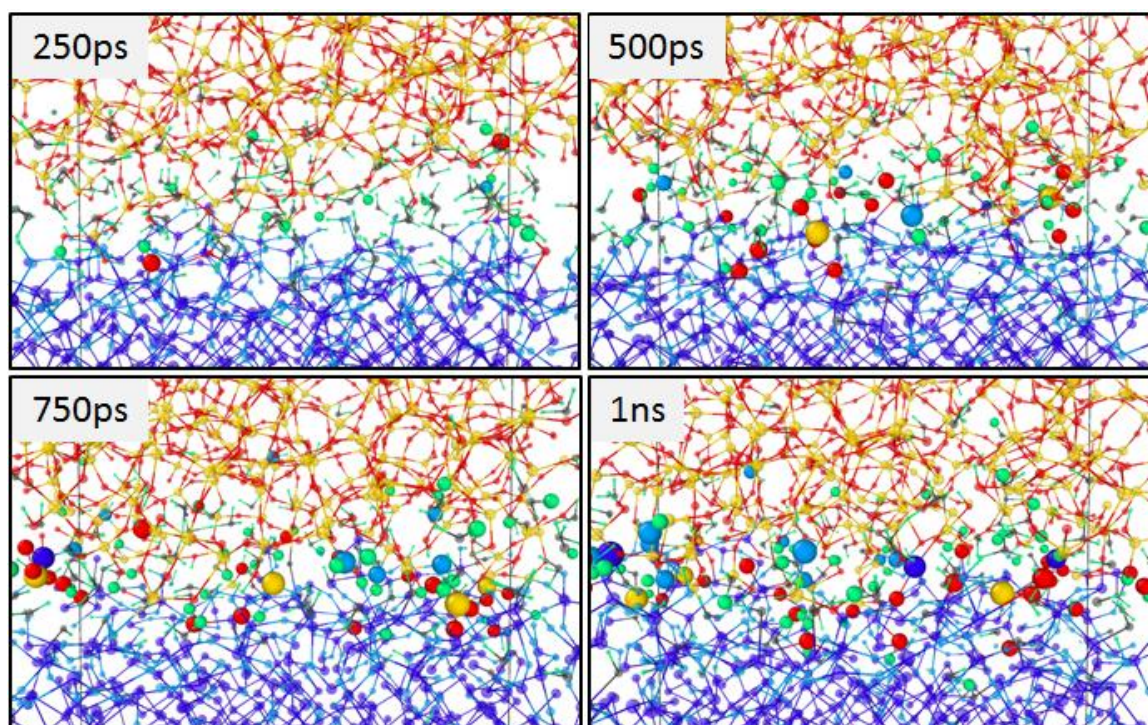


Figure 4-8. Mixing of atoms across the interface during the slide in the presence of 100 water molecules at 300K. The sliding time is shown in each frame. The color codes in the figures are the same as Figure 4-6.

into both slabs. In addition, we observed the formation of small amount of water molecules during the sliding under no water condition for all temperatures. These water molecules are originated from surfaces hydroxyls, from dehydroxylation and collision. At 300K and 500 K, the dissociation rate is slow initially and then accelerated gradually. This acceleration seems to correlate with the progress of the interfacial mixing. Later, as the amount of molecular water decreases substantially, the water dissociation rate decreases gradually. In contrast, at 700K, water molecules dissociate fast as soon as the sliding starts. This data implies that thermal energy at 700K is high enough to facilitate or assist tribochemical reactions.

The initial amount of interfacial water molecules in the system affects the degree of surface hydroxylation during the sliding, in Figure 4-7(b). In figure 4-7(b), we tracked the number of surface hydroxyls. The results from the simulations under dry condition showed

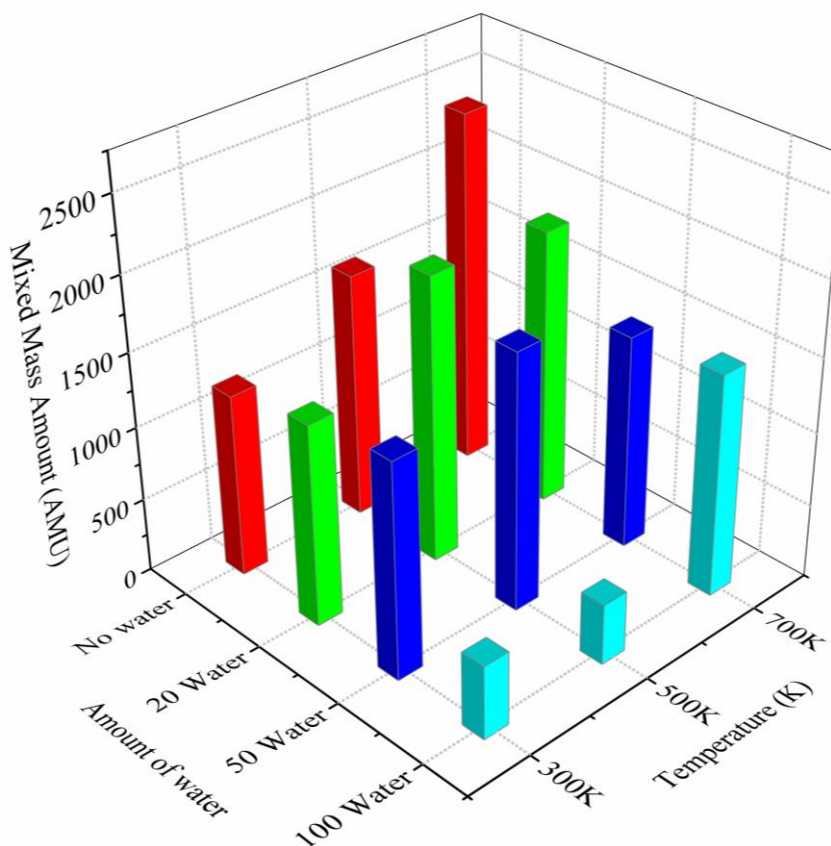


Figure 4-9. Total amount of interfacial mixing, as a function of number of water molecules and system temperature, occurred after sliding at a speed of 10 m/s for 1 ns. The applied normal load is 1 GPa.

decreasing number of hydroxyls regardless of temperature. Simulations with 20 water molecules also presented small decreases in silanols. Simulations with 50 water molecules showed the trends of weak increasing number of silanols. In the case of 100 water molecules, the number of hydroxyls kept increasing during the sliding at all temperature conditions tested. For all cases, no $\text{Si}(\text{OH})_4$ molecules were observed. This is because both slabs were closely adhered to each other under 1GPa of downward pressure. In addition, as the temperature increases, the rate of hydroxylation was increased. This tendency became more prominent at 700K with 100 water molecules.

In the absence of water molecules, the number of surface hydroxyl groups decreases. This decrease is faster at 700 K, compared to the 300 K and 500 K cases. When 20 water molecules are added in the sliding interface, the decrease in hydroxyl group density is slower since the dissociation of water molecules result in production of hydroxyl groups. When the interfacial water loading is increased to 100 molecules (enough to form a full coverage of the surface), then the total OH groups at the interface increases slightly at 300 K and 500 K, and significantly at 700 K.

The presence of large amounts of water molecules sufficient to cover the entire sliding interface resulted in a decrease in the atomic mixing across the interface. Figure 4-8 shows the snapshots of the sliding interface at every 250 ps for the system containing 100 water molecules at 300 K. Compared to Figure 4-6, the amount of transferred oxygen atoms (large red and cyan circles in Figure 4-8) is greatly reduced and a substantial increase in the hydroxyl group concentration is noted (large green circles in Figure 4-8).

Figure 4-9 compares the total amount of atoms transferred from one surface to the other after sliding for 1 ns. Several interesting trends are noted in this plot. In the absence of interfacial water molecules, the degree of atom transfer increases as the system temperature increases. This trend indicates that the atom transfer process is facilitated by the increase in thermal energy of the system. In other words, the atom transfer across the interface is an energetically activated process. At 300 K and 500 K, when less than one monolayer of interfacial water molecules (20 and 50 H₂O molecules in Figure 4-9) are added, the overall mixing or atom transfer across the interface is increased. This must be due to additional reaction pathways facilitated or provided by the presence of water (Figure 4-4). This tendency of mixing also matches well with previous prediction,¹¹⁰ which simulated the role of water molecules not only to build hydrogen bond network, but also initiates strong siloxane bonds across the surface.

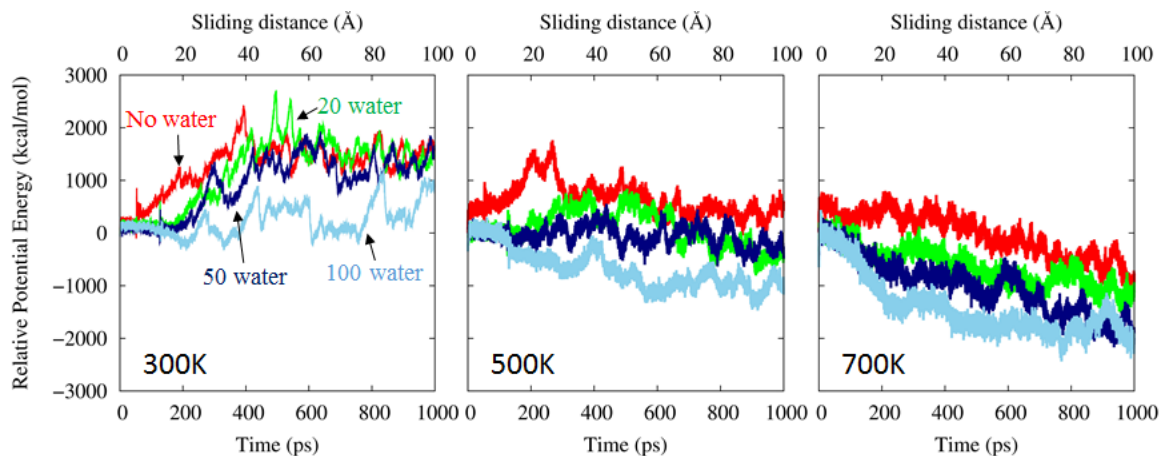


Figure 4-10. Potential energy change during the sliding of the α -SiO₂/oxidized-Si(100) interface system containing 0, 20, 50, and 100 water molecules at 300K, 500K, and 700K. Higher temperature shows smooth and declining potential energy curves, while lower temperature shows numerous peaks and increasing tendency of potential energy.

However, when the interfacial water amount is increased large enough for full coverage of the sliding interface (100 H₂O molecules in Figure 4-9), the interfacial atom transfer is substantially decreased at 300 K and 500 K. In the presence of large number of water molecules, the atom transfer reaction has a higher probability to lead to highly hydroxylated surface state than forming covalent bonds bridging two solid surfaces (Figure 4-5). Also, unreacted water molecules (Figure 4-7(a)) can act as a spacer preventing surface hydroxyl groups of the solid surfaces from reacting each other.

The effects of interfacial water molecules on atom transfer at 700K seem different from those at 300 K and 500 K (Figure 4-9). The degree of interfacial atom transfer is reduced as soon as a small amount of water is introduced to the sliding interface. At 700 K, the water molecules are readily dissociated as soon as the sliding is started (Figure 4-7(a)), which is different from the lower temperature cases (300 K and 500K as shown in Figures 4-7(a)) where the dissociation of water molecules is slow in the first 100 – 300 ps and then facilitated as the sliding continues.

Again, this implies that the thermal energy at 700 K is high enough to assist the water dissociation reaction even before the solid surface is substantially sheared creating reactive sites.

Figure 4-10 shows the changes in potential energy during the sliding at each temperature with different amounts of interfacial water molecules. At 300K, the system energy increases as soon as the sliding starts and then reaches a steady state after ~500 ps. When 20 and 50 water molecules are present at the beginning, the system energy remains almost unchanged for ~200 ps and then increases rapidly in the next ~200 ps period. This implies that intact water molecules could delay the shear-induced interfacial atomic mixing for a while; but, as soon as the water dissociation is initiated (Figure 4-7(a)), the atom transfer process is facilitated. In the presence of 100 interfacial water molecules at 300K, the overall increase of the system potential energy is much smaller. This could be attributed to the lower degree of interfacial atom transfer at this condition compared to the 20 and 50 H₂O molecule cases.

At 500 K with 20 and 50 water molecules, the system energy increases slightly during the first half of the sliding period and then decreases gradually. When the water amount is increased to 100 molecules, then the system energy decreases from the beginning of the slide. At 700 K, the system energy decreases continuously in all cases. This difference from the 300 K case must be due to thermal activation and relaxation of the intermediate species formed by interfacial shear. The large fluctuation of the system energy in a short time (<10 ps) scale also supports this interpretation.

4.2.4. Separation of the interface after sliding for 1 ns

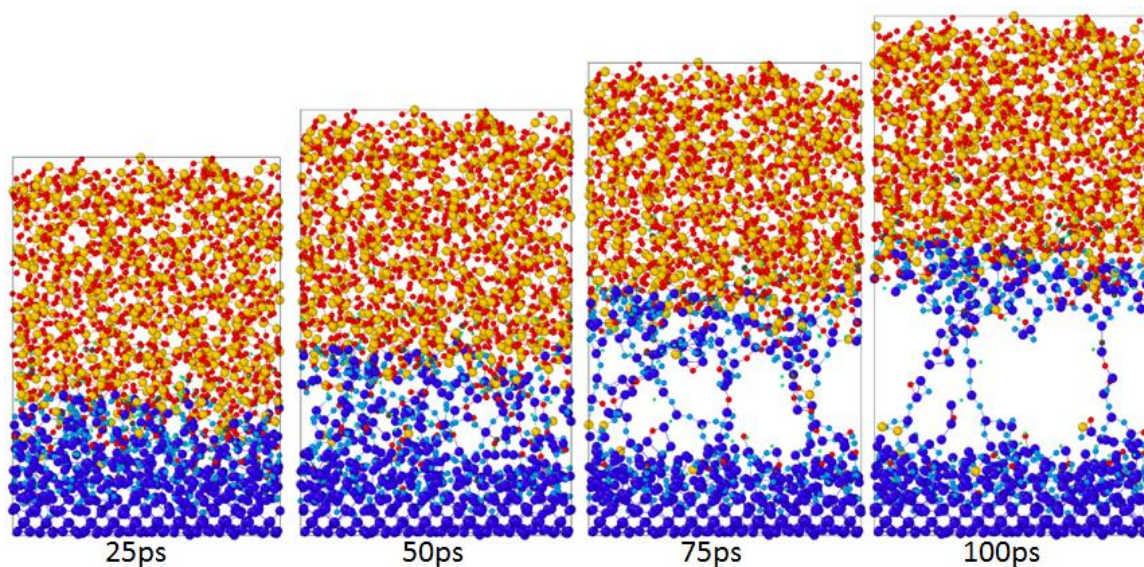


Figure 4-11. Snapshot views of the vertical separation at a 20 m/s speed for 100 ps after sliding for 1 ns in the absence of water molecule at 500K. The separation time is shown in each frame. The color codes in the figures are the same as Figure 2.

Since the ReaxFF-MD simulations were carried out with the slab-on-slab geometry with periodic boundary conditions along the x- and y-directions, the only way to estimate the quantity relevant to the mechanochemical wear measured experimentally was to separate the interface vertically after the sliding. Figure 4-11 shows snapshots of the vertical separation process at a 25 ps interval for the 500 K system after sliding for 1 ns in the absence of interfacial water molecules. At 25 ps, the two solid surfaces still share intimately mixed interface. At 50 ps, two solids start to physically separate and there is a low atomic density region between two solids. It is interesting to note that above this low-density region, substantial amounts of silicon and oxygen atoms originating from the oxidized-Si(100) surface are adhered or transferred to the top α -SiO₂ surface. At 75 ps, there are many Si-O-Si inter-connected chains or strings being stretched by the two solids surfaces. It should be noted that this could be an artifact caused by the fast separation rate (20 m/s). If the vertical separation rate is much slower (for example, less than 1 m/s), then the surface atoms would have much longer time to relax or restructure; thus, the

number of chains or strings being pulled during the vertical separation process is expected to be smaller at a slower separation rate. In any case, the separation and chain-pulling dynamics of the interface would strongly depend on the atomic mixing across the interface during the sliding (Figures 4-6 and 4-9). The interfaces slid in the presence of 20 and 50 water molecules at 300 K and 500 K also showed large amount of Si-O-Si chains during the separation.

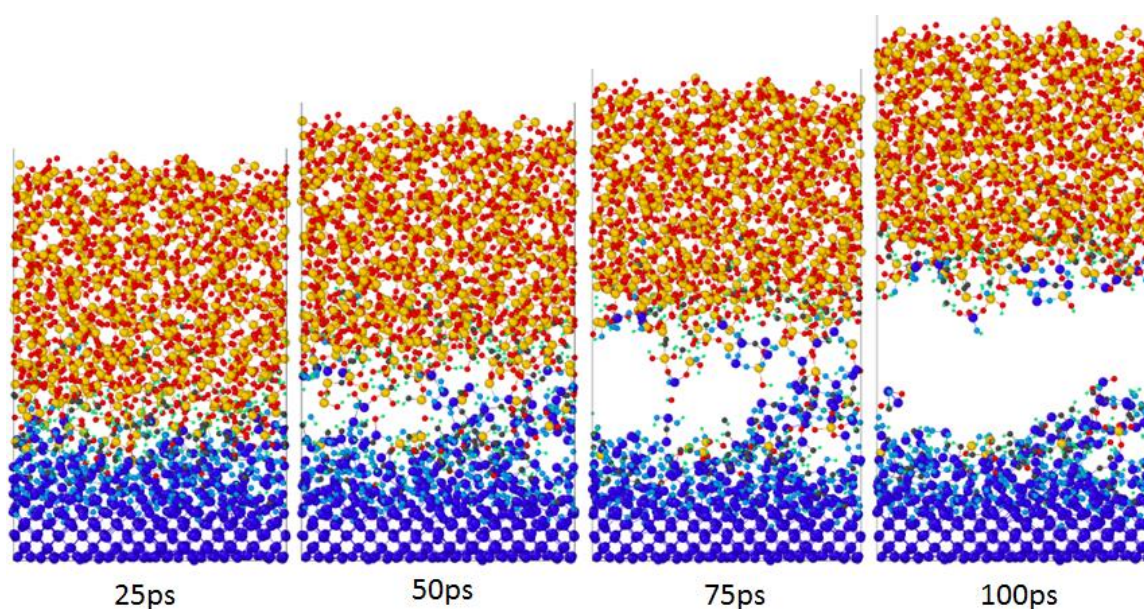


Figure 4-12. Snapshot views of the vertical separation at a 20 m/s speed for 100 ps after sliding for 1 ns in the presence of 100 water molecules at 500K. The separation time is shown in each frame. The color codes in the figures are the same as Figure 2.

Figure 4-12 pictures the separation process at the same 25 ps steps for the case at 500K with 100 interfacial water molecules. Unlike the no water case (Figure 4-11), the low atomic density region can be noticed even at 25 ps. At 50 ps, two surfaces are already almost completely separated and there are no Si-O-Si chains or strings connecting the a-SiO₂ and oxidized-Si(100) surfaces. This is mainly because the interfacial atomic mixing is negligible when 100 water molecules are involved and the system temperature is low (Figures 4-8 and 4-9). At these conditions, the sliding interface is highly hydroxylated.

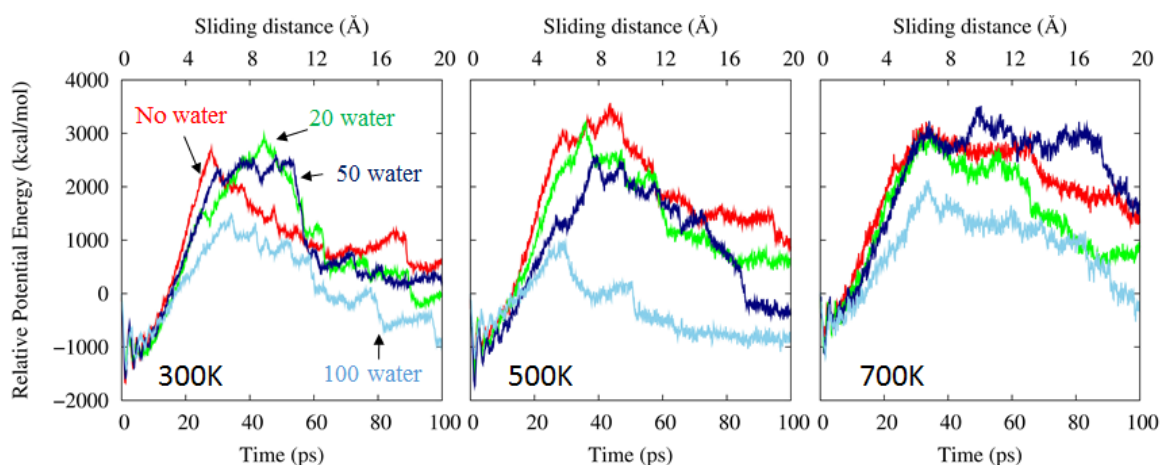


Figure 4-13. Changes in potential energy of the system during the separation, for the systems of 0, 20, 50, and 100 water molecules at 300K, 500K, and 700K.

Potential energy changes during the vertical separation at a 20 m/s speed are plotted in Figure 4-13. In the first 10 – 15 ps, the potential energy of the system decreases in an oscillatory fashion. This is due to the relief of the compressive stress (1 GPa) and tangential shear (10 m/s) applied to the interface. After this period, the potential energy of the system increases as the Si-O-Si chains are stretched, and decreases as the Si-O-Si chains bridging two surfaces are broken upon further increase of the distance between two surfaces. It is noted that in the case of 100 interfacial water molecules, the potential energy increase is much smaller. Again, this is due to the lack of interfacial mixing during the sliding and stretching of Si-O-Si chains during the separation. The slow decrease in potential energy after 50 ps is due to the structural relaxation of the two separated surfaces.

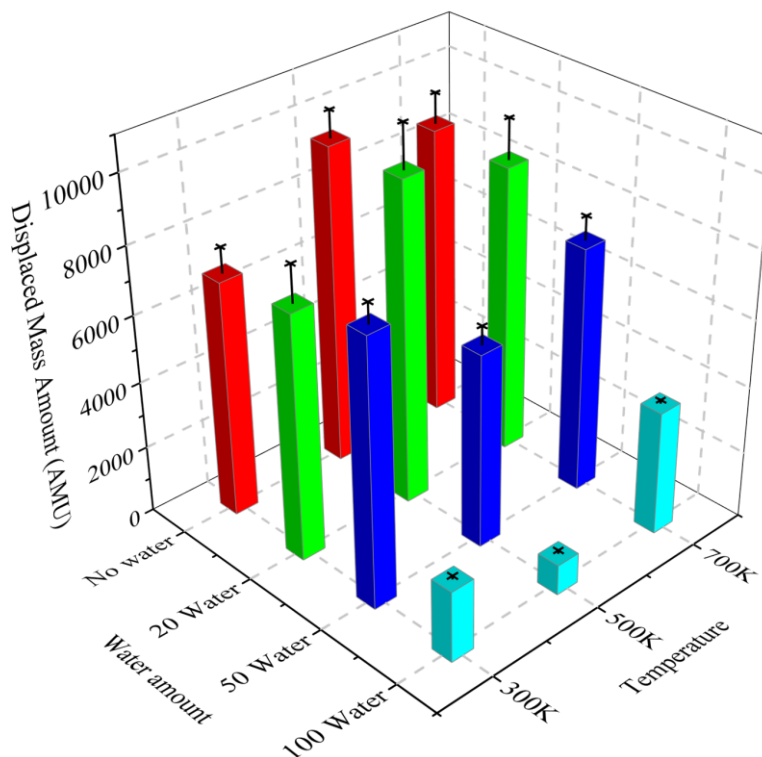


Figure 4-14. Total amount of atoms displaced from their original surfaces after sliding at a speed of 10 m/s for 1 ns followed by vertical separation at 20 m/s for 100 ps. The applied load normal to the surface was 1 GPa.

Since ReaxFF-MD simulations were done in the NVT ensemble, there is no mass loss from the simulation box. The amount of wear that can be related to experimental data could be defined by the amount of atoms displaced or removed from the original surface after the vertical separation of the two surfaces by 2 nm (100 ps at a 20 m/s speed). Again, the atom connectivity algorithm was used to calculate the amount of atoms dissociated from their original solid surface. The calculation results are plotted in Figure 4-14. When there were Si-O-Si chains still bridging two solid surfaces, a half of their mass was included in the removed mass and the other half was considered as the error of the calculation (plotted as error bar in Figure 4-14).

The data summarized in Figure 4-14 reveals many interesting trends for the consequences of tribochemical reactions occurred during the sliding of the a-SiO₂ surface against the oxidized-

Si(100) surface at various temperature and interfacial water conditions. In the dry sliding case, ReaxFF-MD simulations indicate substantial amount of wear of the silicon substrate. This result is consistent with the experimental data observed in the macroscale ball-on-flat tribo-test.¹¹¹ However, this result is not in agreement with the nanoscale AFM test results.⁴⁴ It should be noted that the AFM test is more susceptible to a trace amount of organic contaminants present at the solid surface. Also, the sliding speed in the AFM test is extremely slow (on the order of $10^{-8} - 10^{-5}$ m/s); so the relaxation dynamics of the mechanically sheared interface might be different. We have attempted simulations for the 1 m/s speed for the interfacial shear in the dry condition. The simulation results were very similar to the 10 m/s speed case shown in this paper; but, the simulation time took 10 times longer. Simulating extremely slow sliding speed is still challenge in MD simulations.¹¹²

As interfacial water molecules are introduced, the wear of the silicon wafer is increased. This is congruent with both nanoscale AFM and macroscale ball-on-flat tribo-tests.^{23,25,44} However, the shear-induced tribochemical reaction dynamics are much more complicated than the simple schematic mechanism proposed in the previous AFM study.^{24,108} ReaxFF-MD simulations reveal that the atom transfer across the sliding interface takes place readily during the sliding. This atomic mixing process is enhanced in the presence of sub-monolayer of interfacial water molecules in the sliding interface, resulting in more wear. The exception from this trend is the 700 K case, where the thermal energy is already high enough to drive large amounts of interfacial atom transfer reactions even in the absence of water molecules. The presence of small amounts of interfacial water molecules can enhance atom transfer or mixing process (Figure 4-9), and so does wear (Figure 4-14), since they can provide additional reactions leading to the formation of covalent bonds bridging two solid surfaces.

When the amount of interfacial water molecules is increased large enough for full coverage of the sliding interface, then the shear-induced atom transfer reactions are accompanied with water dissociation and surface hydroxylation reactions. Thus, the connectivity between the α -SiO₂ and oxidized-Si(100) surfaces is reduced (Figure 4-8), which results in the significant reduction of wear (Figure 4-14). This simulation result explains well the experimental observation made with AFM – reduction of wear at high humidity or in liquid water.²⁵

It is interesting to note that in macroscale ball-on-flat wear tests for soda lime silica glass, the wear was observed to decrease as relative humidity was increased.^{29,113} This observation appears to be consistent with the current ReaxFF-MD simulations. However, it should be noted that the current simulations does not include sodium ions; ¹¹⁴ more thorough and realistic simulations for tribochemical reactions of soda lime glass requires the formulation of a Na/Si/O/H force field, which is not currently available and beyond the scope of this study.

Chapter 5

Development of a ReaxFF description for fluorine etching

5.1. Introduction to force field development

The quality of the parameters in the force field is critical, since it determines the overall accuracy of result of simulations. It is essential to check and validate the credibility of the force field before we start any meaningful simulation by training and validating against DFT or any level of quantum mechanics calculation. If the force field fails to predict the expected value, then the parameters of the force field should be fitted with experimental and QM results using a training set. Typically, this training set contains bond dissociation / angle / torsion energies, equation of state, heat of formation and energy relations for important species, reaction barrier and reaction pathway, and transition state results.

The parameters of the force fields are optimized with continuous single-parameter search algorithm.¹¹⁵ The error function for the training set, to minimize the error values between ReaxFF value and QM value, is shown in equation 3.1

$$\text{Error} = \sum_i^n \left(\frac{X_{i,\text{QM}} - X_{i,\text{ReaxFF}}}{\sigma_i} \right)^2, i = 1, 2, 3 \dots n \quad (3.1)$$

Where the $X_{i,\text{QM}}$ is the any energy or values from experiment / quantum mechanics software, while the $X_{i,\text{ReaxFF}}$ is the values from ReaxFF calculation. σ_i is the weight value assigned to each data point. Experimental or quantum mechanics data for force field training are usually gathered from literature and papers, or obtained from research collaborators, or calculated by using QM softwares. Typically, well trained parameters of ReaxFF should reach the comparable

level of energy values when compare to QM or experimental values, within 2 kcal/mol for important heat of formation or energy curves / relations, and 5 kcal/mol for general reaction barriers.

5.2. Force field optimization of Si/F parameters

In order to accurately predict the Si- F interactions during etching simulations, based on previously developed water branch force field developed for silica - water reactions,¹ we trained the several important reaction relations for Si-F system. We trained the bond dissociation, off-diagonal, angle parameters in the SiF₄ and Si₂F₆ molecular structures, as well as 1fold, 2fold, and 4fold SiF energies of a Fluorine atom on Si(100) surface. We also included the DFT data for the SiF, SiF₂, SiF₃ on the reconstructed Si 001 surface, and the heat of formation for SiF₄, SiF₅ to correctly describe the product of etching reaction on the silicon / silica surface. The parameters we trained are the Si-F sigma bond and off diagonal, F-Si-F angle, F-Si-Si angle, F-Si-Si-F and F-Si-Si-F torsions.

Figure 5-1 shows the energy curve for bond dissociation of Si-F from SiF₄, F-Si-F angle from SiF₄, and F-Si-Si angle from Si₂F₆. Used DFT values are calculated from commercial DFT software, Jaguar, using B3LYP functional and 6-311G ** basis set, following previous DFT level

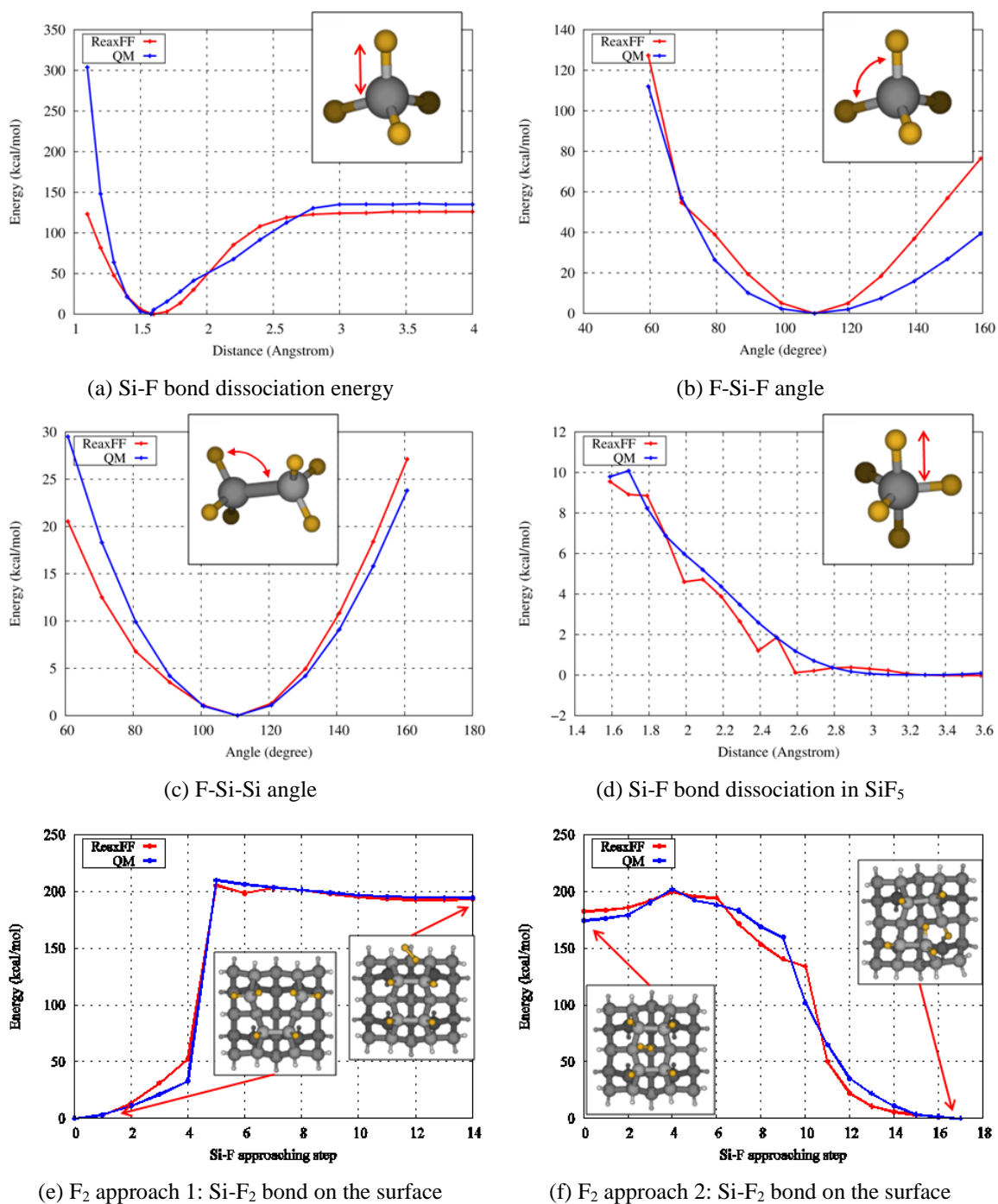
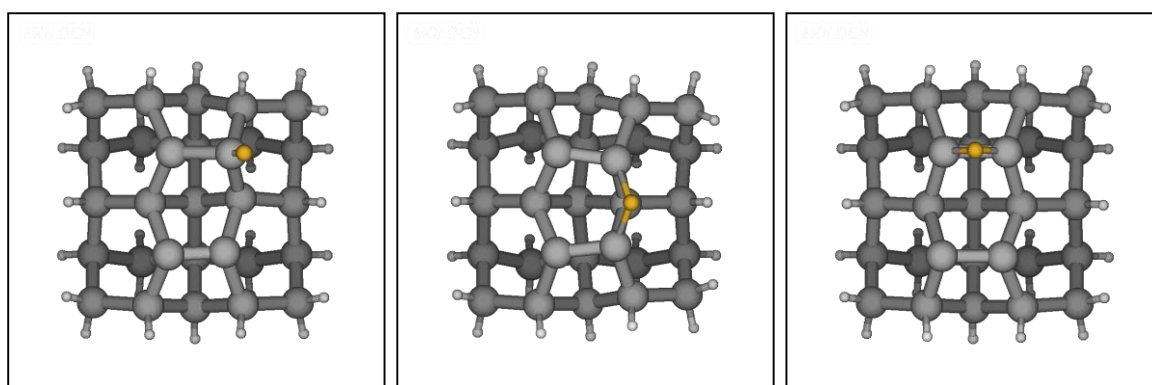


Figure 5-1. Energy curve for (a) Si-F bond dissociation, (b) F-Si-F angle, and (c) F-Si-Si angle, and (d) Si-F overcoordinated dissociation energy in SiF_5 . (e) SiF_2 formation on the surface 1, F_2 approach from edge, (f) SiF_2 formation on the surface 2, F_2 approach from center. Si-F bond energy and F-Si-F valence angle energies are calculated from SiF_4 , while F-Si-Si angle used Si_2F_6 molecule.

Si-F reaction energy studies.^{79,81} Table 5-1 represents the reaction energy relation and heat of formation for Si-F related system. Figure 5-2 shows the geometries for the Si-F training set. We found that ReaxFF successfully follows the energy relations and energy curves from DFT value for the most of the cases. Since too stable SiF₅ formation was a major problem of previous Si/F ReaxFF parameter sets, its energy curve and energy relations regarding SiF₅ has been intensively trained, allowing ReaxFF to correctly calculates the formation of SiF₄, and suppress

Geometry relation	ReaxFF (kcal/mol)	QM or expr. (kcal/mol)
Heat of formation of SiF ₄	-384.7	-386 ¹¹⁶
Heat of formation of SiF ₅	-24.5	-22.31
1fold F on Si(100)	115.3	109.5
2fold F on Si(100)	48	34.1
4fold F on Si(100)	79.1	72.4
SiF ₂ on Si(100) surface Si	602.7	641.4
SiF ₃ on Si(100) surface Si	1000.7	1005.1

Table 5-1. Various energy relation comparison between ReaxFF and QM after Si-F interaction training. (all kcal/mol)



(a) 1fold position F on H-terminated Si(100) slab

(b) 2fold bridge F on H-terminated Si(100)slab

(c) 2fold position F on H-terminated Si(100)slab

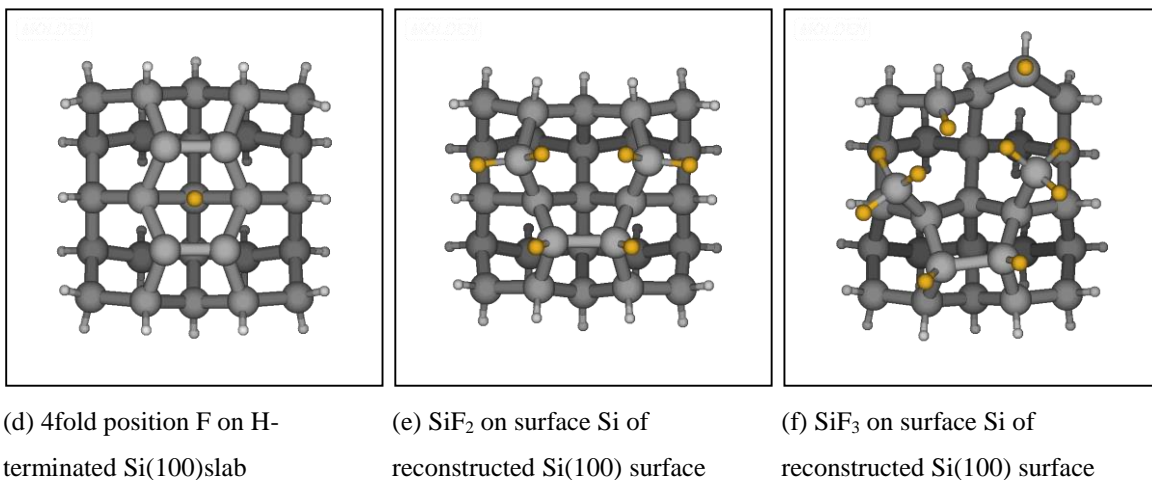


Figure 5-2. Pictures of geometries for Si-F trainset

the SiF₅ formation. Specially, optimization of van der Waals energy parameters was crucial, because the inclination of vdW parameter repaired stable-SiF₅ issue, but at the same time, it deteriorates the Si-F dissociation energy, which could lead poor Si-F interaction. We carefully trained the vdW and bond dissociation parameters, so that the Si-F bond energy curve and formation of SiF₅ are fixed at the same time.

5.3. Force field optimization for F/F and H/F interaction

After several test simulations of gas phase HF molecules and F₂ molecules, we found the clustering anomalies of those gas molecules as shown in figure 3-3 resulting in the crash of the MD simulation. To fix those problems we performed successive training for HF and FF interaction parameters. While the F₂ molecular interactions issue was relatively easy to solve, the HF accumulation problem at room temperature was more problematic. After checking the training results file, we found the divergence of temperature and energy values regarding

accumulated molecules, which was caused by excessive Coulomb energy and charge energy of the system.

To solve this issue, we trained the H-F and F-F bond parameters, H-F off diagonal, F-F-F angle, H-F-H angle, F-H-F angle and H-F-F angle, as well as H-F-H hydrogen bond parameters. Atomic parameters for shielding, electronegativity, and hardness of F was also included in the optimization.

The figure 5-4 shows the energy curves of important bond dissociation energy curves, as well as table 5-2 provides energy comparison of the unphysical molecular clusters, between before and after force field optimization. Optimization successfully stabilized the HF and F₂ molecule's behavior, and no more unphysical accumulation problems were reported.

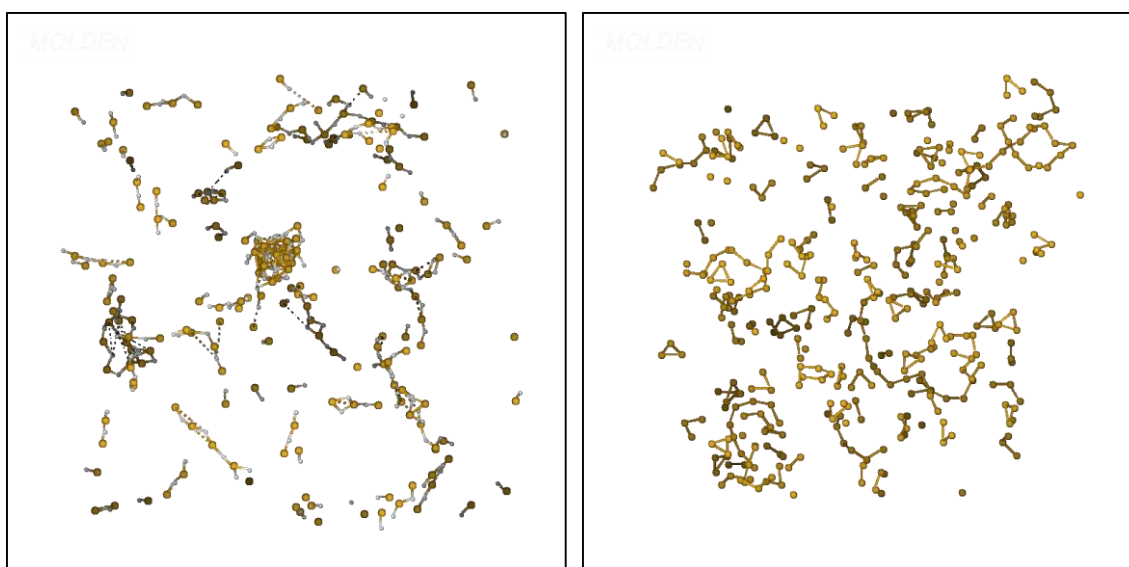


Figure 5-3. (a) Clustering anomalies of HF molecules (left), and (b) F₂ molecules (right)

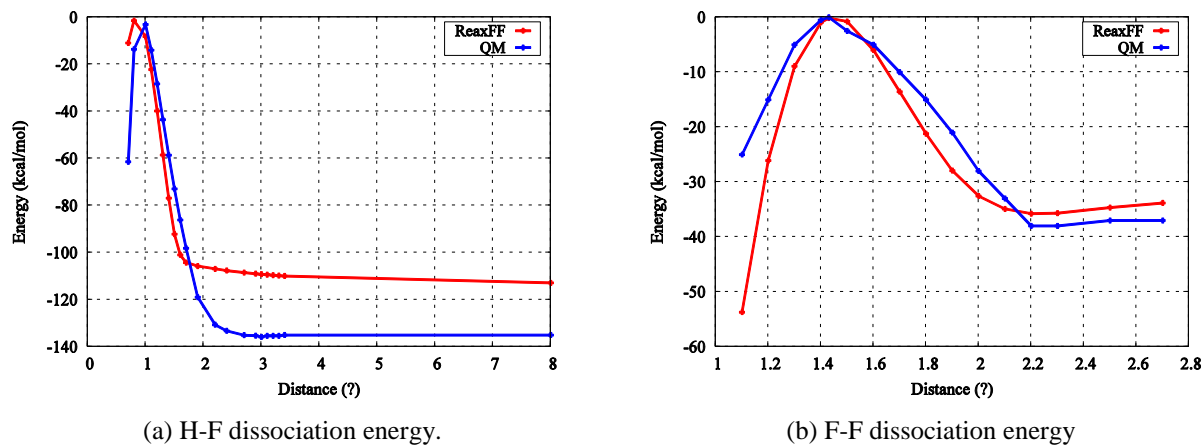


Figure 5-4. Energy curve for ReaxFF and QM comparison

Geometry relation	ReaxFF before	ReaxFF after
20 HF accumulated cluster	-56.3	129.4
5 HF accumulated cluster	-19.1	87.8
3 HF accumulated cluster	-9.6	72.3
20 F ₂ linear chain	-33.8	201.8
10 F ₂ linear chain	-16	90.3
3 F ₂ linear chain	-10.8	49

Table 5-2. Various relative energy comparison before / after training of ReaxFF force field. Those energies were compared with same number of isolated HF or F₂ molecules.

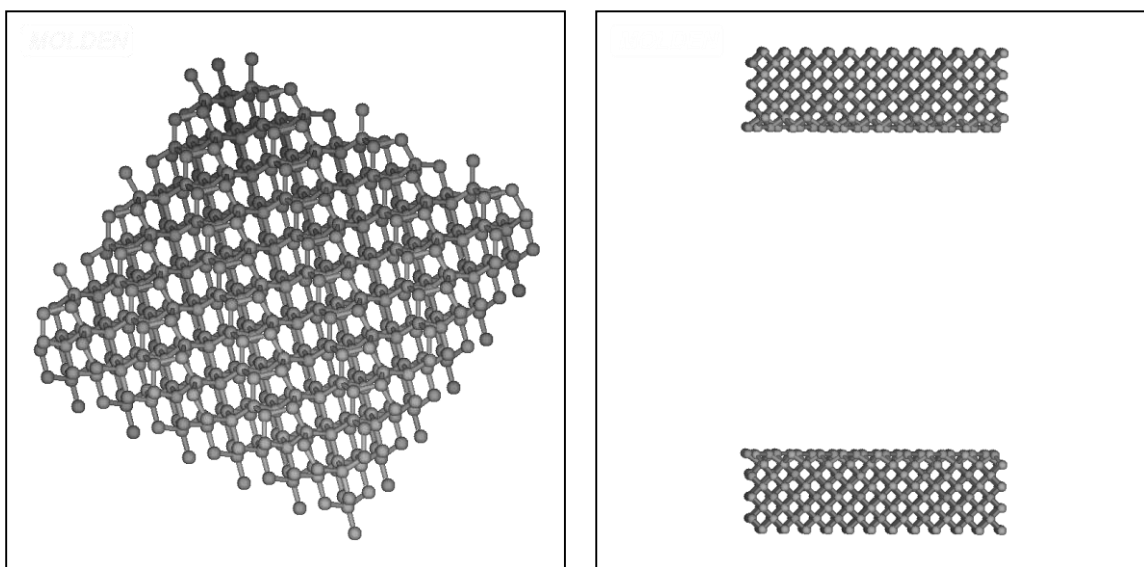
5.4. Etching of Si 001 surface using F₂ and HF molecule

Using the force field developed and discussed in chapter 3.1 and 3.2 of this paper, with improved Si-F, H-F, and F-F parameters, we performed ReaxFF NVT MD simulation, to observe how Fluorine atom etch the Silicon surfaces.

5.4.1. System Preparation

We prepared a double Si(100) slab with reconstructed surface Si atoms. Each slab has 576 Si atoms, placed within the dimension of $31.9\text{\AA} \times 31.9\text{\AA} \times 9.21\text{\AA}$, and the distance between two slabs were 40\AA . as shown in figure 4-21. The number of Si atoms in a very top layer was 72.

In this system, we placed 100, 200, 300, and 400 F_2 molecules in random positions, between two Si(100) slabs. The density of F_2 gas was 0.16, 0.32, 0.48, and 0.64 kg/dm^3 , respectively. All ReaxFF MD simulation was calculated under constant 1500K temperature with NVT ensemble, Nose-Hoover thermostat in LAMMPS environment. We used a 0.1fs time step, 10fs temperature damping constant, and total 200ps of simulation time. The system was pre-minimized with a Conjugate Gradient minimize before the MD simulation was performed.



(a) Si(100) surface with reconstructed Si atoms

(b) Double slit Si(100) system, total 1152 atoms

Figure 5-5. Si(100) slab with reconstructed surface Si atoms

5.4.2. Etching of Fluorine gas to Si(100) surface: ReaxFF MD simulation results

We observed active Si-F interactions on the Si(100) surface, and a significant amount of dissociation of Fluorine molecules. Figure 5-6 ~ 5-9 shows the results from the MD simulation with 100, 200, 300, and 400 F_2 molecules at 0, 50, 150, 200ps of simulation time.

According to these pictures, after 200ps simulation of etching process for different F_2 gas densities, we can make two observations. First, the etching is initiated by interaction between surface Si atom and F_2 molecule. Fluorine molecule approaches and interacts with Si on the surface, forms Si-F bond, and then one of the F atom is dissociated after a very short-lived unstable over-coordinated state. Secondly, the density of Fluorine gas affects the etching process, since at high density of F_2 gas, we observe the creation of significant amounts of F anions in the vacuum which easily react with Si on the surface. This can be also seen in figure 5-10, which shows the number of F_2 , F, and SiF_4 during simulation.

According to figure 4-10, F atoms were formed at the earlier stage of simulation, by unstable Si- F_2 direct interaction, which rapidly expels the F atom to the vacuum. A maximum 19 F atoms were observed from 100 F_2 simulation, 32 F atoms from 200 F_2 , 50 F atoms from 300 F_2 ,

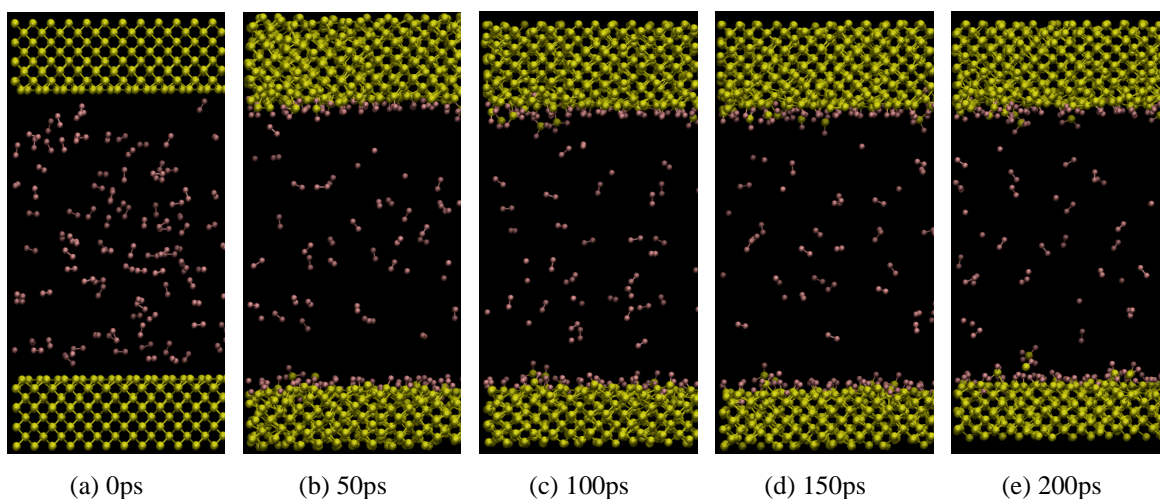


Figure 5-6. Result features of the etching of Si(100) slab with 100 F_2 molecules.

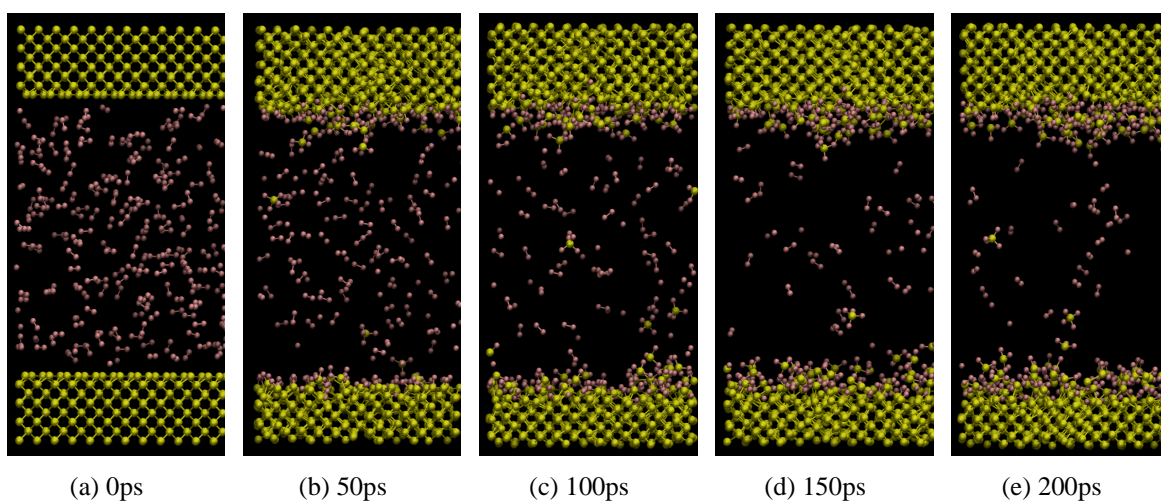


Figure 5-7. Result features of the etching of Si(100) slab with 200 F₂ molecules.

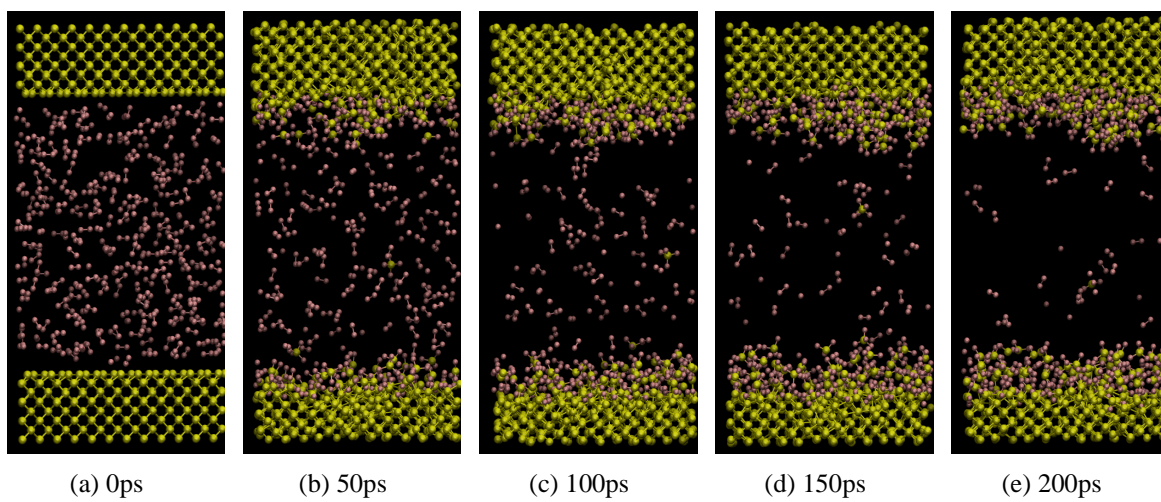
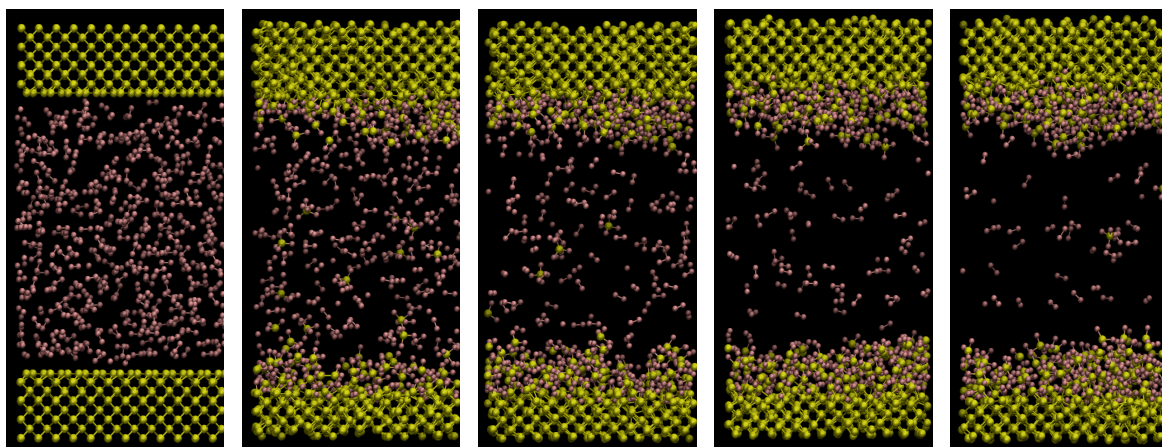


Figure 5-8. Result features of the etching of Si(100) slab with 300 F₂ molecules.



(a) 0ps (b) 50ps (c) 100ps (d) 150ps (e) 200ps

Figure 5-9. Result features of the etching of Si(100) slab with 400 F₂ molecules.

and 55 F atoms from 400 F₂ simulation. It is observable that 400 F₂ simulation shows the fastest decreasing speed of F atoms during simulation, which means that F atoms are more likely to react in the case of high density of F₂ molecules. This is in agreement with a previous study on ReaxFF simulations of Ti-Cl etching.⁹¹ Pictures of the etched surface can be checked in figure 5-11. Here, we observed numerous dangling F atoms on the surface, as well as Si-F₂ and Si-F₃ structure on the surface. F atoms break the Si-Si bonds, and form a 'mixing layer' made up of Si-F₂ and Si-F₃ structures between F₂ gas and Si substrates.

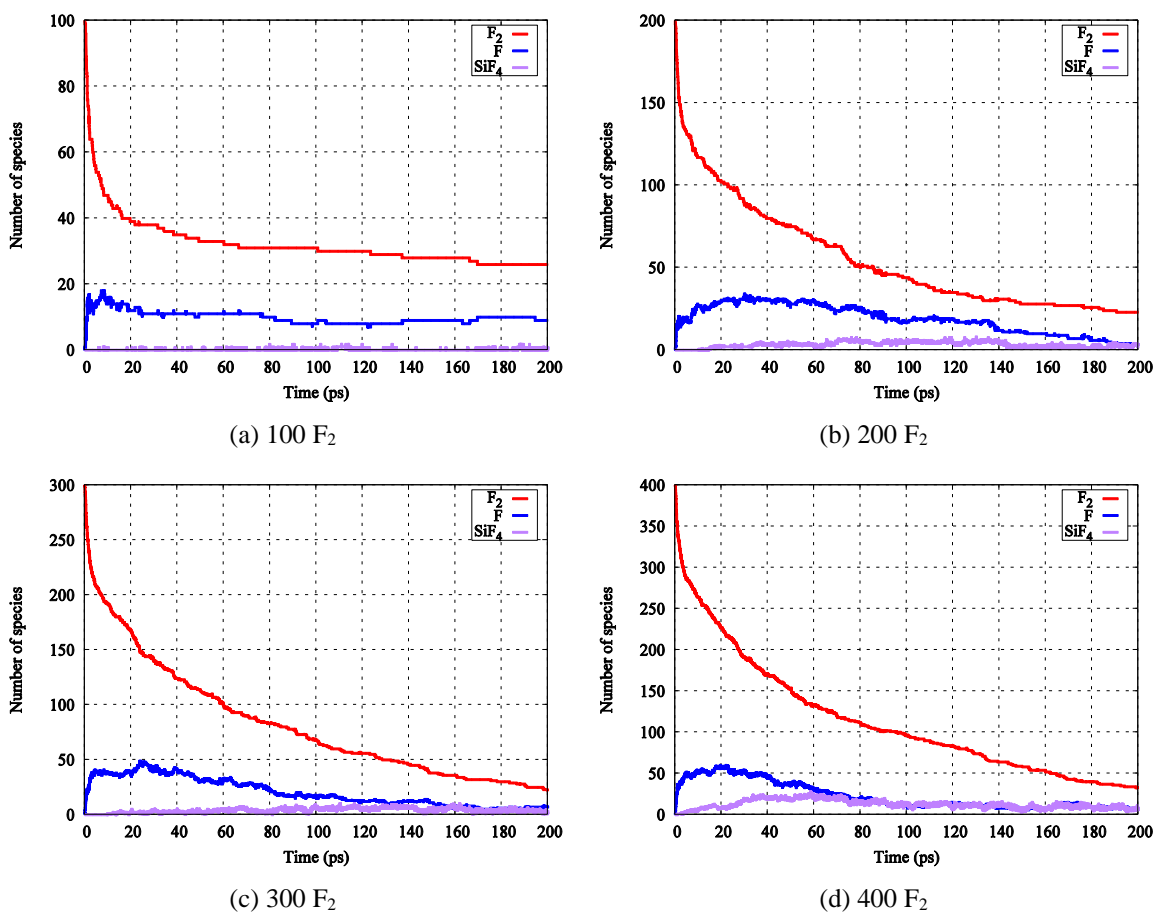
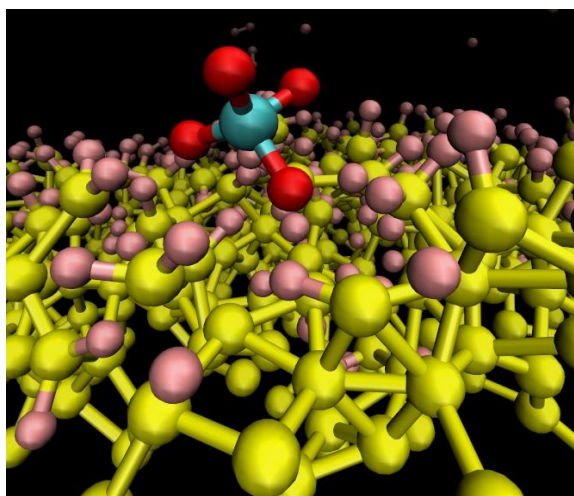
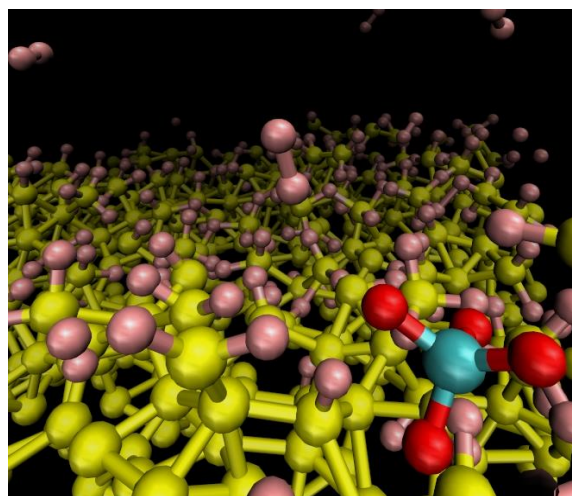


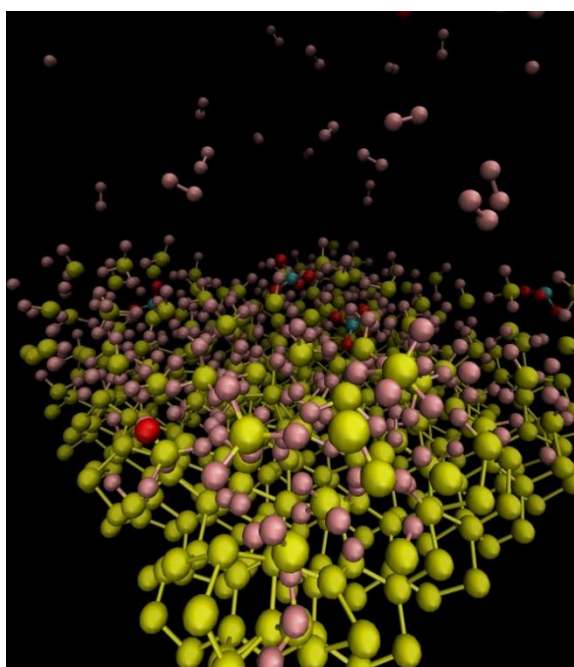
Figure 5-10. Number of species during etching simulations for different F_2 density. Decreasing speed of F atoms, which means adsorption of F anions to the surface, is faster in 400 F_2 simulation results than others.



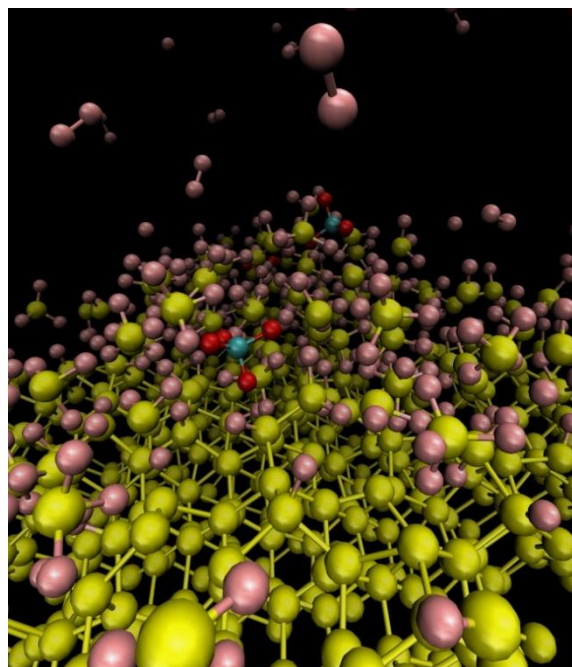
(a) Surface feature from 200 F_2 simulation, 200ps 1



(b) Surface feature from 200 F_2 simulation, 200ps 2



(c) Surface feature from 400 F_2 simulation, 200ps 1



(d) Surface feature from 400 F_2 simulation, 200ps 2

Figure 5-11. Surface features from etching simulation after 200ps. Yellow = Si, Pink = F, Cyan = Si of SiF_4 , and Red = F of SiF_4

Aside from SiF_4 , large amount of other Si-F related molecules were detected, such as SiF_3 , SiF_2 , Si_2F_6 , Si_2F_7 , and Si_3F_{10} . All of them were unstable, dissociated or reattached to the stable state shortly after formation.

On the other hand, we found the several Si-F-Si bridge structures on the surface, which survived for 2~3 ps of the time. This might effect on the etching reaction in a way to suppress the diffusion of F atoms penetrate into the inner layer of Si slab, which bring the rapid etching reaction of the Si slab. As a result, some of current force field parameters regarding Si-F-Si related energies are currently being re-evaluated, to test the feasibility of these Si-F-Si bridge structures. In addition, etching simulation using HF, and longer simulation to compare.

The importance of proper Si-F, F-F, and H-F force field is not only for atomic scale research of etching, but also for the various surface chemistry research. For example, proper Si-F parameters will greatly important to simulate mechano-chemical reaction during sliding and friction, since the many surface coating materials for Si based wafer system contains F atoms. In addition, with the accurate description of Si-F-water interaction, we could reveal the new reaction pathways for the lubrication for various lubricating materials, such as ZDDP.

Chapter 6

Conclusion

We performed ReaxFF-based molecular dynamics (MD) simulations for hydrolysis reactions on the SiO₂/water interface, using both silica nano wire and an amorphous silica slab. First, we provided additional data for the validation of the ReaxFF SiO₂/water model, by comparison with experimental results and DFT data. Specifically, the energy barrier for the hydroxylation for both strained silica dimer and non-strained silica dimer is added to the training set, resulting in more reliable description for the hydroxylation reaction. After retraining, both ReaxFF and DFT showed 20 kcal/mol and 30 kcal/mol of energy barrier for the hydroxylation on the strained and non-strained silica dimer, respectively.

These results indicate that the hydroxylation reaction is more favorable for strained silica compared to that at a non-strained local environment. We observed that a highly strained edge area is preferentially responsible for silanol formation, rather than the lower-strain silicon atoms in the body of the nano wire.

In addition, we detected three specific hydroxylation paths. First, we observed the silanol formation initiated from adsorbed water molecule, forming a hydronium ion by donating its proton to a nearby water molecule, leaving silanol on the surface, and forming –usually solvated - H₃O⁺ as a product. The second path for silanol formation was the dissociation of hydronium ion. A H₃O⁺, formed in the first method of silanol formation, donates one of H ions to the bridge oxygen on the surface, creating silanol on the donated spot, and leaving a water molecule as a product. The third method of silanol formation was the direct dissociation of an adsorbed water

molecule. After adsorption, one of the H of Si-H₂O moves to bridge oxygen, forming two silanols at once.

We observed a strong relationship between the temperature of system, the reaction pathway for the hydroxylation, and the existence of water clusters. Our result implies that high temperatures (>1200K) induced the dissociation of hydrogen bond network, as well as water cluster structures. This indicated the reduced number of hydronium ions, and direct dissociation of adsorbed water molecule become major hydrolysis pathway at such temperature. Meanwhile, from 500K to 1000K of the temperature range, the existence of water dimer and nearby water molecules played important role on hydrolysis reaction involving H₃O⁺ ions. Due to water clusters, water molecules easily find the target – nearby water molecules- for the donation or adsorption of proton ions, inducing the formation and dissociation of hydronium ions. This may suggest the existence of optimum temperature for water – Si interactions.

To investigate the trends of silanol formation on a larger silica structure, an amorphous SiO₂ slab was prepared by ReaxFF simulation. Bulk properties of the surface and slabs were compared to and validated with the experimental results. MD simulations on the interaction of water molecules with the amorphous silica slab confirm that the hydroxyl groups on the silica surface favor the locally strained SiO₂ structure and undercoordinated silicon atoms. The comparison between the surface strain energy map and silanol formation map supports this phenomenon; the silanol formation sites match with the locations of the more highly strained Si atoms. We also observed proton hopping events among the water molecules, producing reactive hydronium molecules, which can donate a proton to the surface oxygen atoms. Highly strained oxygen atoms and undercoordinated oxygen atoms can also be capable of receiving a proton from water. These observations agree with those from the simulation using the silica nano wire, as well as previous studies reported by other researchers.⁶⁵

ReaxFF MD simulation of sliding and separation between a-SiO₂ slab and Si(100) slab was performed, under various temperature and humidity condition.

During sliding phase, considerable amount of mixing and mass transport between two surfaces was observed. Based on our analysis, the amount of mixing is highly depending on boundary condition: temperature and amount of water. Under 300K and 500K condition, small amount of water molecules facilitated the mixing, while the simulation with 100 water molecules showed less amount of mixing. Various reaction pathways for mixing of Si and O atoms were detected during sliding, which include the dehydroxylation of surface, and Si-O-Si connection between two slabs, with O from water molecules. Under 700K condition, however, high temperature influence the mixing result. Due to intense vibration, dry case showed huge amount of mixing, as well as 100 water case brought comparable amount of mixing as the water molecules quickly adsorbed to the surface by hydroxylation.

During separation, under specific conditions, numerous chain-like Si-O column structures and massive surface wear from Si(100) slab were observed. Mixed Si-O connections formed strong mixed region. As a result, weaker Si-Si bonds were dissociated during separation, leading surface damage to the Si(100) slab. Based on our observation, mixed atoms were the source of wear. Generally, amount of wear mass weakly followed the trends of amount of mixed atoms.

This result indicates that the amount of wear mass has weak relationship with the amount of mixing, which was promoted by small amount of water molecules. In other words, small number of water molecules is possible to stimulate the damage of surface during friction. This result supports the observation from previous experimental studies.

Friction force and friction coefficients are available to calculate from ReaxFF MD simulation, but their time scale is limited to compare with any experimental counterparts. In addition, such properties in instantaneous scale of 1ns accompany intense fluctuations. To

achieve the meaningful study of frictional properties in MD scale and comparison with experiment, it is needed to increase the time scale of MD simulation, such as PRD method¹¹⁷, or metadynamics.¹¹⁸ As a future plan, we will investigate to apply PRD or metadynamics method to ReaxFF for sliding simulation.

We optimized a ReaxFF force field parameters for Si/F/H/O system and etching reaction, using DFT data. The training set for these systems contain reaction energy curves of Si-F bond dissociation, F-Si-F angle, F-Si-Si angle, binding energy of F on Si slab, and various energy relation of Si/F system. We also trained our force field to simulate the behavior of HF and F₂ molecules accurately, preventing abnormal accumulation and clustering of those molecules. HF-HF and F₂ - F₂ molecular interaction energies, bond dissociation energy, hydrogen bonding energy and valence angle energy regarding H and F are included in the training set, as well as electronegativity, shielding and hardness parameters of F atom are optimized.

After the optimization of force field, NVT MD simulation for the etching of Si(100) slab was performed with reconstructed Si surface and F₂ molecules. Etching simulation shows the formation of SiF₄ molecules as a product of etching, as well as the atomized F atoms in the vacuum. The formation of F atoms are coming from F₂ - surface Si interaction, as the F₂ easily dissociated after contacts with surface Si atoms. F atoms dissociated from F₂ also react with Si atoms, forming more SiF, SiF₂ or SiF₃ on the surface.

We tested 4 different amount of F₂ gas molecules, 100 F₂, 200 F₂, 300 F₂, and 400 F₂ molecules. We found that the dissociated F atoms are reacting faster with Si atoms in high density F₂ gas case, than lower density case. As a result, the Si/F etching become more reactive as the density of F₂ increases.

References

- (1) Fogarty, J.; Aktulga, H.; Grama, A. A Reactive Molecular Dynamics Simulation of the Silica-Water Interface. *J. Chem.* **2010**, *132* (17), 174704.
- (2) Persson, B. N. J. Theory of Friction: Stress Domains, Relaxation, and Creep. *Phys. Rev. B* **1995**, *51* (19), 13568–13585.
- (3) Rabinowicz, E. *Friction and Wear of Materials*; John Wiley and Sons INC, 1995.
- (4) Hutchings, I. M. *Tribology: Friction and Wear of Engineering Materials*; CRC Press, Boca Raton, FL, 1992.
- (5) Bhushan, B. Nanotribology and Nanomechanics of MEMS/NEMS and BioMEMS/BioNEMS Materials and Devices. *Microelectron. Eng.* **2007**, *84* (3), 387–412.
- (6) Jacob N. Israelachvili. *Intermolecular and Surface Forces*; Elsevier INC, 2011.
- (7) Li, Y. Experimental Studies on Relationships between the Electron Work Function, Adhesion, and Friction for 3d Transition Metals. *J. Appl. Phys.* **2004**, *95* (12), 7961.
- (8) Han, T.-Z.; Dong, G.-C.; Shen, Q.-T.; Zhang, Y.-F.; Jia, J.-F.; Xue, Q.-K. Adhesion Modulation by Quantum Size Effects in PbSi(111) System. *Appl. Phys. Lett.* **2006**, *89* (18), 183109.
- (9) Barthel, A. J.; Al-Azizi, A.; Surdyka, N. D.; Kim, S. H. Effects of Gas or Vapor Adsorption on Adhesion, Friction, and Wear of Solid Interfaces. *Langmuir* **2014**, *30* (11), 2977–2992.
- (10) Alazizi, A.; Barthel, A. J.; Surdyka, N. D.; Luo, J.; Kim, S. H. Vapors in the Ambient - A Complication in Tribological Studies or an Engineering Solution of Tribological Problems? *Friction* **2015**, *3* (2), 85–114.
- (11) Iler, R. K. *The Chemistry of Silica*; John Wiley and Sons INC, 1979.
- (12) Kurkjian, C.; Krause, J. Tensile Strength Characteristics of “Perfect” Silica Fibers. *J. Phys. Colloq.* **1982**, *43* (C9), 585–586.
- (13) Bunker, B. C.; Rieke, P. C.; Tarasevich, B. J.; Campbell, A. A.; Fryxell, G. E.; Graff, G. L.; Song, L.; Liu, J.; Virden, J. W.; McVay, G. L. Ceramic Thin-Film Formation on Functionalized Interfaces through Biomimetic Processing. *Science*. **1994**, *264* (5155), 48–55.
- (14) Bhushan, B. *Modern Tribology Handbook*; Bhushan, B., Ed.; CRC Press, 2001.
- (15) Williams, J. a.; Le, H. Tribology and MEMS. *J. Phys. D. Appl. Phys.* **2006**, *39* (12), 201–214.
- (16) Kaneko, R.; Umemura, S.; Hirano, M.; Andoh, Y.; Miyamoto, T.; Fukui, S. Recent Progress in Microtribology. *Wear* **1996**, *200* (1-2), 296–304.

- (17) Tanaka, H.; Shimada, S.; Anthony, L. Requirements for Ductile-Mode Machining Based on Deformation Analysis of Mono-Crystalline Silicon by Molecular Dynamics Simulation. *CIRP Ann. - Manuf. Technol.* **2007**, *56* (1), 53–56.
- (18) Bhushan, B.; Israelachvili, J. N.; Landman, U. Nanotribology: Friction, Wear and Lubrication at the Atomic Scale. *Nature* **1995**, *374* (13), 607–616.
- (19) Ribeiro, R.; Shan, Z.; Minor, a. M.; Liang, H. In Situ Observation of Nano-Abrasive Wear. *Wear* **2007**, *263* (7-12), 1556–1559.
- (20) Zhang, L.; Tanaka, H. Atomic Scale Deformation in Silicon Monocrystals Induced by Two-Body and Three-Body Contact Sliding. *Tribol. Int.* **1998**, *31* (8), 425–433.
- (21) Eder, S. J.; Feldbauer, G.; Bianchi, D.; Cihak-Bayr, U.; Betz, G.; Vernes, a. Applicability of Macroscopic Wear and Friction Laws on the Atomic Length Scale. *Phys. Rev. Lett.* **2015**, *115* (2), 025502.
- (22) Yu, J. X.; Qian, L. M.; Yu, B. J.; Zhou, Z. R. Nanofretting Behaviors of Monocrystalline Silicon (1 0 0) against Diamond Tips in Atmosphere and Vacuum. *Wear* **2009**, *267* (1-4), 322–329.
- (23) Barnette, A. L.; Asay, D. B.; Kim, D.; Guyer, B. D.; Lim, H.; Janik, M. J.; Kim, S. H. Experimental and Density Functional Theory Study of the Tribochemical Wear Behavior of SiO₂ in Humid and Alcohol Vapor Environments. *Langmuir* **2009**, *25* (22), 13052–13061.
- (24) Yu, J.; Kim, S. H.; Yu, B.; Qian, L.; Zhou, Z. Role of Tribochemistry in Nanowear of Single-Crystalline Silicon. *ACS Appl. Mater. Interfaces* **2012**, *4* (3), 1585–1593.
- (25) Wang, X.; Kim, S. H.; Chen, C.; Chen, L.; He, H.; Qian, L. Humidity Dependence of Tribochemical Wear of Monocrystalline Silicon. *ACS Appl. Mater. Interfaces* **2015**, *7* (27), 14785–14792.
- (26) Chen, L.; He, H.; Wang, X.; Kim, S. H.; Qian, L. Tribology of Si/SiO₂ in Humid Air : Transition from Severe Chemical Wear to Wearless Behavior at Nanoscale. *Langmuir* **2015**, *31* (1), 149–156.
- (27) Barnette, A. L.; Ohlhausen, J. A.; Dugger, M. T.; Kim, S. H. Humidity Effects on In Situ Vapor Phase Lubrication with N-Pentanol. *Tribol. Lett.* **2014**, *55* (1), 177–186.
- (28) Chen, L.; Yang, Y. J.; He, H. T.; Kim, S. H.; Qian, L. M. Effect of Coadsorption of Water and Alcohol Vapor on the Nanowear of Silicon. *Wear* **2015**, *332-333*, 879–884.
- (29) Bradley, L. C.; Dilworth, Z. R.; Barnette, A. L.; Hsiao, E.; Barthel, A. J.; Pantano, C. G.; Kim, S. H. Hydronium Ions in Soda-Lime Silicate Glass Surfaces. *J. Am. Ceram. Soc.* **2013**, *96* (2), 458–463.
- (30) Nian, J.; Si, Y.; Guo, Z. Advances in Atomic-Scale Tribological Mechanisms of Solid Interfaces. *Tribol. Int.* **2015**, *94* (1), 1–13.
- (31) Mo, Y.; Turner, K. T.; Szlufarska, I. Friction Laws at the Nanoscale. *Nature* **2009**, *457* (7233), 1116–1119.
- (32) Chandross, M.; Webb, E.; Stevens, M.; Grest, G.; Garofalini, S. Systematic Study of the

- Effect of Disorder on Nanotribology of Self-Assembled Monolayers. *Phys. Rev. Lett.* **2004**, *93* (16), 166103.
- (33) Chandross, M.; Grest, G. S.; Stevens, M. J. Friction between Alkylsilane Monolayers: Molecular Simulation of Ordered Monolayers. *Langmuir* **2002**, *18* (22), 8392–8399.
- (34) Lan, H. Q.; Liu, C.; Kato, T. Simulations on Sliding Process between Si-DLC and DLC Films on a Water-Lubricated Condition. *Appl. Mech. Mater.* **2010**, *29-32*, 1408–1413.
- (35) Bucholz, E. W.; Phillpot, S. R.; Sinnott, S. B. Molecular Dynamics Investigation of the Lubrication Mechanism of Carbon Nano-Onions. *Comput. Mater. Sci.* **2012**, *54*, 91–96.
- (36) Gao, G. T.; Mikulski, P. T.; Harrison, J. a. Molecular-Scale Tribology of Amorphous Carbon Coatings: Effects of Film Thickness, Adhesion, and Long-Range Interactions. *J. Am. Chem. Soc.* **2002**, *124* (24), 7202–7209.
- (37) van Duin, A. C. T.; Dasgupta, S.; Lorant, F.; Goddard, W. a. ReaxFF: A Reactive Force Field for Hydrocarbons. *J. Phys. Chem. A* **2001**, *105* (41), 9396–9409.
- (38) Buehler, M. J.; Van Duin, A. C. T.; Goddard, W. a. Multiparadigm Modeling of Dynamical Crack Propagation in Silicon Using a Reactive Force Field. *Phys. Rev. Lett.* **2006**, *96* (9), 1–4.
- (39) Verners, O.; van Duin, A. C. T. Comparative Molecular Dynamics Study of Fcc-Ni Nanoplate Stress Corrosion in Water. *Surf. Sci.* **2015**, *633*, 94–101.
- (40) Liu, Y.; Szlufarska, I. Chemical Origins of Frictional Aging. *Phys. Rev. Lett.* **2012**, *109* (18), 186102.
- (41) Li, Q.; Tullis, T. E.; Goldsby, D.; Carpick, R. W. Frictional Ageing from Interfacial Bonding and the Origins of Rate and State Friction. *Nature* **2011**, *480* (7376), 233–236.
- (42) Yue, D. C.; Ma, T. B.; Hu, Y. Z.; Yeon, J.; Van Duin, A. C. T.; Wang, H.; Luo, J. Tribochemistry of Phosphoric Acid Sheared between Quartz Surfaces: A Reactive Molecular Dynamics Study. *J. Phys. Chem. C* **2013**, *117* (48), 25604–25614.
- (43) Yue, D.-C.; Ma, T.-B.; Hu, Y.-Z.; Yeon, J.; van Duin, A. C. T.; Wang, H.; Luo, J. Tribochemical Mechanism of Amorphous Silica Asperities in Aqueous Environment: A Reactive Molecular Dynamics Study. *Langmuir* **2015**, *31* (4), 1429–1436.
- (44) Chen, L.; He, H.; Wang, X.; Kim, S. H.; Qian, L. Tribology of Si/SiO₂ in Humid Air: Transition from Severe Chemical Wear to Wearless Behavior at Nanoscale. *Langmuir* **2015**, *31* (1), 149–156.
- (45) Cruz-Chu, E. R.; Aksimentiev, A.; Schulten, K. Ionic Current Rectification through Silica Nanopores. *J. Phys. Chem. C* **2009**, *113* (5), 1850–1862.
- (46) Bunker, B. Molecular Mechanisms for Corrosion of Silica and Silicate Glasses. *J. Non. Cryst. Solids* **1994**, *179*, 300–308.
- (47) Tan, W.; Wang, K.; He, X.; Zhao, X. J.; Drake, T.; Wang, L.; Bagwe, R. P. Bionanotechnology Based on Silica Nanoparticles. *Med. Res. Rev.* **2004**, *24* (5), 621–638.
- (48) Chanthateyanonth, R.; Alper, H. The First Synthesis of Stable palladium(II) PCP-Type

- Catalysts Supported on Silica—application to the Heck Reaction. *J. Mol. Catal. A Chem.* **2003**, *201* (1-2), 23–31.
- (49) Gaigeot, M.; Sprik, M.; Sulpizi, M. Oxide/water Interfaces: How the Surface Chemistry Modifies Interfacial Water Properties. *J. Phys. Condens. Matter* **2012**, *24* (12), 124106.
- (50) Sulpizi, M.; Gaigeot, M.-P.; Sprik, M. The Silica–Water Interface: How the Silanols Determine the Surface Acidity and Modulate the Water Properties. *J. Chem. Theory Comput.* **2012**, *8* (3), 1037–1047.
- (51) He, Y.; Cao, C.; Trickey, S. B.; Cheng, H.-P. Predictive First-Principles Simulations of Strain-Induced Phenomena at Water–Silica Nanotube Interfaces. *J. Chem. Phys.* **2008**, *129* (1), 011101.
- (52) Michalske, T.; Freiman, S. A Molecular Mechanism for Stress Corrosion in Vitreous Silica. *J. Am. Ceram. Soc.* **1983**, *66* (4), 284–288.
- (53) Michalske, T.; Freiman, S. A Molecular Interpretation of Stress Corrosion in Silica. *Nature* **1982**, *295* (11), 511–512.
- (54) Brown, M. A.; Huthwelker, T.; Redondo, A. B.; Janousch, M.; Faubel, M.; Arrell, C. A.; Scarongella, M.; Chergui, M.; Bokhoven, J. A. Changes in the Silanol Protonation State Measured In Situ at the Silica–Aqueous Interface. *J. Phys. Chem. Lett.* **2012**, *3* (2), 231–235.
- (55) Romero-Vargas Castrillón, S.; Giovambattista, N.; Aksay, I. a; Debenedetti, P. G. Effect of Surface Polarity on the Structure and Dynamics of Water in Nanoscale Confinement. *J. Phys. Chem. B* **2009**, *113* (5), 1438–1446.
- (56) Mischler, C.; Horbach, J.; Kob, W.; Binder, K. Water Adsorption on Amorphous Silica Surfaces: A Car–Parrinello Simulation Study. *J. Phys. Condens. Matter* **2005**, *17* (26), 4005–4013.
- (57) Du, M.-H.; Kolchin, A.; Cheng, H.-P. Hydrolysis of a Two-Membered Silica Ring on the Amorphous Silica Surface. *J. Chem. Phys.* **2004**, *120* (2), 1044–1054.
- (58) Ma, Y.; Foster, a S.; Nieminen, R. M. Reactions and Clustering of Water with Silica Surface. *J. Chem. Phys.* **2005**, *122* (14), 144709.
- (59) Musso, F.; Mignon, P.; Ugliengo, P.; Sodupe, M. Cooperative Effects at Water–crystalline Silica Interfaces Strengthen Surface Silanol Hydrogen Bonding. An Ab Initio Molecular Dynamics Study. *Phys. Chem. Chem. Phys.* **2012**, *14*, 10507–10514.
- (60) Mischler, C.; Kob, W.; Binder, K. Classical and Ab-Initio Molecular Dynamic Simulation of an Amorphous Silica Surface. *Comput. Phys. Commun.* **2002**, *147* (1-2), 222–225.
- (61) Du, J.; Cormack, A. N. Molecular Dynamics Simulation of the Structure and Hydroxylation of Silica Glass Surfaces. *J. Am. Ceram. Soc.* **2005**, *88* (9), 2532–2539.
- (62) Giovambattista, N.; Rossky, P. J.; Debenedetti, P. G. Effect of Temperature on the Structure and Phase Behavior of Water Confined by Hydrophobic, Hydrophilic, and Heterogeneous Surfaces. *J. Phys. Chem. B* **2009**, *113* (42), 13723–13734.
- (63) Huff, N. T.; Demiralp, E.; Çagin, T.; Goddard III, W. A. Factors Affecting Molecular

- Dynamics Simulated Vitreous Silica Structures. *J. Non. Cryst. Solids* **1999**, 253 (1-3), 133–142.
- (64) Mahadevan, T. S.; Garofalini, S. H. Dissociative Chemisorption of Water onto Silica Surfaces and Formation of Hydronium Ions. *J. Phys. Chem. C* **2008**, 112 (5), 1507–1515.
- (65) Lockwood, G. K.; Garofalini, S. H. Proton Dynamics at the Water Silica Interface via Dissociative Molecular Dynamics. *J. Phys. Chem. C* **2014**, 118 (51), 29750–29759.
- (66) Donnelly, V.; Kornblit, A. Plasma Etching: Yesterday, Today, and Tomorrow. *J. Vac. Sci. Technol. A* **2013**, 31 (5).
- (67) Jansen, H.; Gardeniers, H.; Boer, M. De; Elwenspoek, M.; Fluitman, J. A Survey on the Reactive Ion Etching of Silicon in Microtechnology. *J. Micromechanics Microengineering* **1996**, 6 (1), 14–28.
- (68) Harris, G. *Properties of Silicon Carbide*; INSPEC, 1995.
- (69) Kovacs, G. T. *Micromachined Transducers Sourcebook*; McGraw Hill New York, 1998.
- (70) Winters, H.; Coburn, J. Surface Science Aspects of Etching Reactions. *Surf. Sci. Rep.* **1992**, 14, 161–269.
- (71) Coburn, J. W.; Winters, H. F. The Role of Energetic Ion Bombardment in Silicon-Fluorine Chemistry. *Nucl. Instruments Methods Phys. Res. Sect. B Beam Interact. with Mater. Atoms* **1987**, 27 (1), 243–248.
- (72) Chang, J. P.; Coburn, J. W. Plasma–surface Interactions. *J. Vac. Sci. Technol. A Vacuum, Surfaces, Film.* **2003**, 21 (5), S145.
- (73) Jiang, L.; Plank, N. O. V.; Blauw, M. a.; Cheung, R.; Drift, E. Van Der. Dry Etching of SiC in Inductively Coupled Cl₂/Ar Plasma. *J. Phys. D. Appl. Phys.* **2004**, 37 (13), 1809–1814.
- (74) Williams, K.; Bray, J.; Venturo, V.; Fisher, E. Multiphoton Ionization Detection of SiF Radicals in SiF₄ Plasmas. *Chem. Phys. Lett.* **2000**, No. June, 137–144.
- (75) Gou, F.; Kleyn, a. W.; Gleeson, M. a. *The Application of Molecular Dynamics to the Study of Plasma–surface Interactions: CF_x with Silicon*; 2008; Vol. 27.
- (76) Gou, F.; Chen, L. Z. T.; Meng, C.; Qian, Q. Molecular Dynamics Simulations of Reactive Etching of SiC by Energetic Fluorine. *Appl. Phys. A* **2007**, 88 (2), 385–390.
- (77) Garrison, B. J.; Goddard, W. a. Dissociation Energetics of SiF Systems of Relevance to Etching Reactions. *J. Chem. Phys.* **1987**, 87 (2), 1307.
- (78) Garrison, J.; Goddard, W. A.; Amos, A.; Si, Q. Reaction Mechanism for Fluorine Etching of Silicon. *Phys. Rev. B* **1987**, 36 (18), 9805–9808.
- (79) King, R. a.; Mastryukov, V. S.; Schaefer, H. F. The Electron Affinities of the Silicon Fluorides SiF_n (n=1–5). *J. Chem. Phys.* **1996**, 105 (16), 6880.
- (80) Walsh, R. Bond Dissociation Energy Values in Silicon-Containing Compounds and Some of Their Implications. *Acc. Chem. Res.* **1981**, 1537 (4), 246–252.

- (81) Hiraoka, K.; Nasu, M.; Akihito, M.; Akitaka, S. On the Structure and Stability of Gas-Phase Cluster Ions SiF_3^+ (CO) N, $\text{SiF}_3\text{OH}_2^+$ (SiF₄) N, SiF_4H^+ (SiF₄) N, and F-(SiF₄) N. *J. Phys. Chem. A* **2000**, *104*, 8353–8359.
- (82) Darcy, a; Galijatovic, a; Barth, R.; Kenny, T.; Krantzman, K. D.; Schoolcraft, T. a. Molecular Dynamics Simulations of Silicon-Fluorine Etching. *J. Mol. Graph.* **1996**, *14* (5), 260–271, 278.
- (83) Abrams, C. F.; Graves, D. B. Molecular Dynamics Simulations of Si Etching by Energetic CF_3^+ . *J. Appl. Phys.* **1999**, *86* (11), 5938.
- (84) Gou, F.; Liang, M. C.; Chen, Z.; Qian, Q. Etching of SiC by Energetic F₂: Molecular Dynamics Simulation. *Appl. Surf. Sci.* **2007**, *253* (21), 8743–8748.
- (85) Gou, F.; Gleeson, M. a.; Kleyn, a. W. CF_3 Interaction with Si(100)-(2×1): Molecular Dynamics Simulation. *Surf. Sci.* **2007**, *601* (18), 4250–4255.
- (86) Zhao, C.; Deng, C.; Sun, W.; Zhang, J.; Chen, F.; He, P.; Chen, X.; Gou, F. Etching Mechanisms of CF_3 Etching Fluorinated Si: Molecular Dynamics Simulation. *Plasma Sci. Technol.* **2012**, *14* (7), 670–674.
- (87) Wu, C. J.; Carter, E. A. Mechanistic Predictions for Fluorine Etching of Si (100). **1991**, No. 19, 9061–9062.
- (88) Weakliem, P. C.; Wu, C. J.; Carter, E. A. First-Principles-Derived Dynamics of a Surface Reaction: Fluorine Etching of Si(100). *Phys. Rev. Lett.* **1992**, *69* (1), 200–204.
- (89) Carter, L. E.; Carter, E. A. Ab Initio-Derived Dynamics for F₂ Reactions with Partially Fluorinated Si (100) Surfaces : Translational Activation as a Possible Etching Tool. **1996**, No. 100, 873–887.
- (90) Duin, A. C. T. Van; Strachan, A.; Stewman, S.; Zhang, Q.; Xu, X.; Goddard, W. A. Reactive Force Field for Silicon and Silicon Oxide Systems. **2003**, No. 1, 3803–3811.
- (91) Kim, S. Y.; van Duin, A. C. T. Simulation of Titanium Metal/titanium Dioxide Etching with Chlorine and Hydrogen Chloride Gases Using the ReaxFF Reactive Force Field. *J. Phys. Chem. A* **2013**, *117* (27), 5655–5663.
- (92) Kim, S.-Y.; van Duin, A. C. T.; Kubicki, J. D. Molecular Dynamics Simulations of the Interactions between TiO₂ Nanoparticles and Water with Na⁺ and Cl⁻, Methanol, and Formic Acid Using a Reactive Force Field. *J. Mater. Res.* **2012**, *28* (03), 513–520.
- (93) Tersoff, J. Empirical Interatomic Potential for Carbon, with Applications to Amorphous Carbon. *Phys. Rev. Lett.* **1988**, *61* (25), 2879–2882.
- (94) Abell, G. Empirical Chemical Pseudopotential Theory of Molecular and Metallic Bonding. *Phys. Rev. B* **1985**, *31* (10), 6184–6196.
- (95) Brenner, D. W. Empirical Potential for Hydrocarbons for Use in Simulating the Chemical Vapor Deposition of Diamond Films. *Phys. Rev. B* **1990**, *42* (15), 9458–9471.
- (96) Mortier, W. J.; Ghosh, S. K.; Shankar, S. Electronegativity-Equalization Method for the Calculation of Atomic Charges in Molecules. *J. Am. Chem. Soc.* **1986**, *108* (15), 4315–4320.

- (97) Rappe, A. K.; Goddard III, W. A. Charge Equilibration for Molecular Dynamics Simulations. *J. Phys. Chem.* **1991**, *95* (8), 3358–3363.
- (98) Chenoweth, K.; van Duin, A. C. T.; Goddard, W. a. ReaxFF Reactive Force Field for Molecular Dynamics Simulations of Hydrocarbon Oxidation. *J. Phys. Chem. A* **2008**, *112* (5), 1040–1053.
- (99) Stukowski, A. Visualization and Analysis of Atomistic Simulation Data with OVITO—the Open Visualization Tool. *Model. Simul. Mater. Sci. Eng.* **2009**, *18* (1), 015012.
- (100) Silva, E. C. C. M.; Li, J.; Liao, D.; Subramanian, S.; Zhu, T.; Yip, S. Atomic Scale Chemo-Mechanics of Silica: Nano-Rod Deformation and Water Reaction. *J. Comput. Mater. Des.* **2006**, *13* (1-3), 135–159.
- (101) Zhu, T.; Li, J.; Lin, X.; Yip, S. Stress-Dependent Molecular Pathways of Silica–water Reaction. *J. Mech. Phys. Solids* **2005**, *53* (7), 1597–1623.
- (102) Gopalan, S.; Savage, P. E. Reaction Mechanism for Phenol Oxidation in Supercritical Water. *J. Phys. Chem.* **1994**, *98* (48), 12646–12652.
- (103) Brunner, G. Near Critical and Supercritical Water. Part I. Hydrolytic and Hydrothermal Processes. *J. Supercrit. Fluids* **2009**, *47* (3), 373–381.
- (104) Chandrasekharan, R.; Zhang, L.; Ostroverkhov, V.; Prakash, S.; Wu, Y.; Shen, Y. R.; Shannon, M. a. High-Temperature Hydroxylation of Alumina Crystalline Surfaces. *Surf. Sci.* **2008**, *602* (7), 1466–1474.
- (105) Kubicki, J. D.; Xiao, Y.; Lasaga, A. C. Theoretical Reaction Pathways for the Formation of [Si(OH)₅]¹⁻ and the Deprotonation of Orthosilicic Acid in Basic Solution. *Geochim. Cosmochim. Acta* **1993**, *57* (16), 3847–3853.
- (106) Mozzi, R.; Warren, B. The Structure of Vitreous Silica. *J. Appl. Crystallogr.* **1969**, *2*, 164–172.
- (107) Zhuravlev, L. The Surface Chemistry of Amorphous Silica. Zhuravlev Model. *Colloids Surfaces A Physicochem.* **2000**.
- (108) Chen, L.; Kim, S. H.; Wang, X.; Qian, L. Running-in Process of Si-SiO_x/SiO₂ Pair at nanoscale—Sharp Drops in Friction and Wear Rate during Initial Cycles. *Friction* **2013**, *1* (1), 81–91.
- (109) Khalilov, U.; Pourtois, G.; van Duin, a C. T.; Neyts, E. C. Hyperthermal Oxidation of Si(100)2x1 Surfaces: Effect of Growth Temperature. *J. Phys. Chem. C* **2012**, *116* (100), 8649–8656.
- (110) Litton, D. A.; Garofalini, S. H. Modeling of Hydrophilic Wafer Bonding by Molecular Dynamics Simulations. *J. Appl. Phys.* **2001**, *89* (11), 6013.
- (111) Barnette, A. L.; Asay, D. B.; Ohlhausen, J. a.; Dugger, M. T.; Kim, S. H. Tribochemical Polymerization of Adsorbed N-Pentanol on SiO₂ during Rubbing: When Does It Occur and Is It Responsible for Effective Vapor Phase Lubrication? *Langmuir* **2010**, *26* (21), 16299–16304.
- (112) Liu, X.-Z.; Ye, Z.; Dong, Y.; Egberts, P.; Carpick, R. W.; Martini, A. Dynamics of

- Atomic Stick-Slip Friction Examined with Atomic Force Microscopy and Atomistic Simulations at Overlapping Speeds. *Phys. Rev. Lett.* **2015**, *114* (14), 1–5.
- (113) He, H.; Qian, L.; Pantano, C. G.; Kim, S. H. Mechanochemical Wear of Soda Lime Silica Glass in Humid Environments. *J. Am. Ceram. Soc.* **2014**, *97* (7), 2061–2068.
- (114) Dove, P. M.; Han, N.; Wallace, A. F.; De Yoreo, J. J. Kinetics of Amorphous Silica Dissolution and the Paradox of the Silica Polymorphs. *Proc. Natl. Acad. Sci. U. S. A.* **2008**, *105* (29), 9903–9908.
- (115) van Duin, A. C. T.; Baas, J. M. A.; van de Graaf, B. Delft Molecular Mechanics A New Approach to Hydrocarbon Force Fields. *J. Chem. Soc. Faraday Trans.* **1994**, *90* (19), 2881–2895.
- (116) Chase, M. W. *NIST-JANAF Thermochemical Tables, Fourth Edition*; J. Phys. Chem. Ref. Data, Monograph 9, 1998.
- (117) Joshi, K. L.; Raman, S.; Van Duin, A. C. T. Connectivity-Based Parallel Replica Dynamics for Chemically Reactive Systems: From Femtoseconds to Microseconds. *J. Phys. Chem. Lett.* **2013**, *4* (21), 3792–3797.
- (118) Ensing, B.; De Vivo, M.; Liu, Z.; Moore, P.; Klein, M. L. Metadynamics as a Tool for Exploring Free Energy Landscapes of Chemical Reactions. *Acc. Chem. Res.* **2006**, *39* (MARCH), 73–81.

Jejoon Yeon | Curriculum Vitae

117 Academic Office Annex, 5200 North Lake Road, Merced, CA 95343

814-441-7217, jyeon3@ucmerced.edu

Research Experience

- Post-doctoral researcher** – University of California, Merced [Jan 2016 – Current]
Computational chemistry research using reactive MD potential and DFT, for the study on interfacial science, tribo-chemistry of Si surface sliding with hydrocarbons, and mechano-chemical reactions of methyl thiolates with Au/Cu surface.
- Graduate Research Assistant, Ph.D.** – The Pennsylvania State University [Aug 2011 – May 2016]
Computational chemistry research using reactive MD potential and DFT, for the study on hydroxylation on Silicon surface, etching of the Fluorine on Silicon, and Si/SiO₂ sliding under different humidity, and ReaxFF force field development for Si/F/O/H.
- Associate Researcher** – Doosan Corps [Jan 2009 – May 2011]
Experimental and analytical research Noise Analysis of Hydraulic system of Excavators and Possible Improvements for CFD Analysis of Engine-Rooms in Large Forklifts and Possible Improvements, Calculation and analysis of heat damage and transformation of machine tools
- Graduate Research Assistant, M.S.** – POSTECH [Mar 2007 – Feb 2009]
Experimental research for dry cleaning of surface using laser-induced shock wave. Shockwave magnification using geometric reflector, and visualization of shock wave using shadowgraph visualization method.

Publications

- (1) Yeon, J.; van Duin, A. C. T.; Kim, S. H. Effects of Water on Tribochemical Wear of Silicon Oxide Interface: Molecular Dynamics (MD) Study with Reactive Force Field (ReaxFF). *Langmuir* 2016, No. Md, acs.langmuir.5b04062.
- (2) Yeon, J.; van Duin, A. C. T. ReaxFF Molecular Dynamics Simulations of Hydroxylation Kinetics for Amorphous and Nano-Silica Structure, and Its Relations with Atomic Strain Energy. *J. Phys. Chem. C* 2016, 120, 305-317.
- (3) Yue, D.-C.; Ma, T.-B.; Hu, Y.-Z.; Yeon, J.; van Duin, A. C. T.; Wang, H.; Luo, J. Tribochemical Mechanism of Amorphous Silica Asperities in Aqueous Environment: A Reactive Molecular Dynamics Study. *Langmuir* 2015, 31 (4), 1429-1436.
- (4) Yue, D.-C.; Ma, T.-B.; Hu, Y.-Z.; Yeon, J.; van Duin, A. C. T.; Wang, H.; Luo, J. Tribochemistry of Phosphoric Acid Sheared between Quartz Surfaces: A Reactive Molecular Dynamics Study. *J. Phys. Chem. C* 2013, 117 (48), 25604-25614.

Awards

- Honors Scholarship**, Department of Mechanical Engineering, Chung-Ang University, Seoul, Korea 2004-2006
- Magna Cum Laude**, Department of Mechanical Engineering, Chung-Ang University, Seoul, Korea 2007
- Best Squad Leader Prize of 2003**, R.O.K. Army 22nd Infantry Division, Korea 2003